Reconstructing sea surface temperature in the South Pacific using organic proxies

Dissertation zur Erlangung des akademischen Grades

eines Doktors der Naturwissenschaften

Dr. rer. nat.

an der Fakultät für Geowissenschaften der Universität Bremen

vorgelegt von

Sze Ling Ho

Bremerhaven, 2012

Gutachter der Dissertation

Prof. Dr. Ralf Tiedemann
Prof. Dr. Gesine Mollenhauer

Erklärung

Name: Sze Ling Ho

Anschrift: Sielstrasse 12, 27568 Bremerhaven.

Hiermit versichere ich, dass ich

1. die Arbeit ohne unerlaubte fremde Hilfe angefertigt habe,

2. keine anderen als die von mir angegebenen Quellen und Hilfsmittel benutzt habe und

3. die den benutzten Werken wörtlich oder inhaltlich entnommenen Stellen als solche kenntlich gemacht habe.

Bremerhaven, 20th September 2012

…….

(Unterschrift)

The most exciting phrase to hear in science, the one that heralds new discoveries, is not 'Eureka!', but 'That's funny…'

Isaac Asimov (1920-1992)

Abstract

Sea surface temperature (SST), at the interface between the atmosphere and the ocean, is an important element in the global climate system. Accurate estimates of past SSTs are indispensable for studying global climate and for validating the numerical models used for projections of future climate. SSTs prior to the instrumentation era could be reconstructed using climatically sensitive biomarkers such as alkenones and glycerol dialkyl glycerol tetraethers (GDGTs). Herein I use marine sediments, both core-tops and long piston cores, to further examine the applicability of organic SST proxies derived from the aforementioned biomarkers, with an emphasis on the relatively under-studied subantarctic Southeast Pacific. The appraisal of these proxies is based on the correlation of the core-top proxy index values with present-day climatological SST, and the comparison of the SST records inferred from these proxies with other regional SST records.

The alkenone index (U^{K}_{37} and $U^{K'}_{37}$) values in the South Pacific core-tops display linear relationships with climatological World Ocean Atlas 2009 (WOA09) SST at low temperatures (1 -12°C), with equally high r^2 values (>0.93). These results suggest that both alkenone indices are highly correlated to SST even at high latitudes, rendering them appropriate for reconstructing SST in the subantarctic Pacific. However, these indices yield different Pleistocene SST patterns for study sites in the subantarctic sector of the Southern Ocean. Judging from the better structural fit of U^{K}_{37} SST records with other subantarctic surface proxy records, including foraminiferal $\delta^{18}O$ and SST records inferred from diatom- and foraminiferal assemblages, it appears that the U^{K}_{37} index results in more plausible paleo SST records in this region, as opposed to the commonly used $U^{K'}_{37}$ index.

The GDGT index (TEX_{86} and TEX_{86}^{L}) values in the subpolar and polar core-tops (with overlying SSTs of -2 to 17°C) are not highly correlated (r^2 values < 0.3) to the annual mean WOA09 SST. Plotting these indices against seasonal SSTs and water temperatures at various hydrographic boundaries does not improve the correlation. Nevertheless, when these data are combined with previously published core-top data (n = 630) spanning a SST range of -2 to 30°C, the r^2 values of these relationships improve to ~ 0.8, with a better correlation for the TEX_{86} compared to TEX_{86}^{L}. The TEX_{86} calibration yields SST estimates that are in better agreement with the WOA09 SST for subpolar and polar regions, rendering it a better SST index in these regions. Meanwhile, applying the GDGT index on a Southeast Pacific sediment core yields SSTs that are colder than those inferred from the alkenones, and the GDGT-

derived interglacial SSTs are ~3°C colder than annual mean WOA09 SST. Given the lack of seasonality in the archaeal abundance here, the cold-biased GDGT estimates probably reflect subsurface temperature instead of SST.

The three SST records presented here allow for further understanding of the surface oceanographic variability in the subtropical and subantarctic Southeast Pacific over the past 700 kyr. The extent of glacial cooling increases with latitude, up to ~8°C in the subantarctic as opposed to the ~4°C in the subtropics. Intense cooling at high latitudes results in larger latitudinal SST gradients during glacials than interglacials. The alkenone-inferred SSTs along the latitudinal range of the Peru-Chile Current (PCC) imply massive equatorward migrations of the Southern Ocean frontal systems and increased equatorward transport of subantarctic waters owing to a stronger PCC during glacials. In addition, GDGT-derived temperatures suggest enhanced subsurface warming during MIS 11 and 13 in the subtropical Southeast Pacific, plausibly due to water column reorganization analogous to that occurring during modern-day El-Niño conditions.

Zusammenfassung

Die Meeresoberflächentemperatur, am unmittelbaren Kontakt zwischen Atmosphäre und Ozean, ist ein wichtiges Element im globalen Klimasystem. Die genaue Bestimmung vergangener Meeresoberflächentemperaturen ist deswegen unabdingbar für die Erforschung der globalen Klimaprozesse und zur Evaluierung numerischer Modelle für die Klimaprojektion. Meeresoberflächentemperaturen zu Zeiten vor der instrumentellen Messung können anhand von klimasensitiven Biomarkern wie Alkenone und Glycerol Dialkyl Glycerol Tetraether (GDGTs) rekonstruiert werden. In der vorliegenden Arbeit nutze ich sowohl die obersten Abschnitte von Sedimentkernen also auch lange Kolbenlote aus dem bisher relativ wenig untersuchten subantarktischen Südostpazifik, um das Potential der oben genannten organischen Biomarker als Proxies für die Meeresoberflächentemperatur zu erfassen. Die Beurteilung dieser Proxies basiert auf der Korrelation der Werte der Proxy-Indizes der Sedimentoberflächen mit aktuellen, klimatologischen Meeresoberflächentemperaturen. Des weiteren werden die rekonstruierten Meeresoberflächentemperaturen mit anderen regionalen Rekonstruktionen der Meeresoberflächentemperaturen verglichen.

In den Sedimentoberflächen des Südpazifiks ist die Beziehung zwischen den Werten der Alkenon-Indizes (U^{K}_{37} und $U^{K'}_{37}$) und den klimatologischen Meeresoberflächentemperaturen des World Ocean Atlas 2009 (WOA09) im niedrigen Temperaturbereich (1 –12°C) linear. Die gleichermaßen hohen r^2-Werten für beide Indizes (> 0.93) deuten an, dass die Korrelation beider Alkenon-Indizes mit der Meeresoberflächentemperatur auch im subantarktischen Südpazifik hoch ist und somit beide Indizes zur Rekonstruktion der Meeresoberflächentemperaturen in den hohen südlichen Breiten geeignet sind. Trotzdem ergeben beide Indizes jedoch unterschiedliche Meeresoberflächentemperaturen für das Pleistozän. Das Ergebnis der U^{K}_{37}-basierten Rekonstruktionen der Meeresoberflächentemperaturen entspricht dabei eher den Resultaten anderer proxy-basierten Rekonstruktionen des Oberflächenwassers des subantarktischen Südpazifiks, z.B. den auf Diatomeen und Foraminiferen-Vergesellschaftungen basierenden Meeresoberflächentemperaturen und Foraminiferen-$\delta^{18}O$. Daher erscheint der U^{K}_{37}-Index, im Gegensatz zum häufig genutzten $U^{K'}_{37}$-Index, besser geeignet zu sein um plausible Rekonstruktionen der Meeresoberflächentemperaturen zu liefern.

Die Korrelation zwischen den Werten der GDGT-Indizes (TEX_{86} and TEX_{86}^{L}) in den subpolaren und polaren Sedimentkernoberflächen (Temperaturen in den darüberliegenden Wasseroberflächen -2 bis 17°C) und den WOA09-basierten Jahresmitteln der

Meeresoberflächentemperaturen ist nicht hoch (r^2 values < 0.3). Das Auftragen dieser Indizes sowohl gegen saisonale Meeresoberflächentemperaturen als auch gegen Wassertemperaturen an den verschiedenen hydrographischen Grenzschichten verbessert die Korrelation nicht. Die Kombination dieser Daten mit bereits publizierten Daten von Kernoberflächen (n = 630), welche Meeresoberflächentemperaturen von -2 bis 30°C umfassen, ergibt r^2-Werte von ~ 0.8, mit einer besseren Korrelation für TEX_{86} als für TEX_{86}^L. Da die Abschätzung der Meeresoberflächentemperaturen mit Hilfe der TEX_{86} Kalibrierung besser mit den WOA09-Meeresoberflächentemperaturen polarer und subpolarer Regionen übereinstimmt, ist dieser Index eher zur Abschätzung der Meeresoberflächentemperaturen in diesen Regionen geeignet. In einem Sedimentkern im Südostpazifik ergibt der GDGT-Index kältere Meeresoberflächentemperaturen als der Alkenon-Index und die GDGT-basierten interglazialen Meeresoberflächentemperaturen sind ~ 3°C kälter als die WOA09-Jahresmitteltemperaturen. Da die Archaea keine saisonalen Schwankungen in der Abundanz aufweisen, spiegeln die zu kalten, GDGT-basierten Abschätzungen wahrscheinlich nicht die Temperaturen direkt an der Meeresoberfläche sondern die der darunter liegenden Wasserschichten wider.

Die drei Rekonstruktionen der Meeresoberflächentemperaturen in der vorliegenden Arbeit tragen zum besseren Verständnis der ozeanographischen Oberflächenvariabilität im subtropischen und subantarktischen Südpazifik der letzten 700.000 Jahre bei. Die Abnahme der glazialen Temperaturen nimmt mit den Breitengraden zu, bis zu ~ 8°C in subantarktischen und bis zu ~ 4°C in subtropischen Regionen. Die starke Abkühlung in den hohen Breiten führt zu größeren latitudinalen Temperaturgradienten während der Kaltzeiten (Glazialen) als während der Warmzeiten (Interglazialen). Darüber hinaus deuten die Alkenon-basierten Meeresoberflächentemperaturen entlang des Humboldt Stroms eine massive, äquatorwärts gerichtete Verlagerung des Frontensystems des Südlichen Ozeans sowie einen zunehmenden, äquatorwärts gerichteten Transport von subantarktischem Wasser an. Diese Veränderungen werden wahrscheinlich durch einen verstärkten Humboldt Strom während der Kaltzeiten bedingt. Außerdem zeigen die GDGT-basierten Temperaturen eine verstärkte Erwärmung im subtropischen Südpazifik während der Marinen Isotopen Stadien 11 und 13 an, welche womöglich durch eine Umstrukturierung der Wassersäule, analog zu den modernen El-Nino-Verhältnissen, bedingt ist.

Acknowledgments

Completing this PhD work was no bed of roses. The thesis would definitely not come into existence if not for the help from many people around me. In line with my firm belief that science is about people and also the fact that I am a tad on the melodramatic side, here I would like to dedicate some pages to thank these people specifically.

First of all, I would like to thank my PhD committee, comprised of Ralf Tiedemann, Frank Lamy and Gesine Mollenhauer, for giving me the opportunity to carry out this interesting interdisciplinary research, for their free reign-style supervision that gave me plenty of freedom to plan and carry out my research as independently as possible, and for always having time for me when their help was needed. I would like to thank Ralf for providing various travel funds and for his effort in getting me the 2-months contract prolongation which bought me some extra time to complete my thesis. Thanks to Frank my PhD study was not 3 monotonous years of laboratory work and writing. I had my fair share of adventures, i.e., sea-going experience and scientific-stays abroad, and the occasional BBQ and beers on sunny days in the Fishtown. Heaps of thanks go to Gesine: for being the role model I could look up to, for teaching by demonstration the importance of communication skills and scientific integrity, for encouraging me when I hit a rough patch and for steering me in the right direction when I could not find my way in the confusing "jungle of academia".

I cannot thank B. David A. Naafs and Susanne Fietz enough. David has been a huge influence in my "formative years" in academia (much like Obi-wan Kenobi to Luke Skywalker), as he often said to me: 'My young *padawan*, you have so much to learn'. I especially appreciate his very "Dutch way" of helping – dishing out blunt, sometimes unbearable, ego-hurting critical comments, in line with his maxim – you learn from criticism not from praises. Thanks for being the "board" where I could bounce ideas off, for helping me with software problems, for exchanging views on how academia should and should not be (illustrated with stories and gossips), for barging into my office every 2 hours to shove his latest super-nice-data-sets-that-match-his-geofantasy in my face, for motivating and bearing with me in general. Similarly, Susanne provided stimulating discussions (on the *Manolitos* a.k.a. GDGTs among many other subjects), and tried by constant repetition to get it through my thick skull that my data are not crap. Many thanks for those fun-, gossip-, wine-, tapas-, advices-, heated discussion-filled months in Barcelona! Thanks for having faith in my scientific ability – it's a source of motivation.

Thanks are also due to various people who contributed ideas, suggestions, advices and encouragements, which had not only improved the quality of my PhD work tremendously but also made the journey more fun: Mahyar Mohtadi, Alfredo Martinez-Garcia, Carme Huguet, Oliver Esper, Jens Hefter, Kalle Baumann, Thom Laepple, Peppe Cortese, Amelia Shevenell, Valerie Masson-Delmotte, Gerald Langer, Tom Russon, Birgit Schneider and Ralph Schneider. I especially appreciate the fact that the geographical distance between some of us did not deter these people to lend a helping hand by putting in extra effort via numerous email exchanges and phone / Skype calls.

Special thanks to Peppe Cortese for meticulous proofreading and improving the quality of this thesis. Thanks also go to Susanne Fietz and Michael Shreck for their assistance in the translation of the thesis abstract into German.

I would like to thank Rainer Gersonde, Rüdiger Stein, and Dierk Hebbeln for providing sediment samples, without which the project would have not been possible. Technical assistance from Walter Luttmer, Ralph Kreutz and Stephan Heckendorff (on ODV) is also appreciated. I am grateful to Antoni Rosell-Melé and Carina B. Lange for hosting me during the short-stays at the ICTA, Autonomous University of Barcelona and the COPAS, University of Concepcion, respectively. I would like to thank POLMAR Graduate School for funding my study at AWI-Bremerhaven, without which none of this work would have happened. Administrative assistance from Claudia Sprengel and Claudia Hanfland is highly appreciated. A SCAR Fellowship 2010/2011 is acknowledged for funding the short-stay at the ICTA, Barcelona.

Research was a big part of my life in Bremerhaven, thus I might not have made it to the end if not for the companionship of work-related people, who have added colors to my life here in the past 3 years, especially Verena, Mieke, Reza, Marie, Franziska, Micha, Thomas, Johannes, Ines and Evgenia. Thanks also go to the friendly people at ICTA, i.e., Gemma, Bastian, Anna and especially Carme for her many hilarious and sarcastic remarks regarding TEX_{86} that never fail to crack me up, and for her contagious enthusiasm for science. Special thanks go to Mariem (my twin sister!) for being the best companion one could have during this PhD journey.

And of course, I am indebted to my parents for their unconditional support and for encouraging me to pursue my passion for science, even if it would mean that they have to be thousands of miles away from me and get to see me twice in the past 3 years. Last but not

least, I cannot thank Raúl enough, who was always there (and thus contributed significantly to Deutsche Bahn via his many 4-hours journeys to Bremerhaven), who bore the brunt of my frustrations and listened to my incessant complaints with endless patience. Thanks for distracting me from work, especially during those stressful and disillusioned dark months when it was almost impossible to find the strength and reason to go on.

Table of Contents

Abstract I
Zusammenfassung III
Acknowledgments V

Chapter 1: General overview

1.1 Global climate and sea surface temperature (SST) 1
1.2 Obtaining SST data 2
1.2.1 Instrumental SST measurements 2
1.2.2 Indirect SST data via proxy 3
1.2.2.1 Alkenone-based paleothermometry 5
1.2.2.2 Glycerol dialkyl glycerol tetraether (GDGT) –based paleothermometry 7
1.3 Subantarctic Southeast Pacific SST: present and past 9
1.4 Outstanding research issues 12
1.4.1 Occurrence of alkenones and GDGTs in the South Pacific 12
1.4.2 Is TEX_{86} paleothermometry applicable in (sub)polar regions? 12
1.4.3 Which alkenone index is more suitable for paleo SST reconstruction in the South Pacific? 13
1.4.4 How has the Southeast Pacific SST evolved during the Pleistocene? 14
1.4.5 How do the TEX_{86}-derived SSTs compare to the alkenone-derived SSTs during the Pleistocene? 15
1.5 Material and methods 15
1.5.1 Marine sediments 15
1.5.2 Sample preparation 17
1.5.3 Alkenone analysis 18
1.5.4 GDGT analysis 20
1.5.5 Choice of environmental data for calibration 20
1.6 Thesis outline 21

Chapter 2: Appraisal of the TEX_{86} and TEX_{86}^{L} thermometries in the subpolar and polar regions: implications for global core-top calibrations

2.0 Abstract 23
2.1 Introduction 24
2.2 Materials and Methods 26
2.2.1 Sediment Extraction 26
2.2.2 GDGTs Analysis 27
2.2.3 TEX_{86} calculation and SST estimations 29
2.2.4 Environmental data 29
2.3 Results 30
2.3.1 Relationship between individual GDGTs 30
2.3.2 Fractional abundance of GDGTs 31
2.3.3 TEX_{86} and TEX_{86}^{L} values 31
2.3.3.1 Correlation to temperature at various water depths 33
2.3.3.2 Correlation to SST of various seasons 34
2.3.4 Residuals of SST estimates 34
2.4 Discussion 38
2.4.1 GDGT contribution from methanogenic archaea 38
2.4.2 Correlation of TEX_{86} / TEX_{86}^{L} indices to subsurface temperature 39
2.4.3 Deviant SST estimates in the Arctic 40

2.4.4 Effect of sedimentation setting and/or seasonality 41
2.4.5 Implications for global core-top calibrations 43
2.4.6 Applicability in (sub)polar regions and conclusions 45
2.5 Acknowledgments 46

Chapter 3: Sea surface temperature variability in the Pacific sector of the Southern Ocean over the past 700 kyr

3.0 Abstract 47
3.1 Introduction 48
3.2 Oceanographic setting 50
3.3 Materials and methods 51
3.3.1 Materials 51
3.3.2 $\delta^{18}O$ measurement on foraminifera 52
3.3.3 Alkenone analysis 53
3.3.4 Alkenone-based indices and calibrations 54
3.3.5 SST gradient calculation 55
3.4 Results 55
3.4.1 Stratigraphy 55
3.4.2 South Pacific core-top alkenone calibrations 58
3.4.3 Downcore SST estimates and planktic $\delta^{18}O$ values 58
3.4.3.1 Core GeoB 3388-1 58
3.4.3.2 Core GeoB 3327-5 58
3.4.3.3 Core PS75/034-2 59
3.5 Discussion 60
3.5.1 Alkenone-based calibrations for application in the subantarctic Pacific 60
3.5.2 Assessing contrasting temporal trends in U^{K}_{37}- and $U^{K'}_{37}$-derived SST records 62
3.5.3 Southern Ocean SST evolution: circum-Antarctic comparison 64
3.5.4 Meridional SST gradients: equatorward cold water transport 67
3.6 Conclusions 70
3.7 Acknowledgments 71

Chapter 4: Diverging Pleistocene SST trends revealed by U^{K}_{37} and TEX_{86}^{H} in the Southeast Pacific

4.0 Abstract 72
4.1 Introduction 73
4.2 Study site 74
4.3 Materials and methods 75
4.4 Results and discussion 77
4.4.1 High BIT values: potential terrestrial bias on TEX_{86}^{H} SST? 78
4.4.2 Comparison with alkenone-derived SSTs 79
4.4.3 Paleoceanographic implications 82
4.5 Conclusions 84
4.6 Acknowledgments 84
4.7 Supplementary information 84

Chapter 5: Conclusions and Outlook

5.1 Summary and conclusions 86
5.1.1 Lipids occurrence: Where the proxies may be applied 86
5.1.2 Proxy indices and calibrations: Diverging views from the core-top and downcore application 86

5.1.3 Paleo SST estimates: Pleistocene climatic implications 88
5.2 Perspectives for future work 89
5.2.1 Refining U^{K}_{37} calibration 90
5.2.2 Refining GDGT-based SST calibrations 92
5.2.3 Constraining paleo SST reconstruction: Multi-proxy approach 95
5.2.4 Towards the "big picture" 96

References 97
Data handling 113
Appendix 1: Abbreviations and acronyms 114
Appendix 2: Units and chemical nomenclatures 116
Appendix 3: List of figures 117
Appendix 4: List of tables 119
Appendix 5: Additional first-authored manuscripts 120

Chapter 1: General overview

1.1. Global climate and sea surface temperature (SST)

One of the pressing issues that plague humanity is climate change. A concerted effort from the scientific community shows that the earth surface temperature has risen by almost 1°C since the Industrial Revolution [*IPCC*, 2007, http://www.ipcc.ch]. While there is no doubt that climate strongly affects our societies, there is still ongoing debates on whether the warming is attributed to natural variability or human activities. It is also crucial to know how the climate may change in the future in order to develop the best possible mitigation policies. Consequently, substantial amount of effort and funding have been invested in the development of earth climate models over the years.

These earth system models are built based on our knowledge on the interaction of various climatic components and feedback mechanisms (**Figure 1.1**). In this regard, the ocean is a vital component of the global climate, through its close interaction with the atmosphere,

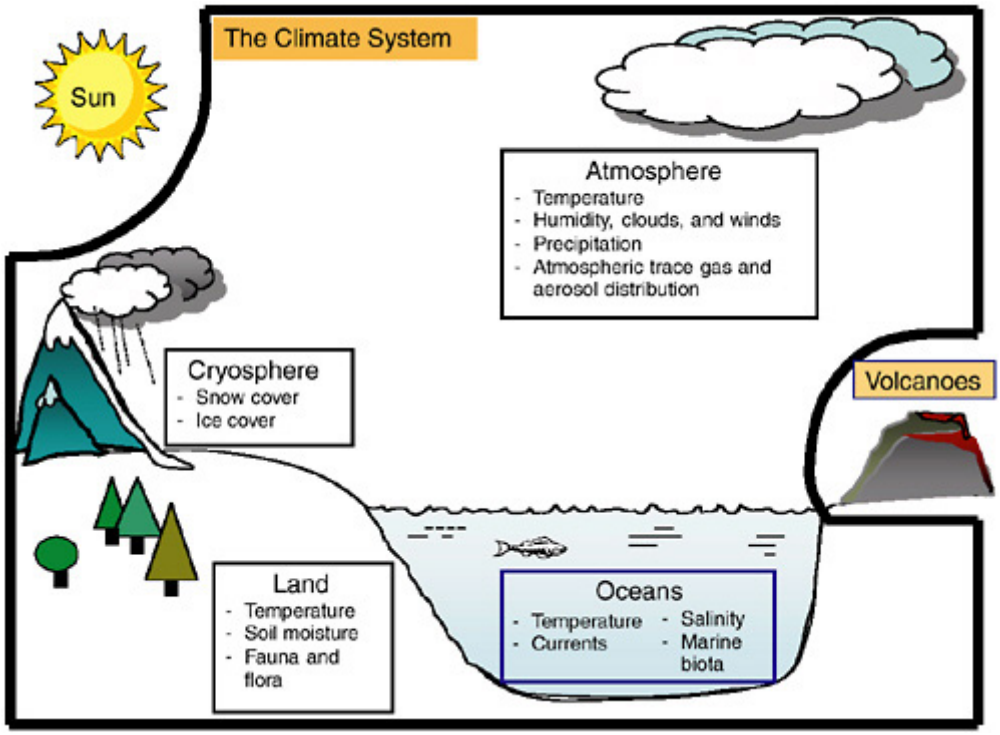

Figure 1.1: Major components of the climate system. (from Roger Pielke Sr.'s www.pielkeclimatesci.wordpress.com).

the land and the cryosphere. Due to its sheer size and high heat capacity, the ocean stores a large amount of energy, which is communicated to the atmosphere via turbulent and radiative energy exchange at the air-sea interface [*Deser et al.*, 2010]. For instance, the condensation of moisture from the ocean releases latent heat that contributes to drive the atmospheric circulation, which in turn affects the sea surface temperature (SST) [*Tomczak and Godfrey*, 2003]. Therefore, the temperature at the sea surface is an important parameter that links the atmosphere and the ocean, rendering it an indispensable boundary parameter in earth climate models (**Figure 1.2**). Records of past SST changes are therefore useful for two reasons. Firstly, these records help us to understand how and why the climate has changed in the past. Secondly, we need these records to validate the climate models in order to improve the credibility of the projections they simulate.

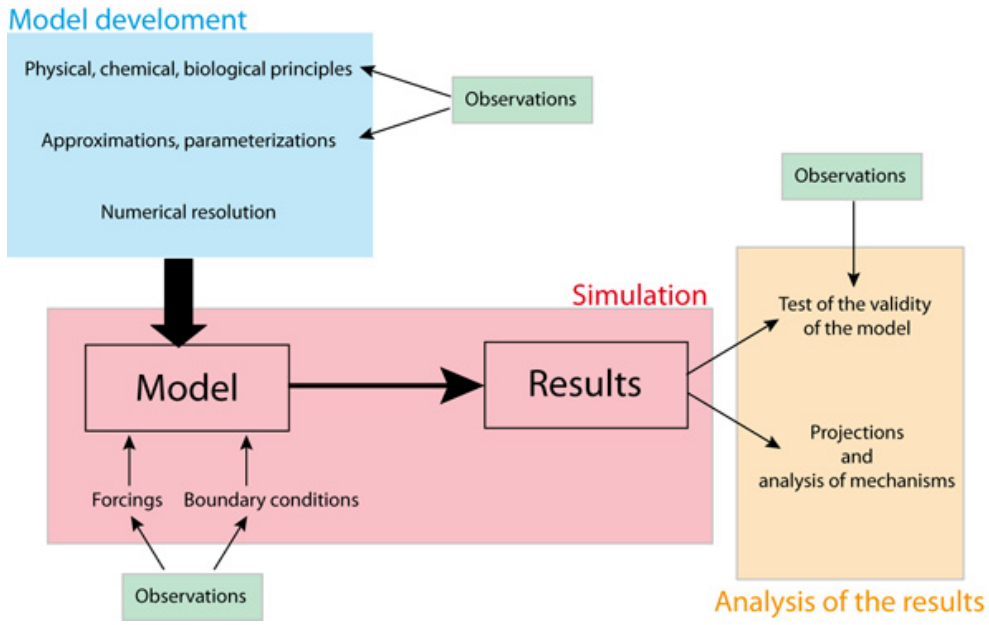

Figure 1.2: A schematic of the framework for projecting future climate using climate models (from *Goosse et al.*'s online textbook at www.climate.be/textbook/).

1.2. Obtaining SST data

1.2.1. Instrumental SST measurements

In modern oceanography, SST data are obtained using instruments such as thermistors and thermometers employed on ships and buoys, or the more recently developed infrared radiometers (such as the Advanced Very High Resolution Radiometer AVHRR) mounted on satellites. Ship-based data have lower and uneven spatial coverage but extend further back in

time to the late 18th century. The voyage of the HMS Challenger in year 1872 marked the first global-scale study of the ocean [*Roemmich et al.*, 2012]. Many more organized efforts would follow, including the International Geophysical Year (1957-1958), the World Ocean Circulation Experiment (WOCE; 1990-2000) and the ARGO program (2004-2010), all of which contributed important data sets of various oceanic parameters, including SST. On the other hand, satellite SST data have global coverage at high resolution (0.25 degree), but only go back to the early 1980s [for more details see *Deser et al.*, 2010]. To get the best spatial and temporal coverage to meet the demands of oceanographic research, in-situ and satellite data could be combined into a single data set, such as the International Comprehensive Atmosphere-Ocean Data Set (ICOADS). Alternatively, observations could be analyzed objectively, interpolated and weighted (to account for irregular sampling in time and space) to construct climatologies, such as the World Ocean Database (WOD). Climatological data are the mean values (of a given oceanic parameter) over many years [*Talley et al.*, 2011]. They are usually constructed for the annual mean, individual months and seasons. Spatially gridded climatological atlases, such as the World Ocean Atlas (WOA) are useful for visualization of climatological fields and are widely used in SST proxy calibration work (**Section 1.5.5**).

1.2.2. Indirect SST data via proxy

Instrumental SST records span approximately the past two centuries (**Section 1.2.1**). Beyond that, we have to rely on indirect SST data inferred from various proxies, which are mostly biogeochemical in nature. Organic or inorganic fossil remains of marine organisms represent SST proxies that are incorporated in marine sediments. These proxies are based on observed relationships between these compounds/species and SST, e.g., the ratio of chemical elements found in the tests of marine organisms, the relative abundance of marine organism and the relative distribution of organic compounds within the cells. Considering the importance of SST in the climate system (**Section 1.1**), since the 1950s large arrays of SST proxies have been developed to reconstruct SST in the geological past. In a broad sense, paleo SST proxies could be categorized into geochemical proxies (oxygen isotope, Mg/Ca, $U^{K'}_{37}$ and TEX_{86}) and faunal/floral census proxies (foraminifera, diatom, radiolaria and coccolithophores). Each proxy has its own advantages and weaknesses. In a recent international Multiproxy Approach for the Reconstruction of the Glacial Ocean surface

(MARGO) project, *Kucera et al.* [2005] concluded that no single proxy is "right" and "right everywhere". A short description of paleo SST proxies is available in **Table 1.1**.

Table 1.1: Overview of paleo sea surface temperature (SST) proxies.

Proxy	Working assumptions	Limitations / Caveats	References
Faunal transfer functions (foraminifera, radiolaria, diatom, coccolithophores)	Temperature as the major environmental parameter causing the changes in faunal assemblages; relationship quantified using statistical methods e.g., IKM [*Imbrie and Kipp*, 1977], MAT [*Prell*, 1985], GAM [*Hastie and Tibshirani*, 1990], RAM [*Waelbroeck et al.*, 1998], ANN [*Malmgren et al.*, 2001], SIMMAX [*Pflaumann et al.*, 1996]	- Lack of diversity at temperature extremes - Evolutionary events - Preferential preservation	*Gersonde et al.* [2005] *Barrows and Juggins* [2005] *Cortese and Abelmann* [2002] *Saavedra-Pellitero et al.* [2011]
Oxygen isotopes $\delta^{18}O$ (foraminifera, corals, opal)	Thermodynamic fractionation between ^{16}O and ^{18}O that occurs during precipitation is a logarithmic function of temperature	- Vital effects (e.g., carbonate ion concentration, ontogenic effect) - Unknown $\delta^{18}O$ of regional seawater - Diagenesis (e.g., partial shell dissolution)	*Urey* [1947] *Epstein et al.* [1953] *Emiliani* [1955] *Hays et al.* [1976] *Gagan et al.* [2000] *Shemesh et al.* [1992]
Mg/Ca (foraminifera)	Incorporation of Mg in calcite varies exponentially as a function of temperature	- Dissolution - Salinity - Vital effects (e.g., species, pH)	*Chave* [1954] *Nuernberg* [1995] *Barker et al.* [2005]
Sr/Ca (corals)	Incorporation of Sr in calcite varies as a negative function of temperature	- Vital effects (e.g., growth rate and symbiont activity) - Seawater Sr/Ca overprint	*Beck et al.* [1992] *Hendy et al.* [2002]
U^{K}_{37} (Unsaturation index of Ketones with 37 carbons)	Unsaturation extent in C_{37} alkenones varies as a linear function of haptophyte growth temperature for achieving optimum density or enzymatic pathway	- Lateral advection - Seasonality of production - Non-thermal physiological effects	*Brassell et al.* [1986] *Prahl et al.* [1988] *Herbert* [2003]
TEX_{86} (TetraEther indeX with 86 carbons)	Ring moieties in glycerol dialkyl glycerol tetraether (GDGT) archaeal lipid vary as a linear function of growth temperature to regulate the fluidity of membrane	- Terrigenous overprint - Unknown depth origin - Uncertain source organism	*Schouten et al.* [2002] *Kim et al.* [2010]
LDI (Long chain Diol Index)	Fractional abundances of long chain diols vary as a function of temperature	- Unknown mechanism of temperature control - Unknown source organism - Relatively new, thus remains to be tested	*Versteegh et al.* [1997] *Rampen et al.* [2012] *Naafs et al.* [2012]

Abbreviations: IKM = Imbrie and Kipp method; MAT = Modern analog technique; GAM = Generalized additive model; RAM = Revised analog method; ANN = Artificial neural network; SIMMAX is an acronym for a modern analog technique using a similarity index

Over the years, advancement in analytical instrumentation and methods has enabled more accurate quantification of compounds / elements used in marine sediment-based SST proxies. This development has encouraged the paleoclimatic community to turn to geochemical proxies which are generally deemed more quantitative and less time-consuming. Among them, organic proxies i.e., U^{K}_{37} (**Section 1.2.2.1**) and TEX_{86} (**Section 1.2.2.2**), based on specific lipid biomarkers, are currently standard tools for inferring paleo SSTs (along with

Mg/Ca on foraminiferal calcite). The advantage of these lipid-based proxies is that they can be obtained simultaneously via routine organic geochemical methods, rendering multi-proxy comparison less labor-intensive. Furthermore, these lipids, especially the GDGTs, are ubiquitous in the global ocean spanning broad biogeographical provinces, enabling comparison of SST records derived from a single proxy covering a large latitudinal range. This is especially valuable in light of the discrepancies often observed in different SST proxies due to seasonality, depth habitat of source organisms and statistical methods / calibrations employed.

1.2.2.1. Alkenone-based paleothermometry

Alkenone paleothermometry [*Brassell et al.*, 1986; *Prahl and Wakeham*, 1987] is one of the most commonly used SST proxies nowadays and has been extensively studied in the past two decades (for detailed overview see **Appendix 5** and *Herbert* [2003]). It is based on long-chain alkenones with 37 carbon atoms (**Figure 1.3**), found in marine haptophyte algae such as coccolithophores of the family *Noelaerhabdaceae*, including the extant species *Emiliani huxleyi* and *Gephyrocapsa oceanica*. This SST proxy is based on the alkenone unsaturation extent, which varies as a function of growth temperature of the source organism. In the early days of alkenone paleothermometry, it was hypothesized that the alkenones are membrane-bound lipids [*Prahl et al.*, 1988], and that the dependency of lipid unsaturation on

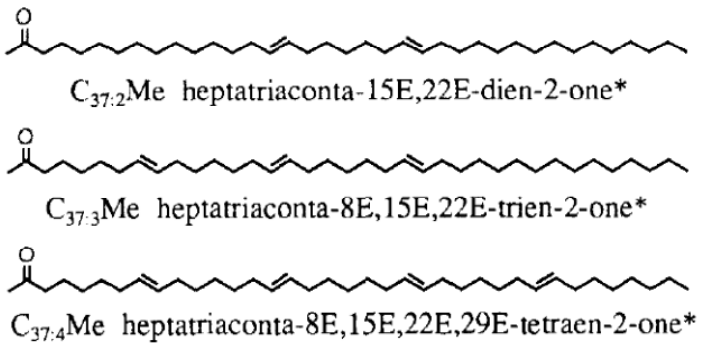

Figure 1.3: Molecular structure and standard IUPAC names of C_{37} alkenones with 2, 3, and 4 double bonds (Figure from *Marlowe et al.* [1990], following structure verification by *Rechka and Maxwell* [1988] and double-bond position identification by *de Leeuw* et al. [1980]).

temperature is for maintaining the membrane fluidity at low temperatures, a phenomenon known as homeoviscous adaptation [*Hazel*, 1988]. However, more recent studies suggested that alkenones are not membrane-bound [*Conte and Eglinton*, 1993; *Sawada and Shiraiwa*, 2004] and they probably serve as metabolic storage lipids [*Bell and Pond*, 1996; *Epstein et al.*, 2001]. The temperature dependence of alkenone unsaturation in the haptophyte is therefore not straightforward and could plausibly be attributed to differences in melting point, density or enzymatic optima of biochemical pathways of the alkenones [*Epstein et al.*, 2001].

In spite of our limited understanding on the biochemical role of the unsaturation in the alkenones, the empirical correlation between the unsaturation extent and temperature has resulted in numerous high-quality paleo SST records spanning various geological time-scales. *Brassell et al.* [1986] first proposed an index known as U^{K}_{37} (U = unsaturation, K = Ketone (alkenone), 37 = chain length of ketone) to quantify the unsaturation extent in alkenones:

$$U^{K}_{37} = \frac{C_{37:2} - C_{37:4}}{C_{37:2} + C_{37:3} + C_{37:4}}$$

As pointed out by *Bendle and Rosell-Melé* [2004], there is no apparent biogeochemical rationale for the form of the numerator in this index and it was derived by empirical trial-and-error (until an index that correlates best with temperature is obtained). Indeed, *Calvo et al.* [2002] speculated that the inclusion of $C_{37:4}$ in the numerator might lead to "overly" low index values, hence an overestimation of cooling. This index was later simplified as $U^{K'}_{37}$ by *Prahl and Wakeham* [1987] by removing the $C_{37:4}$ alkenones from the equation since the inclusion of this compound did not improve the unsaturation extent – temperature correlation in laboratory *E. huxleyi* cultures.

$$U^{K'}_{37} = \frac{C_{37:2}}{C_{37:2} + C_{37:3}}$$

Subsequent studies, mostly in the mid and low latitudes, found no $C_{37:4}$ alkenones in the marine sediments and suspended matters in sea water above SST of 15°C. As a result, most of the alkenone-related studies available in literature at present are based on the simplified $U^{K'}_{37}$ index.

The most commonly used calibration to convert the alkenone index values into SSTs is *Prahl et al.* [1988]'s culture-based $U^{K'}_{37}$ calibration. In this work, Prahl and co-workers grew *E. huxleyi* cultures (strain VAN55 isolated from North Pacific waters) at temperatures

between 8 and 25°C, and observed linear relationships between growth temperatures with U^{K}_{37} and $U^{K'}_{37}$ values (the latter showed a slightly better correlation). The $U^{K'}_{37}$ calibration has since been attested by two global core-top $U^{K'}_{37}$ calibrations, proposed by *Müller et al.* [1998] (n=370) and *Conte et al.* [2006] (n=592), respectively. All three of these calibrations are statistically similar.

1.2.2.2. Glycerol dialkyl glycerol tetraether (GDGT) –based paleothermometry

It was not until year 2002, 16 years after the introduction of alkenone paleothermometry, that another organic SST proxy came along. Schouten and co-workers [2002] found that the relative distribution of GDGTs (with different ring moieties; **Figure 1.4**) in 42 marine sediment samples varies as a function of SST. The authors speculated that the source organisms of these lipids, i.e., non-thermophilic Thaumarchaeota (formerly known as Marine Group 1 Crenarchaeota), increase the ring moieties in their membrane lipids at higher temperatures. Such modification of archaeal lipids as a response to temperature has been observed previously in hyperthermophilic Crenarchaeota [*De Rosa and Gambacorta*, 1988; *Gliozzi et al.*, 1983; *Uda et al.*, 2001]. The increased ring moieties were thought to provide a better packing of the membrane at higher temperatures [*Gliozzi et al.*, 2002]. As mentioned by *Schouten et al.* [2002], microbiologists [*De Rosa and Gambacorta*, 1988; *Gliozzi et al.*, 1983; *Uda et al.*, 2001] quantified the ring moiety – temperature relationship in extremophiles using the weighted average number of rings in GDGTs. However, the ring index values in marine sediments did not correlate well with overlying SSTs. After some trial-and-errors, *Schouten et al.* [2002] found that the best fit was obtained by an index termed TEX_{86} (TetraEther index of tetraethers consisting of 86 carbon atoms):

$$TEX_{86} = \frac{GDGT\text{-}2 + GDGT\text{-}3 + Cren'}{GDGT\text{-}1 + GDGT\text{-}2 + GDGT\text{-}3 + Cren'}$$

The two most abundant isomers, i.e., GDGT-0 and Crenarchaeol, were not included in the index because the occurrence of GDGT-0 is not exclusive to Thaumarchaeota – they were previously found in methanogenic archaea [*Schouten et al.*, 2000]. Secondly, the abundance of Crenarchaeol is one magnitude higher than GDGT-1, -2 and-3, thus it might overwhelm the correlation found between these latter compounds with temperature.

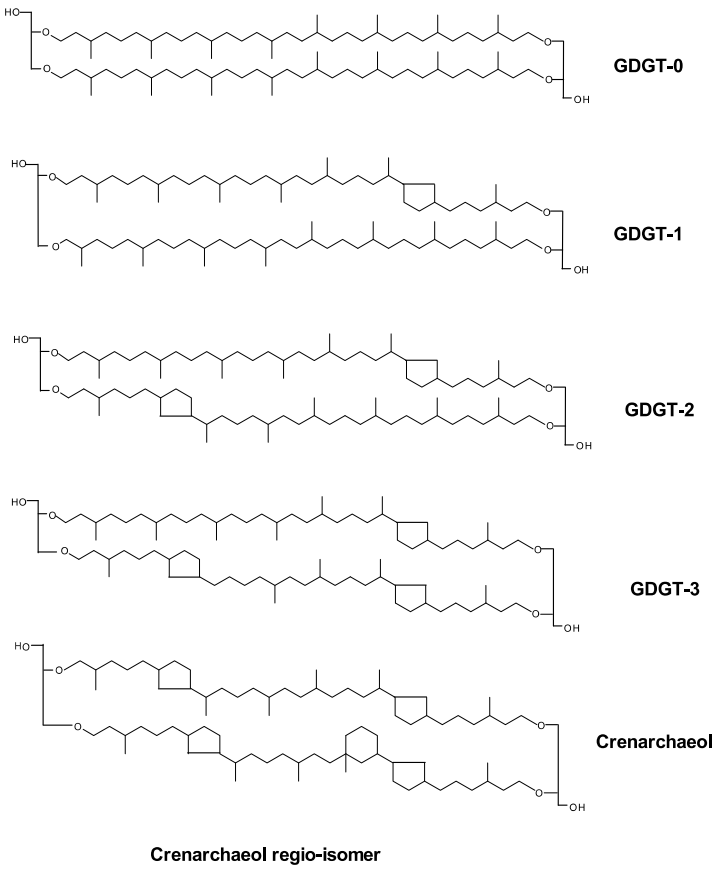

Figure1.4: Molecular structure of isoprenoid glycerol dialkyl glycerol tetraether (GDGT) lipids with different ring moieties (from *Ho et al*. [2011]).

Later studies [*Kim et al.*, 2010] with a much larger data set (n= 396) showed that a better correlation was found between SST and a modified GDGT-based index known as TEX_{86}^{L}:

$$TEX_{86}^{L} = \mathrm{Log}\left(\frac{GDGT\text{-}2}{GDGT\text{-}1 + GDGT\text{-}2 + GDGT\text{-}3}\right)$$

Notably, this index emerged as the best among all 1953 combinations consisting of the 6 archaeal isoprenoid GDGTs (**Figure 1.4**) assessed by Kim and co-workers. Nevertheless, as is the case with alkenone paleothermometry, these GDGT indices are empirical. While there is a biochemical reason for the temperature dependency of the ring moieties in GDGTs, the definition of the indices are derived based on the outcome of many trial-and-errors, performed with a priority in finding the one that fits best to SST.

Calibrations commonly used to convert the index values into SST estimates are based on marine sediment studies [*Kim et al.*, 2008; *Kim et al.*, 2010; *Schouten et al.*, 2002]. Marine

Thaumarchaeota have not yet been successfully cultured. Whilst a mesocosm study on North Sea waters by *Wuchter et al.* [2004] demonstrated a first-order relationship between TEX_{86} and growth temperature, the equation is different from that found in marine sediments, casting doubt on its applicability in paleo SST reconstruction. Interestingly, recent development in TEX_{86} paleothermometry has seen several cases in which the index, thereby also the calibration, was adapted for a specific study site in order to obtain "more reasonable" SST estimates (shortly described in **Table 1.2**). The global applicability of these indices is not granted as they have never been applied elsewhere except in the study they were proposed.

Table 1.2: Short description of several modified GDGT-based indices and calibrations that deviate from the commonly applied global core-top calibrations of *Schouten et al.* [2002], *Kim et al.* [2008] and *Kim et al.* [2010].

Index	Calibration	Studied area and timescale	Reference
$TEX_{86}' = \frac{GDGT-2 + GDGT-3 + Cren'}{GDGT-1 + GDGT-2 + Cren'}$	104 unspecified core-top data vs. atlas SST	Arctic; Paleocene – Eocene thermal maximum	*Sluijs et al.* [2006]
$\frac{1}{TEX_{86}} = \frac{GDGT-1}{GDGT-2 + GDGT-3 + Cren'} + 1$	*Kim et al.* [2008]'s TEX_{86} data vs. atlas SST data (n=287)	Global; Eocene-Oligocene climate transition	*Liu et al.* [2009]
TEX_{86} (see text above, proposed by *Schouten et al.*, [2002])	*Kim et al.* [2008]'s core-top TEX_{86} data (n=287) vs. atlas SST; combined with 7 AP core-top TEX_{86} vs. measured SST	Antarctic Peninsula (AP), Holocene	*Shevenell et al.* [2011]

1.3. Subantarctic Southeast Pacific SST: present and past

To get a grasp on how the climate system operates, one first needs to understand its components, including the ocean (**Section 1.1**). Oceanographic studies could be divided into two domains, i.e., modern oceanography and paleoceanography. Historical SST data (e.g., from merchant ship-based measurements) are heavily concentrated in the North Atlantic, western South Atlantic and northern Indian oceans [*Deser et al.*, 2010]. The Southern Ocean, on the other hand, is poorly sampled due to a scarcity of trading ports in the Southern hemisphere, expensive logistics, and its uninviting rough seas. The same could be said about the paleo domain – progress in Southern Ocean research, especially in the Pacific sector, is hampered by a dearth of data. This situation partly arises from logistical difficulty since most well-funded oceanographic institutions are located in the Northern hemisphere on both sides of the North Atlantic. Another contributing factor is the "obsession" with the North Atlantic

since the early days of paleoceanography. As dramatically put by *Huybers and Wunsch* [2010], "*Like the Genesis story, the idea that the North Atlantic Ocean meridional overturning circulation is the major controller of the climate system has taken on an almost mythic status*". Nevertheless, recent studies suggest that the upwelling of intermediate and deep waters in the Southern Ocean is one of the main components of the global overturning circulation, and it influences the exchange of heat and carbon between the deep and the surface ocean and the atmosphere [*Marshall and Speer*, 2012] Therefore, not unlike the North Atlantic (one of the locations in the global ocean where deep waters are formed), the Southern Ocean too plays an important role in global climate [see review by *Fischer et al.*, 2010], via its linkages with the intense wind field [*Toggweiler and Russell*, 2008] and its seasonally varied sea-ice cover [*Stephens and Keeling*, 2000]. Incidentally, SST is a key element in these physical processes, as it either steers them, or it is modified by them.

The geographic pattern of SST is strongly linked to, and controlled by, atmospheric and oceanic processes. Among the latter, physical processes such as heat transport by currents and vertical mixing play a major role. The single most important surface current in the Southern Ocean is the formidable Antarctic Circumpolar Current (ACC) that flows unimpeded around Antarctica, connecting the Atlantic, the Pacific and the Indian Oceans. It is also the largest current in the world, transporting around 110 Sv of water [*Cunningham et al.*, 2003], and its latitudinal position and intensity have implications for the global ocean and climate. In the east Pacific sector of the Southern Ocean, a very vigorous eastern boundary current i.e., the Peru-Chile Current (PCC; also known as the Humboldt Current and the Peru Current) is formed as a result of the bifurcation of the ACC as it approaches the South American continent (**Figure 3.1**). The PCC brings cold and nutrient-rich subantarctic water equatorward, feeding the east Pacific equatorial cold tongue. This current is therefore a heat conduit and forms the link between high and low latitudes in this sector of the Southern Ocean. Furthermore, it provides nutrients that sustain the high productivity in the upwelling regions off northern Chile and Peru, without which the profitable fishery industry here, one of the largest on the planet [*Chavez and Messié*, 2009], would perish. More detailed description of these surface currents is available in **Chapter 3**.

In spite of the remarkable difficulties in logistic and in finding suitable and datable sediments, several studies have been conducted in the Pacific sector of the subantarctic Southern Ocean to examine past SST changes (see **Figure 1.5**). These studies made use of various paleo SST proxies described in section **1.2.2** and **Table 1.1**. An emerging picture

from these studies is that different proxies suggest dissimilar extents of glacial cooling in this region, plausibly due to differences in production seasonality and habitat depth of the source

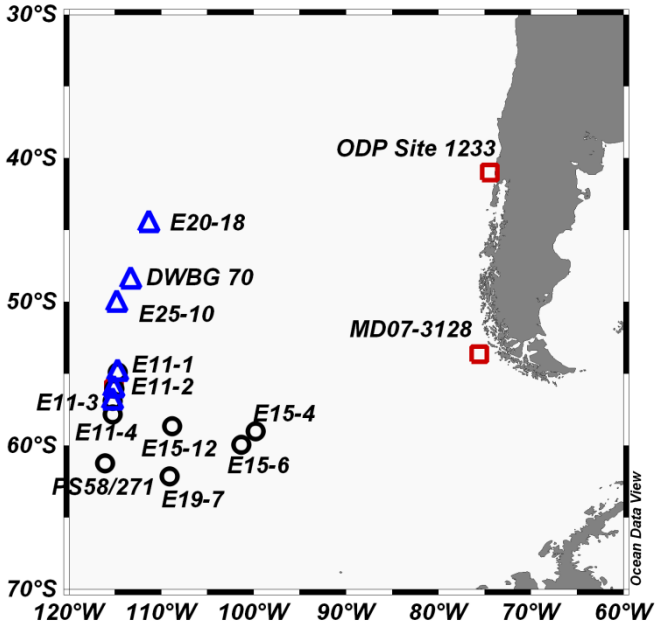

Figure 1.5: Literature review of paleo sea surface temperature reconstruction in the subantarctic South Pacific south of 40°S. Red squares denote continuous downcore reconstructions; blue triangles denote the Last Glacial Maximum (LGM) time-slice study of *Luz* [1977]; black circles denote LGM time-slice study of *Gersonde et al.* [2005]. For more details see **Table 1.3**.

Table 1.3: Details of previous paleo sea surface temperature studies in the subantarctic Southeast Pacific (south of 40°S).

Site	Time scale	Type of Proxy	Glacial-interglacial amplitude	Reference
ODP 1233	70 kyr	Alkenone ($U^{K'}_{37}$)	~7°C	*Lamy et al.* [2004]; *Kaiser et al.* [2005]
	27 kyr	Coccolithophorid TF	~5°C	*Saavedra-Pellitero et al.* [2011]
MD07-3128	60 kyr	Alkenone ($U^{K'}_{37}$)	~8°C	*Caniupán et al.* [2011]
E11-1	LGM (time-slice)	Foraminiferal TF	2.3°C	*Luz* [1977]
	LGM (time-slice)	Diatom TF	0.7°C	*Gersonde et al.* [2005]
E11-2	110 kyr	Mg/Ca on *N. pachyderma (s)*	~3°C	*Mashiotta et al.* [1999]
	LGM (time-slice)	Foraminiferal TF	2.5°C	*Luz* [1977]
	LGM (time-slice)	Diatom TF	0 °C	*Gersonde et al.* [2005]
E11-3	LGM (time-slice)	Foraminiferal TF	1.5°C	*Luz* [1977]
	LGM (time-slice)	Diatom TF	1.6°C	*Gersonde et al.* [2005]
E11-4	LGM (time-slice)	Diatom TF	0.3°C	*Gersonde et al.* [2005]
E15-4	LGM (time-slice)	Diatom TF	0.7°C	*Gersonde et al.* [2005]
E15-6	LGM (time-slice)	Diatom TF	0.2°C (LGM warmer than present)	*Gersonde et al.* [2005]
E15-12	LGM (time-slice)	Diatom TF	0.9°C	*Gersonde et al.* [2005]
E19-7	LGM (time-slice)	Diatom TF	1.4°C	*Gersonde et al.* [2005]
E20-18	LGM (time-slice)	Foraminiferal TF	0.2°C (LGM warmer than present)	*Luz* [1977]
E25-10	LGM (time-slice)	Foraminiferal TF	4.9°C	*Luz* [1977]
PS58/271-1	LGM (time-slice)	Diatom TF	1.3°C	*Gersonde et al.* [2005]
DWBG 70	LGM (time-slice)	Foraminiferal TF	3.4°C	*Luz* [1977]

Abbreviations: LGM = Last Glacial Maximum; TF = transfer function

organisms. SST estimates based on diatom assemblages (max. 1.5°C; *Gersonde et al.* [2005]) and Mg/Ca on planktonic foraminifera *N. pachyderma* (~3°C; *Mashiotta et al.* [1999]) suggested less severe glacial cooling, as opposed to stronger cooling indicated by alkenone unsaturation ($U^{K'}_{37}$) (~7°C; *Caniupán et al.* [2011]; *Kaiser et al.* [2005]; *Lamy et al.* [2004]), coccolithophorid assemblages (6°C; *Saavedra-Pellitero et al.* [2011]), and foraminiferal assemblages (max. 5°C; *Luz* [1977]). Since these studies linked the SST changes to the latitudinal migrations of key climatic elements in the Southern Ocean - the ACC and its associated oceanic frontal systems, the southern hemisphere Westerlies and the sea-ice extent – dissimilar glacial cooling leads to diverging view on the latitudinal positions of these climatic features.

1.4. Outstanding research issues

1.4.1. Occurrence of alkenones and GDGTs in the South Pacific

To date there is no report on the occurrence of alkenones and GDGTs in surface sediments between the shallow waters off New Zealand [*Sikes et al.*, 1997] and the continental shelves off Chile [*Kim et al.*, 2002], casting some uncertainties on the potential of these biomarkers for paleo SST reconstruction work in this region.

1.4.2. Is TEX_{86} paleothermometry applicable in (sub)polar regions?

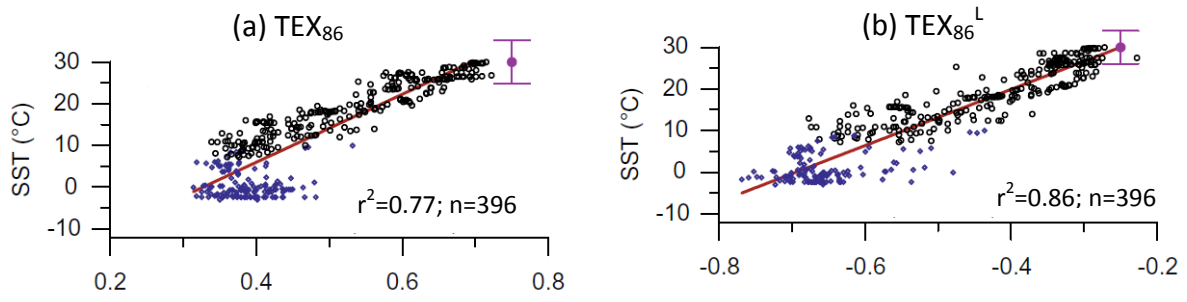

Figure 1.6: Crossplots of GDGT-based indices (a) TEX_{86} and (b) TEX_{86}^{L} with satellite SSTs from *Kim et al.* [2010]. Blue symbols represent subpolar and polar samples from the Arctic, the Barents Sea, off Svalbard, the Southern Ocean, and off Antarctica (see **Figure 2.1** for location). Purple whisker bars denote residual standard error (±1σ).

The applicability of TEX_{86} in the subpolar and polar regions has not been rigorously tested, especially in the context of late Pleistocene glacial-interglacial SST shifts. A recent

reconstruction by *Shevenell et al.* [2011] on Holocene SST changes off Antarctic Peninsula demonstrated that although the TEX_{86} index did show climatic shift that were qualitatively consistent with other proxy data, both the latest global core-top calibrations of TEX_{86} and TEX_{86}^{L} of *Kim et al.* [2010] resulted in unrealistic SST estimates. As mentioned by *Kim et al.* [2010], the crossplots of both indices versus SST (**Figure 1.6**) show large scatter at the low temperature end, where the indices seem to be invariant with temperature. The fact that the scatter at low temperature in the TEX_{86}^{L}-SST correlation is as large as, if not larger, than that in the TEX_{86}-SST relationship, casts doubts on the justification of the TEX_{86}^{L} as the better index at low temperature range (recommended by *Kim et al.* [2010]). The marginally improved r^2 value in the TEX_{86}^{L}-SST relationship is probably a statistical artifact due to the amplified variance of TEX_{86}^{L} at the low temperature end. Furthermore, since most of the data forming the scatter are retrieved from continental shelves prone to terrestrial GDGT input, it is not clear whether the scatter is due to the physiological limit of archaeal response to temperature, or other underlying cause (e.g., terrigenous overprint).

In addition, there are very few data from the Southern Ocean and the Pacific (see **Chapter 2**; **Figure 2.1**), so the TEX_{86}-SST relationship in these regions is currently not well constrained. Although a study by *Ho et al.* [2011] suggested that there is no apparent regional bias in the South Pacific (see **Appendix 5**), the study is based on only 20 data points. More data are necessary to appraise the applicability of TEX_{86} paleothermometry in this region.

A further complicating factor is represented by the two modified versions of TEX_{86}, namely the TEX_{86}^{L} and TEX_{86}^{H} for application at sites <15°C proposed by *Kim et al.* [2010]. Applying different indices at opposite temperature ends adds more uncertainty in comparing SST records from high and low latitudes (which are not directly comparable since they are based on different indices and calibrations). Therefore, work is needed in order to establish a universal calibration which is applicable throughout the entire temperature range.

1.4.3. Which alkenone index is more suitable for paleo SST reconstruction in the South Pacific?

The few marine sediment and water column studies in the high latitudes show contradictory findings on the applicability of U^{K}_{37} and $U^{K'}_{37}$. The U^{K}_{37} index appears to be a better SST proxy in the Nordic Sea [*Bendle and Rosell-Melé*, 2004] while the $U^{K'}_{37}$ seems to

be a better choice in the Southern Ocean [*Sikes et al.*, 1997]. Multi-proxy downcore SST reconstructions in the North Atlantic by *Bard* [2001] showed that the U^{K}_{37}, instead of the simplified $U^{K'}_{37}$, resulted in SST estimates that are more comparable with other proxy data. This is somehow to be expected, considering the working principle of alkenone paleothermometry, which dictates that the unsaturation extent in alkenones increases with decreasing temperature. The abundance of the more unsaturated alkenones (i.e., $C_{37:4}$) becomes numerically important at low temperatures, hence the exclusion of this compound from the SST index might undermine its predictive power (as is the case in the simplified $U^{K'}_{37}$).

Notwithstanding, *Sikes et al.* [1997] found better correlation in the $U^{K'}_{37}$-SST relationship in the Southern Ocean. Notably, the U^{K}_{37} values in the Southern Ocean surface sediment reported by *Sikes et al.* [1997] are systematically lower than those observed in the *E. huxleyi* culture of *Prahl et al.* [1988] (The $U^{K'}_{37}$-SST relationship in the latter study has been attested by two global core-top calibration studies and is the most commonly employed calibration). The discrepancy between these two data sets is due to the higher relative abundance of $C_{37:4}$ alkenones in the Southern Ocean surface sediment, which amounted to ~15% at 15°C and even as high as 38% at 9°C, while the cultured *E. huxleyi* started producing this compound at relatively low abundance at 10°C (absolute concentration data not reported). Therefore, it is still debatable which alkenone index is more suitable for paleo SST reconstruction in the Southern Ocean.

1.4.4. How has the Southeast Pacific SST evolved during the Pleistocene?

In spite of climatically important oceanic features in the east Pacific sector of the Southern Ocean such as the ACC and the PCC, studies are scarce in this region (see **Chapter 3**). In the past 50 years, there have been fewer than a dozen studies on paleo SST here using marine sediment-based proxies (see **Section 1.3**). These SST records also do not go very far back in time, with the longest record [*Kaiser et al.*, 2005] spanning merely 70 kyr. Therefore, the late Pleistocene SST evolution prior to MIS 4 here is virtually unknown, a fact that has important implications, as we lack information on the warmer-than-present MIS 5 and MIS 11, and on the Mid-Brunhes Event (MBE), a climatic reorganization of the glacial-interglacial cycles which is well-expressed in the ice core records from Antarctica and is thought to play a

key role in the global carbon cycle. The data scarcity also impedes circumpolar comparison of climatic evolution in the Southern Ocean and Antarctica.

1.4.5. How do the TEX_{86}-derived SSTs compare to the U^{K}_{37}-derived SSTs during the Pleistocene?

As the MARGO community [*Kucera et al.*, 2005] concluded, no single proxy is "right" and "right everywhere", highlighting the importance of a multi-proxy approach to better constrain SST reconstruction. Within the context of organic SST proxies, multi-proxy studies comparing alkenone- and GDGT-derived SST estimates are still not widespread but are on the rise, including studies from *Castañeda et al.* [2010]; *Huguet et al.* [2006b], , *Huguet et al.* [2011], , *Lopes dos Santos et al.* [2010] and *McClymont et al.* [2012]. Most of these studies are based on sediment records from shallow continental margins with high sedimentation rates. The emerging picture from these studies is a complex one, with some studies suggesting diverging SST evolutions [*Huguet et al.*, 2006b; *Lopes dos Santos et al.*, 2010], while other studies do not support this scenario [*Castañeda et al.*, 2010; *Huguet et al.*, 2011; *McClymont et al.*, 2012]. In light of the recent finding that sedimentation settings (coastal vs. offshore) result in contrasting biases in TEX_{86}-derived SSTs [*Leider et al.*, 2010], a study based on material from an open ocean setting with moderate to low sedimentation rate would further add to our understanding of these organic SST proxies.

1.5. Material and methods

Marine sediments are the climatic archive used in this thesis to address the issues discussed above (**Section 1.4**). These sediment samples were analyzed using organic geochemical methods outlined in the following sub-sections.

1.5.1. Marine sediments

Various chemical (e.g., degradation and remineralization) and physical (e.g., advection) processes occurring in the water column during the sinking of biomarkers from the sea surface to the sediment might alter the empirical relationship between biomarkers and environmental parameters, resulting in dissimilar calibrations in the suspended organic matter

and in the sediment [e.g., *Conte et al.*, 2006]. Hence, temporally and spatially averaged surface sediments are appropriate for assessing the applicability of a proxy in downcore reconstruction, as the sediments have undergone similar processes in the water column before being incorporated into the sediments. In this thesis, an extensive set of surface sediments were analyzed (**Figure 1.7**). These sediments are the upper most 0-1 cm of multicores, retrieved during various cruises in under-sampled regions such as the North Pacific, the Arctic and the Southern Ocean (see **Section 2.6**). The core sites are strategically located to fill the geographical voids in the global core-top calibration data sets (see **Figure 2.1**).

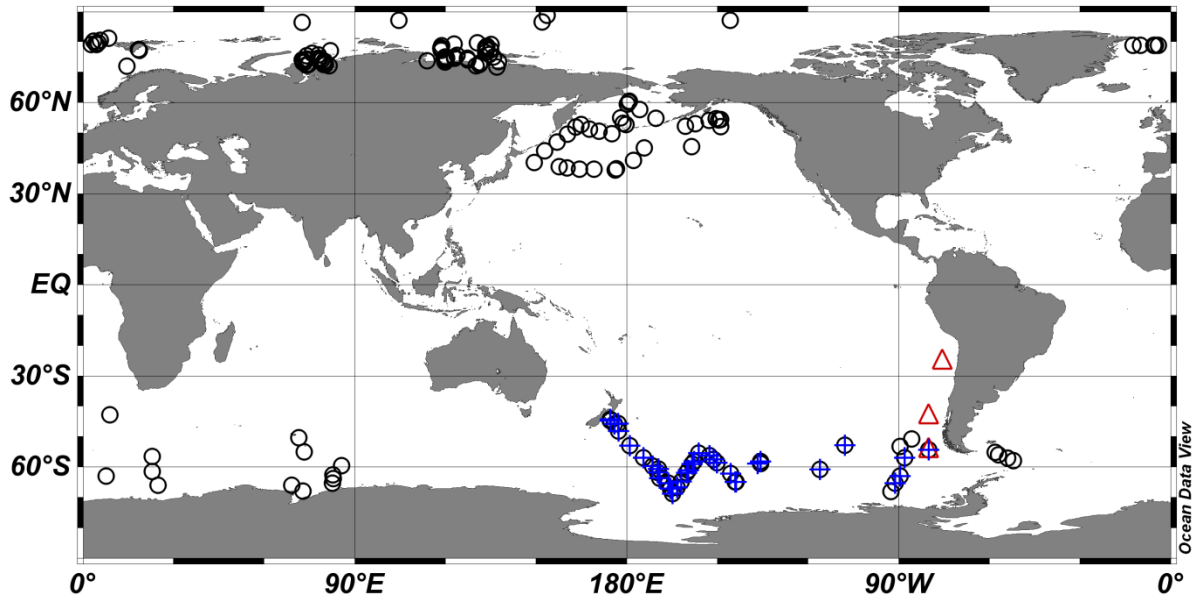

Figure 1.7: Location of marine sediments used in this study. Red triangles denote long piston cores for downcore reconstruction (**Chapter 3** and **4**); black circles denote surface sediments used for TEX_{86} calibration (**Chapter 2**); blue crosses denote surface sediments used for U^{K}_{37} calibration (**Chapter 3**).

To examine the evolution of SST in the Southeast Pacific at different latitudes on orbital time scale, we analyzed three marine sediment cores obtained via piston coring along the latitudinal range of the Peru-Chile Current (see **Section 3.3.1**). These sediments span at least 500 kyr, and the oldest core extends back to 700 kyr, according to the stratigraphic framework established via graphic alignment of benthic foraminiferal $\delta^{18}O$ to the global stack LR04 [*Lisiecki and Raymo*, 2005], or visual tuning of the SST record to the air temperature record in the EPICA ice core at Dome C, Antarctica (see **Section 3.4.1**).

1.5.2. Sample preparation

Standard organic geochemical techniques were employed in this work. All sediment samples were freeze-dried and homogenized before being subjected to extraction using organic solvents. Freeze-drying is preferred for sediments used for alkenone analysis because air-drying (commonly used for samples prior to microfossil analysis) might lead to significant loss of alkenones and potentially bias the temperature estimation [*McClymont et al.*, 2007]. Several extraction methods were applied in this work, such as the Accelerated Solvent Extractor (DIONEX 200), ultrasonication, and microwave-assisted extraction (see **Section 2.2.1**). It is conceivable that different extraction techniques might lead to dissimilar recovery rates of extractable compounds which could affect the absolute compound concentration per sediment weight. However, this is not a concern for this thesis since the focus is not on comparing the concentration of biomarkers at various study sites. Furthermore there is no evidence of extraction method-induced bias in index values.

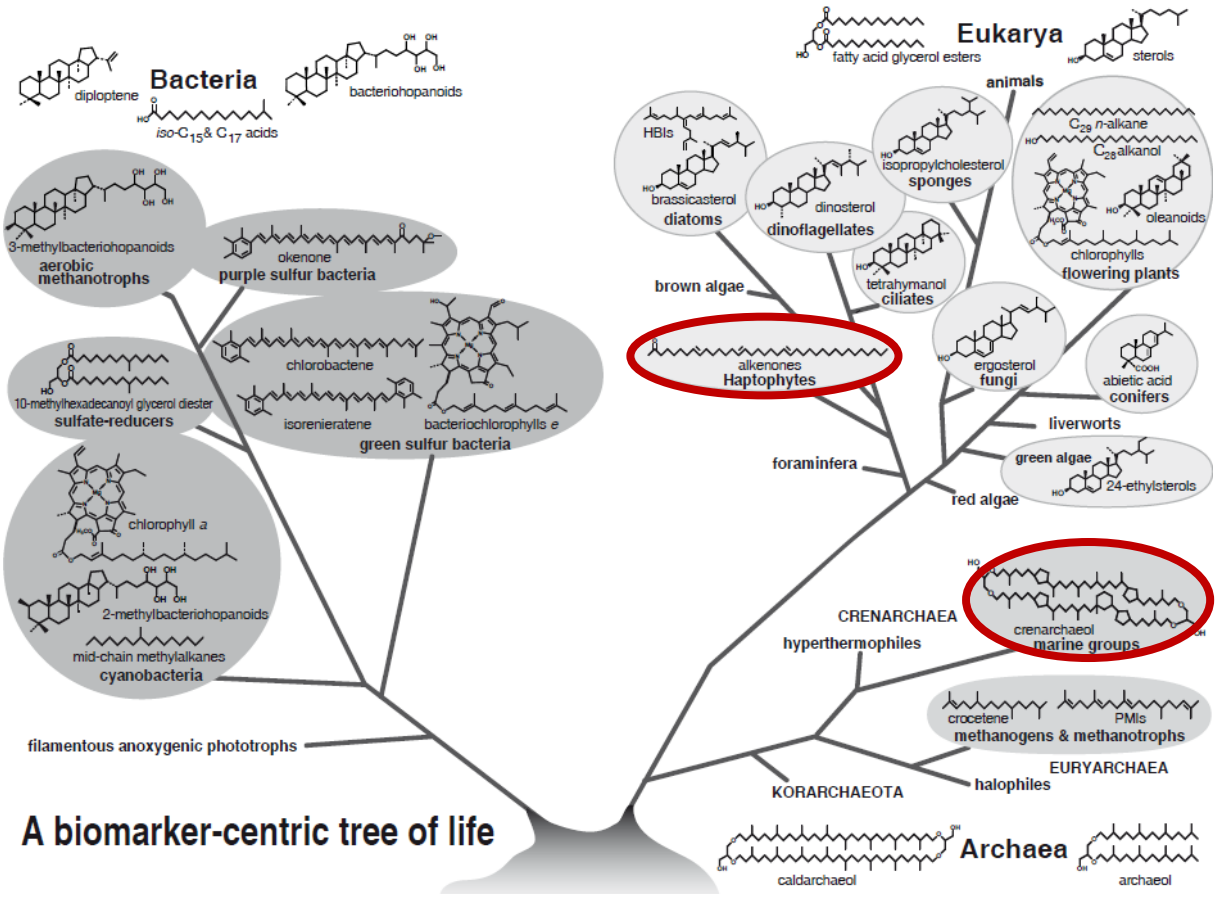

Figure 1.8: Types of biomarkers and their precursors in the three domains of life. Red circles denote biomarkers used in this study for paleo SST reconstruction. (Figure courtesy of Florian Rommerkirschen; in *Gaines et al.* [2008]).

The total lipid extract is composed of a large suite of biomarkers derived from organisms spanning archaea, bacteria and eucarya (i.e., the three domains of life), as illustrated in **Figure 1.8**. To have purer samples for a better quantification, the total lipid extracts were partitioned into different fractions by means of silica gel chromatography or via a high performance liquid chromatography system equipped with a silicon dioxide column (details in **Section 2.2.1** and **3.3.3**).

Organic compounds move through silica or alumina columns at different rates depending on the type of column (stationary phase) and solvents (mobile phase) used, as illustrated in **Figure 1.9**. There is higher affinity between silica / alumina and polar compounds, hence the less polar alkenones elute through the columns before the more polar GDGTs.

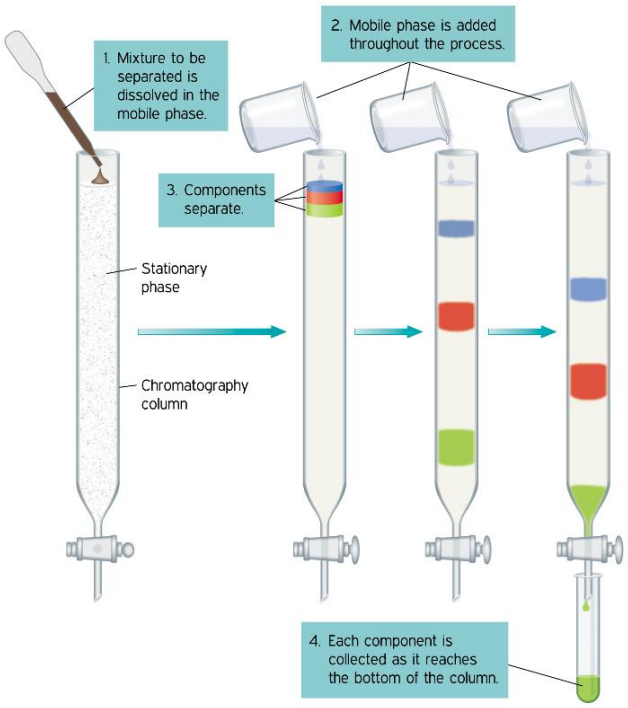

Figure 1.9: Schematic of silica or alumina column chromatography to separate a mixture of organic compounds into different fractions prior to analysis. (Figure from explow.com/chromatography)

1.5.3. Alkenone analysis

After the separation of total lipid extracts, the fraction containing alkenones was saponified using weak potassium hydroxide (KOH) in methanol to remove ester-bound

compounds such as alkenoates which might co-elute with alkenones in gas chromatography. In general, saponification is not a standard protocol of alkenone analysis, especially for pelagic sediments which are usually depleted in organic matter. However, it was essential for the sediment core-tops examined here as co-elution of an unknown compound with the $C_{37:4}$ alkenones occurred in many samples from sites with overlaying SST < 10°C, resulting in similar $U^{K'}_{37}$ values but different U^{K}_{37} values (**Figure 1.10**). The co-elution artificially increased the $\%C_{37:4}$ and lowered the U^{K}_{37}-derived temperature estimates. Notably, this unknown compound was not found in deeper sediments in piston core PS75/034-2, suggesting that it is probably not as refractory as the alkenones and was degraded in the upper few centimeters. Saponification of six samples with $\%C_{37:4}$ of 10% to 20% did not result in different temperature estimates and $\%C_{37:4}$ values, as they were comparable to those obtained from untreated samples. Therefore, the alkenone samples for core PS75/034-2 were not saponified prior to analysis.

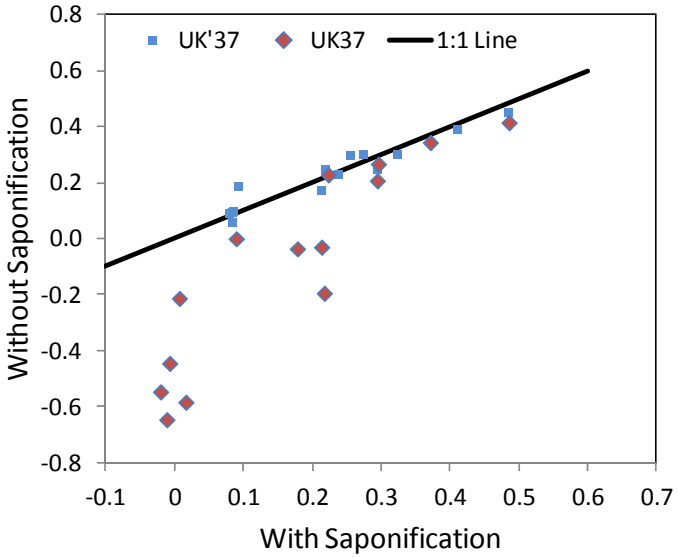

Figure 1.10: South Pacific core-top alkenone index values with and without saponification.

Alkenones were analyzed using gas chromatography (GC) equipped with a flame ionization detector. In a GC system, injected samples are vaporized and pushed through the column by a carrier gas (mobile phase). The separation of different compounds is achieved via differences in boiling point, molecular size and affinity for the mobile phase. The identification of alkenones was done by comparing the sample chromatogram to that of a reference standard extracted from an *Emiliania huxleyi* culture (similar compounds should

have similar retention times). The instrumental precision for alkenones analysis is estimated to be ~0.2 °C based on replicate measurements.

1.5.4. GDGT analysis

Unlike for alkenones, gas chromatography is not adequate for analyzing the relatively high-molecular-weight GDGTs. Instead, a high performance liquid chromatography (HPLC) was used. In this work, GDGT analysis was carried out using HPLC systems coupled to a mass spectrometer, operating with an atmospheric pressure chemical ionization (APCI) interface (see **Section 2.2.2** for details). The TEX_{86} values obtained using these systems were not compared directly, but significant bias is unlikely since an interlaboratory comparison study suggests that different HPLC systems result in comparable TEX_{86} values [*Schouten et al.*, 2007]. Samples were passed through polytetrafluoroethylene (PTFE) filters prior to injection to prevent clogging in the column. The detection of the GDGTs was achieved by Selected ion Monitoring (SIM) of the [M+H]+ ions in the m/z ranges described by *Hopmans et al.* [2000].

1.5.5. Choice of environmental data for calibration

To calibrate alkenone- and GDGT-based proxies, the indices were plotted against various environmental data sets retrieved from the World Ocean Atlas 2009 [*Locarnini et al.*, 2010]. These include the annual mean and seasonal SSTs, in addition to temperature data at different water depths. As mentioned in **Section 1.2.1**, several reanalyzed and climatological SST products are available for research purposes. The WOA09 data sets were employed in this work, in consistency with most calibration studies in the past which opted for earlier versions of WOA data sets [e.g., *Kim et al.*, 2008; *Müller et al.*, 1998; *Sikes et al.*, 1997]. However, *Kim et al.* [2010] used the NSIPP AVHRR Pathfinder and Erosion Global 9 km climatology data [*Casey and Cornillon*, 1999] in their most recent global core-top TEX_{86} study. This data set is not significantly different from the WOA09 data set, rendering calibrations based on these data sets comparable. The deviations between these data sets occur at the low temperature end (**Figure 1.11**), where the Pathfinder SST values are colder than those from the WOA09, and can get as low as -2.4°C. Such low SST values are probably

errors related to the processing of satellite data, given the theoretical coldest seawater temperature is -1.8°C.

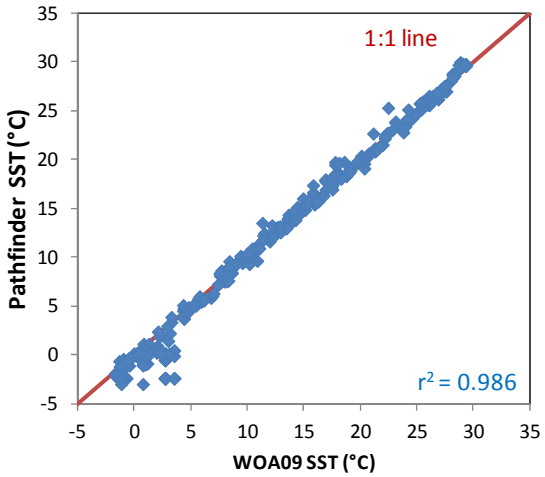

Figure 1.11: Correlation between the climatology SST data sets from the NSIPP AVHRR Pathfinder and Erosion Global 9km [*Casey and Cornillon*, 1999] and the World Ocean Atlas 2009 [*Locarnini et al.*, 2010].

1.6. Thesis outline

The outstanding research issues outlined in **Section 1.4** are addressed in **Chapter 2** to **4** of this thesis, presented in the form of three manuscripts submitted or to be submitted to international peer-reviewed journals. Two additional manuscripts produced during the course of this PhD study, i.e. a review paper on alkenone paleothermometry and a Pacific TEX_{86} core-top calibration paper based on the data generated during MSc. study, are included in **Appendix 5**.

Chapter 2 presents 160 new (sub)polar core-top TEX_{86} and TEX_{86}^{L} data that greatly enhance the spatial coverage and the temperature range of the previous global core-top calibration of *Kim et al.* [2010]. In this chapter, the implications of new data addition for the global core-top calibrations are appraised. The suitability of TEX_{86} and TEX_{86}^{L} as SST proxy in subpolar and polar regions are further evaluated based on temperature residuals. The extensive compilation (~600 data) comprising data presented here and published data is rigorously assessed for any potential bias between the high- and low latitudes, and between different sedimentation settings.

Chapter 3 contributes to the spatial mapping of alkenones in surface sediment in the South Pacific, which is of great importance for the planning of future paleoceanographic

studies in this region. The assessment of the suitability of alkenone indices as SST proxy in the Southeast Pacific is carried out with a two-pronged approach, i.e., by examining the correlation of core-top alkenone index values with modern SST; and by comparing the alkenone indices-derived SST records with other proxy records. After establishing the more appropriate alkenone index for paleo SST estimation, the SST records are used to infer the latitudinal migration of the oceanic frontal systems during the late Pleistocene, with an emphasis on the glacial-interglacial amplitude and notable climatic events such as the MBE.

Chapter 4 presents a comparison of alkenone- and GDGT-based Pleistocene SST records in the Southeast Pacific. Several scenarios related to climatic events and proxies are suggested to reconcile the differences in the absolute values and the temporal trends of these SST records.

Chapter 5 summarizes the findings discussed in abovementioned chapters. In light of these findings, perspectives for future work to further improve the proxies and their application are proposed.

Chapter 2: Appraisal of the TEX_{86} and TEX_{86}^{L} thermometries in the subpolar and polar regions: implications for global core-top calibrations

Sze Ling Ho [a]*, Gesine Mollenhauer [a], Susanne Fietz [b], Alfredo Martínez-Garcia [b,1], Frank Lamy [a], Gemma Rueda [b], Konstanze Schipper [a,c], Marie Méheust [a], Antoni Rosell-Melé [b,d], Rüdiger Stein [a], Ralf Tiedemann [a]

[a] Alfred Wegener Institute for Polar and Marine Research, P.O.Box 12 01 61, 27515 Bremerhaven, Germany.
[b] Institut de Ciència i Tecnologia Ambientals, Universitat Autònoma de Barcelona, 08193 Bellatera, Spain.
[c] Department of Geosciences, University of Bremen, 28334 Bremen, Germany.
[d] Also at Institució Catalana de Recerca i Estudis Avançats, Barcelona, Catalonia, Spain.
[1] Presently at Geological Institute, Swiss Federal Institute of Technology Zürich, NO G 55, Sonneggstrasse 5, CH-8092 Zürich, Switzerland.

(Under review with Geochimica et Cosmochimica Acta)

2.0. Abstract

TEX_{86} (TetraEther indeX of tetraethers consisting of 86 carbon atoms) paleothermometry is an organic sea surface temperature (SST) proxy based on the archaeal isoprenoid glycerol dialkyl glycerol tetraethers (GDGTs). In this study, we improved the spatial coverage of the global core-top TEX_{86} calibration by contributing additional core-top data from the subpolar and polar regions, and appraised the applicability of the TEX_{86} and a modified version, i.e., TEX_{86}^{L}, in these regions. The SST estimates derived from both TEX_{86} and TEX_{86}^{L} are anomalously warm in the Arctic especially in the vicinity of the sea ice margin, calling for caution in interpreting paleo TEX_{86}/TEX_{86}^{L} reconstruction in this region. Judging from the temperature residuals, the TEX_{86} calibration resulted in better SST estimates in subpolar and polar regions, especially the Southern Ocean and the North Pacific, where the TEX_{86}^{L}-inferred SSTs are considerably warmer than summer SSTs, in spite of the fact that the TEX_{86}^{L} is recommended for application at sites with SST < 15°C. Linear regressions through our compiled global data set (excluding the Arctic data) resulted in TEX_{86} (n = 482) and TEX_{86}^{L} (n = 480) calibrations with r^2 values of 0.8 and 0.73 respectively, further confirm the robust relationship between both GDGT-based indices and SST for a broader geographical coverage. Between these indices, TEX_{86} appears to be a more suitable SST proxy for the

application in subpolar and polar regions, judging from better correlation in TEX_{86}-SST calibration and smaller TEX_{86}-derived temperature estimates residuals in these regions.

2.1. Introduction

TEX_{86} (TetraEther indeX of tetraethers consisting of 86 carbon atoms) paleothermometry is an organic sea surface temperature (SST) proxy based on the relative distribution of isoprenoid glycerol dialkyl glycerol tetraethers (GDGTs) in archaeal lipids [*Schouten et al.*, 2002]. These lipids appear to be mostly biosynthesized by Thaumarchaeota (previously known as Group I.1a Crenarchaeota) [*Brochier-Armanet et al.*, 2008] that are omnipresent in the global ocean. The number of cyclopentane moieties of these archaeal GDGT lipids in marine sediments was found to demonstrate an empirical linear relationship with the annual mean temperature of the overlaying sea surface water [*Schouten et al.*, 2002], suggesting its potential as a proxy for paleo-environmental conditions. Later on, a mesocosm study confirmed that indeed the relative distribution of the GDGTs in seawater varied as a function of the growth temperature of the source organism [*Wuchter et al.*, 2005].

Since then, many more studies have been carried out to scrutinize the potential of TEX_{86}, revealing that the ring numbers in the GDGTs seem to be responsive solely to the growth temperature, and are not influenced by salinity and nutrient availability [*Wuchter et al.*, 2004], sediment maturity [*Schouten et al.*, 2004], or grazing [*Huguet et al.*, 2006a]. It was also found that the isoprenoid GDGTs are less susceptible to long distance lateral transport relative to alkenones used for the more established organic SST proxy [*Mollenhauer et al.*, 2008; *Mollenhauer et al.*, 2007; *Shah et al.*, 2008]. In addition, the fact that the GDGTs are found at all latitudes of the global ocean, including the polar regions that are often devoid of alkenones, and hence preclude the application of the well established organic SST proxy $U^{K'}_{37}$ [*Kim et al.*, 2010], suggest a potential advantage of the TEX_{86} paleothermometer in this region.

However, there are some uncertainties and caveats associated with the GDGT-based proxy. For instance, the GDGTs have been found throughout the water column and in the sediments [*Lipp and Hinrichs*, 2009], sometimes even more abundant at subsurface than surface waters [*Huguet et al.*, 2007; *Sinninghe Damsté et al.*, 2002a; *Wuchter et al.*, 2005] and may reflect subsurface water temperature in some settings [*Huguet et al.*, 2007; *Lee et al.*,

2008]. Moreover, a lack of understanding on the ecology, metabolic pathways and energy sources of the Thaumarchaeota, and the processes that control the sedimentary deposition of GDGTs, makes it difficult to constrain the water depth where the sedimentary GDGTs might have originated, thus complicating the interpretation of TEX_{86} values as SST estimates.

Initially, TEX_{86} has been defined by *Schouten et al.* [2002] based on a global core-top study (n = 44) as:

$$TEX_{86} = \frac{[GDGT-2]+[GDGT-3]+[Cren']}{[GDGT-1]+[GDGT-2]+[GDGT-3]+[Cren']}$$

where GDGT-1, GDGT-2, GDGT-3 denote GDGTs containing 1, 2 and 3 cyclopentane moieties respectively; and Cren' the crenarchaeol regioisomer. Recently, based on the comparison of the correlation of all the possible combinations of GDGTs with SST, performed on a more extensive core-top data set (n = 396), a modified version of TEX_{86}, known as TEX_{86}^{L}, was proposed [*Kim et al.*, 2010]:

$$TEX_{86}^{L} = \log\left(\frac{[GDGT-2]}{[GDGT-1]+[GDGT-2]+[GDGT-3]}\right)$$

The differences between these two indices are twofold. Firstly, the TEX_{86}^{L} does not include the crenarchaeol regioisomer, which could be difficult to quantify especially in subpolar regions where its abundance is usually low, rendering possibly better applicability of the modified equation in this realm. On the other hand, the logarithmic function of the TEX_{86}^{L} indeed affords a better linearity to the regression line by amplifying the variability in the low temperature range, but at the same time also magnifying its uncertainty.

The TEX_{86} values could be converted to SST by means of the empirical linear regressions based on global sediment core-tops [*Kim et al.*, 2008; *Kim et al.*, 2010; *Schouten et al.*, 2002]. There have been some successful paleo SST reconstruction in the subtropical

area such as in the Arabian Sea [*Huguet et al.*, 2006b], the Mediterrenean Sea [*Castañeda et al.*, 2010; *Huguet et al.*, 2011] and the Agulhas current system [*Caley et al.*, 2011]. However, the applicability of the global core-tops calibration of TEX_{86} and TEX_{86}^{L} in the subpolar and polar regions is more uncertain. Thus far there are few reported successful studies. In some cases modified TEX_{86} indices and calibrations are proposed, such as demonstrated by *Sluijs et al.* [2006] in the Arctic and *Shevenell et al.* [2011] at the Antarctic Peninsula. Furthermore, the substantial scatter in the TEX_{86} – SST correlation [*Kim et al.*, 2010] especially in the lower temperature range of the calibration, suggests the possibility of additional factors that might influence the TEX_{86} indices in these regions.

Therefore, this study was carried out to assess the applicability of the TEX_{86} and TEX_{86}^{L} indices in low-temperature environments. In light of the important role played by the polar regions in the global climate, the emphasis of this study is focused on the mid and high latitudes where the annual mean surface water temperatures are in the range of -2 to 17 °C. In addition, this study also aims at providing more TEX_{86} core-top data from the Southern Ocean and the Pacific, the two regions that still suffer from a lack of geographical coverage in the present global core-top data set.

2.2. Materials and Methods

2.2.1. Sediment Extraction

The 160 marine sediment core-tops (0-1cm) analyzed in this study were obtained via multicoring during several Alfred Wegener Institute (AWI) and German-Russian scientific expeditions on various research vessels (R/Vs Polarstern, Sonne, Ivan Kireyev and Akademik Boris Petrov) in the Southern Ocean, the North Pacific, the Fram Strait and the Arctic Ocean (**Figure 2.1**).

All core-top sediments were freeze-fried and homogenized. The GDGT extraction of the core-tops from the Southern Ocean (ANT-XXIII/9) and the Arctic (ARK-IX/4, ARK-XI/1, Transdrift-1 and SIRRO 1997 - 2000) was done according to *Müller et al.* [1998]. Briefly, the sediments were subjected to 3 times of ultrasonication using UP200H sonic disruptor probes in successively less polar solvent mixtures (dichloromethane/methanol). From the North Pacific samples (SO202), the GDGTs were extracted using an DIONEX™ accelerated solvent extractor (DIONEX ASE 350), according to the NIOZ protocol [*Schouten*

et al., 2002]: heating for 5 minutes at 100°C, static time of 5 minutes, 3 cycles and solvent mixture of dichloromethane/methanol in the ratio of 9:1, v/v. After extraction, the total lipid extracts were fractionated by column chromatography (SiO cartridges, Varian Bond-Elut) using dichloromethane/methanol.

The core-tops from the central Arctic (ARK-XXII/2), the Fram Strait (ARK-XXI/1) and the Southern Ocean core-tops other than those from ANT-XXIII/9, were subjected to microwave assisted extraction as described by *Fietz et al.* [2011] by using a mixture of dichloromethane:methanol (3/1, v/v). The extracts were then injected manually onto a Thermo Surveyor HPLC system equipped with a Lichrosphere Silicon dioxide column (4.6 x 250 mm, 5 µm; Teknokroma) and a stainless steel inline filter (2 µm pore size). Compound class fractionation was achieved running sequentially n-hexane, dichloromethane, and acetone.

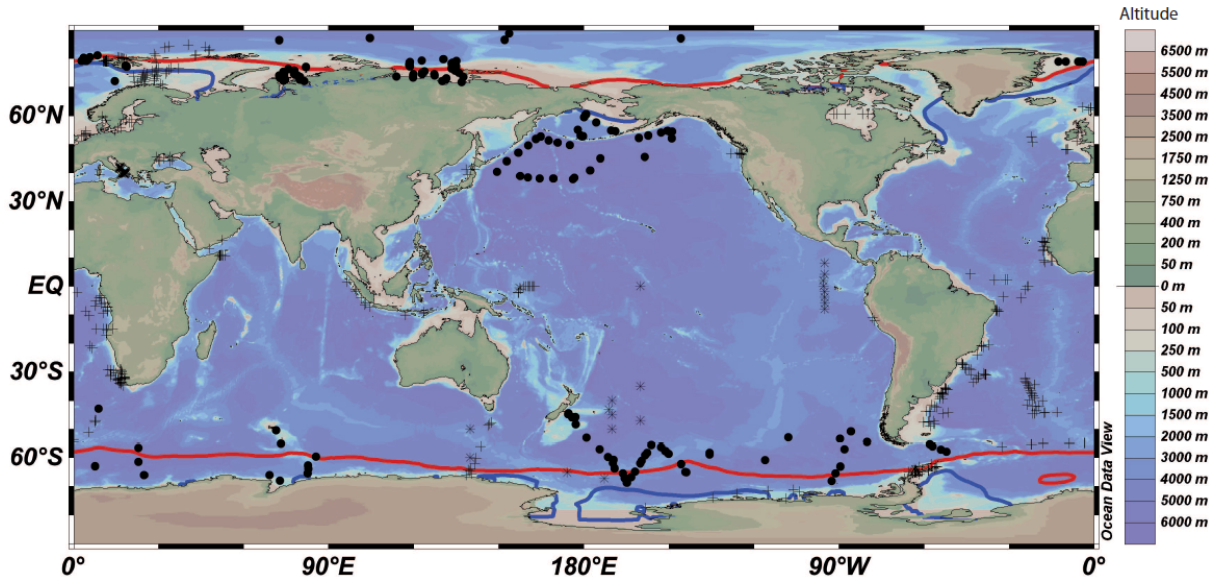

Figure 2.1: Location of study sites in the global ocean. Black circles denote sites in this study, while previously published data are marked by different symbols: black crosses - *Kim et al.* [2008] and *Kim et al.* [2010]; black asterisks - *Ho et al.* [2011]; open triangles – *Shevenell et al.* [2011]; diagonal crosses – *Leider et al.* [2010]. Blue and red lines illustrate the monthly sea ice extent (in March and September) incorporated in the ODV software [*Schlitzer*, 2011] based on data from *Walsh* [1978] and *Zwally et al.* [1983]. Color bar indicates the altitude and the depth of seafloor.

2.2.2. GDGTs Analysis

The GDGTs in samples from expeditions ANT-XXIII/9, SO202, ARK-XI/1, ARK-IX/4, Transdrift-1 and SIRRO 1997 - 2001 were quantified using liquid chromatography with a method derived from *Hopmans et al.* [2000]. The polar fractions were pre-filtered through a 4 µm diameter PTFE filter (0.45 µm pore size) to prevent clogging in the column. Filtered

samples were then dissolved in hexane:isopropanol (99:1; v/v) and were injected onto a high performance liquid chromatography system (Agilent 1200 series HPLC system) coupled to an Agilent 6120 MSD mass spectrometer, operating with atmospheric pressure chemical ionization (APCI). The injection volume was 20 µL. A Prevail Cyano 3µm column (Grace, 150mm x 2.1mm) maintained at 30°C was used to separate the GDGTs. The injected samples were eluted with a mixture of solvents, i.e., solvent A = hexane and solvent B = 5% isopropanol in hexane. The mixture of solvents (solvents A:B in the ratio of 80:20 v/v) was eluted isocratically for 5 min, then the volume of solvent B was increased linearly to 36% in 40 min. The column was back-flushed with 100% solvent B for 8 min after each analysis to eliminate any compound that remains in the column. The spray chamber of the APCI-MS was set in the following conditions: drying gas flow 5 l/min and temperature 350°C, nebulizer pressure 60 psi, vaporizer gas temperature 450°C, capillary voltage -3 kV and corona current +4 µA. The detection of the GDGTs was achieved by Selected Ion Monitoring (SIM) of the $[M+H]^+$ ions (dwell time 67 ms) in the m/z range of 1022 – 1302.

Meanwhile, the remaining core-tops (ANT-X/5, ANT-XI/2, ANT-XII/4, ANT-XX, ANT-XXVI/2, ARK-XXI/1 and ARK-XXII/2) were analyzed as described by *Fietz et al*. [2011]. The dry polar fractions were re-dissolved in hexane/n-propanol (99/1, v/v) and filtered through 0.50 µm PTFE filters (Advantec). A Dionex P680 HPLC system coupled to a Thermo Finnigan TSQ Quantum Discovery Max quadrupole mass spectrometer with an APCI interface was used. The target compounds were separated with a Tracer Excel CN column (0.4 x 20 cm, 3 µm; Teknokroma) equipped with a precolumn filter and a guard column. The solvent program was modified from *Schouten et al.* [2007] and *Escala et al.* [2007]. Samples were eluted with hexane/n-propanol at 0.6 mL / min. The amount of n-propanol was held at 1.5 % for 4 min, increased gradually to 5.0 % during 11 min, then increased to 10 % during 1 min and held at 10 % for 4 min, then decreased to 1.5 % during 1 min and held at 1.5 % for 9 min until the end of the run. The parameters of the APCI were set as follows to generate positive ion spectra: corona discharge 3 µA, vaporizer temperature 400ºC, sheath gas pressure 49 mTorr, auxiliary gas (N_2) pressure 5 mTorr and capillary temperature 200ºC. GDGTs were monitored in SIM mode.

The samples preparation and GDGT analysis were carried out at the University of Bremen, the Autonomous University of Barcelona and the Alfred Wegener Institute. We contend that the results obtained from different laboratories using different analytical methods should result in comparable data since it was reported that the TEX_{86} measurement is not

significantly biased by extraction techniques or HPLC/APCI-MS set-ups [*Schouten et al*., 2007].

2.2.3. TEX_{86} calculation and SST estimations

The values for TEX_{86} and TEX_{86}^{L} are calculated following the equations as reported by *Schouten et al.* [2002] and *Kim et al*. [2010], respectively. These values are converted to SST estimates using the latest global core-top TEX_{86} / TEX_{86}^{L} - SST calibrations proposed by *Kim et al.* [2010]. Additionally, we calculated the Branched and Isoprenoid Tetraether Index (BIT) according to *Hopmans et al.* [2004], which was proposed as a qualitative indicator for fluvial terrigenous GDGTs input (cutoff value suggested to be 0.3 by *Weijers et al.* [2006]).

2.2.4. Environmental data

The objectively analyzed climatological data utilized in this study, i.e., water temperature at different depths, are extracted from the World Ocean Atlas 2009 (WOA09) [*Locarnini et al.*, 2010]. The WOA09 dataset is preferred (over the NSIPP AVHRR Pathfinder and Erosion Global 9 km SST Climatology dataset used in *Kim et al*. [2010] which does not include subsurface water temperature data, see **Figure 1.11**) in this study on the grounds that all the environmental data used to discuss our TEX_{86} values should be from a consistent source.

For comparison of our index data with seasonal mean SST, we used seasons as defined by the WOA09 (i.e., Northern/Southern hemisphere spring/autumn: AMJ, summer/winter: JAS, autumn/spring: OND, winter/summer: JFM) [*Locarnini et al*., 2010]. The water temperatures at various depths (e.g., base of thermocline) are determined manually from the temperature-depth profile at each study site using the ODV software [*Schlitzer*, 2011]. Instead of a fixed depth, we opt to compare TEX_{86} values with water temperatures at a particular physical or chemical hydrographic boundary. This is because our study sites vary considerably in terms of water depths (20m to 5500m), hence a fixed depth (e.g., 200m) could correlate to very different hydrographic features, potentially introducing more scatter in the correlation of the water temperature with the TEX_{86} values. In fact, if there is indeed a significant subsurface GDGTs export, it is more likely to occur at a hydrographic boundary,

physical or chemical, rather than a fixed depth, due to specific biological niche development or physical factors such as preferential detention of lipids at the interface of water masses with large density difference. Therefore, three water depths are chosen, i.e., the base of thermocline, the base of oxycline, and the bottom waters close to the water-sediment interface (defined for the purpose of our study as the deepest temperature datum available for a given site in WOA09).

2.3. Results

2.3.1. Relationship between individual GDGTs

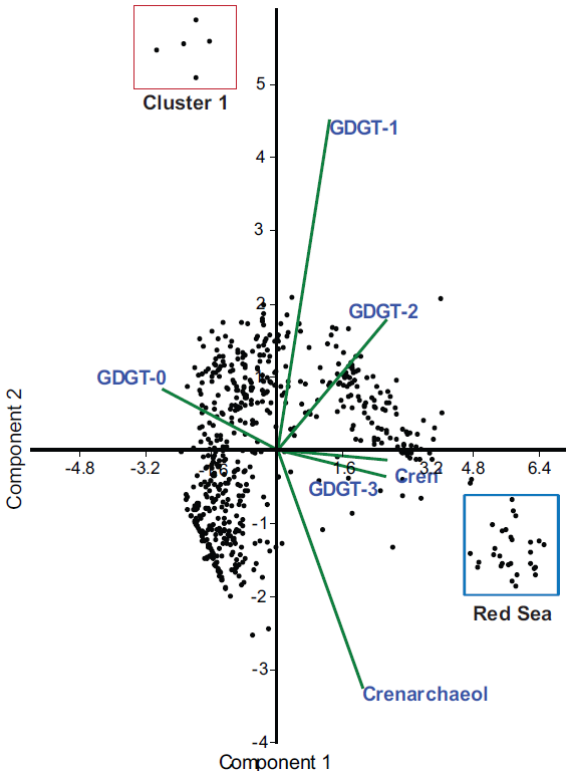

Figure 2.2: Principal component analysis on the individual GDGTs in the compilation of the data in this study and the published core-top data by *Kim et al.* [2008], *Kim et al*. [2010] and *Ho et al*. [2011].

The PCA on the compilation of our data, the global core-top data set from *Kim et al*. [2008; 2010] and the Pacific data set from *Ho et al.* [2011] spanning a large temperature range (-2 to 30°C), shows that in general the relative relationship between individual GDGTs at our core sites are not different from that of the global ocean. The exceptions are five North Pacific samples (Cluster 1, **Figure 2.2**) and the Red Sea data set (previously discussed in *Kim et al.*

[2008]) that form separate clusters. The first two principal components explain approximately 92% of the variance (PC1: 70 % and PC2: 22 %), similar to the values reported in the global core-top study [*Kim et al*., 2010]. On the Component 1 axis, all the GDGTs included in the TEX_{86} indices are positively correlated, while GDGT-1 and GDGT-2 are negatively correlated with GDGT-3 and crenarchaeol regioisomer on the Component 2 axis. This pattern of GDGTs distribution is essentially the same as reported in the latest global core-top study [*Kim et al*., 2010].

2.3.2. Fractional abundance of GDGTs

In a broad sense, the fractional abundance of GDGTs increases with the WOA09 annual mean SST, except the GDGT-0, which exhibits an opposite trend (see **Figure 2.3**). Some of the Arctic marginal sea data reveal a different relationship with SST compared to the Southern Ocean and the North Pacific data set, especially evident in terms of the relative fractional abundance of GDGT-3 (Laptev Sea and Kara Sea), crenarchaeol (Laptev Sea and Kara Sea) and crenarchaeol regioisomer (Fram Strait and Central Arctic). Meanwhile, the distribution of GDGTs from Cluster 1 displays a completely different behavior relative to the rest of the data set. The fractional abundances of GDGT-0, -1 and -2 are remarkably high while those of crenarchaeol and crenarchaeol regioisomer are substantially lower than in the rest of the data set.

2.3.3. TEX_{86} and TEX_{86}^{L} values

For a broader geographical coverage in the appraisal of the applicability of TEX_{86} and TEX_{86}^{L} thermometries in the subpolar and polar regions, we include also previously published data [*Ho et al*., 2011; *Kim et al.*, 2008; *Kim et al*., 2010; *Shevenell et al*., 2011] from regions that are comparable in terms of SST (<17°C) and latitudes (>37°N/S) with those presented in this study.

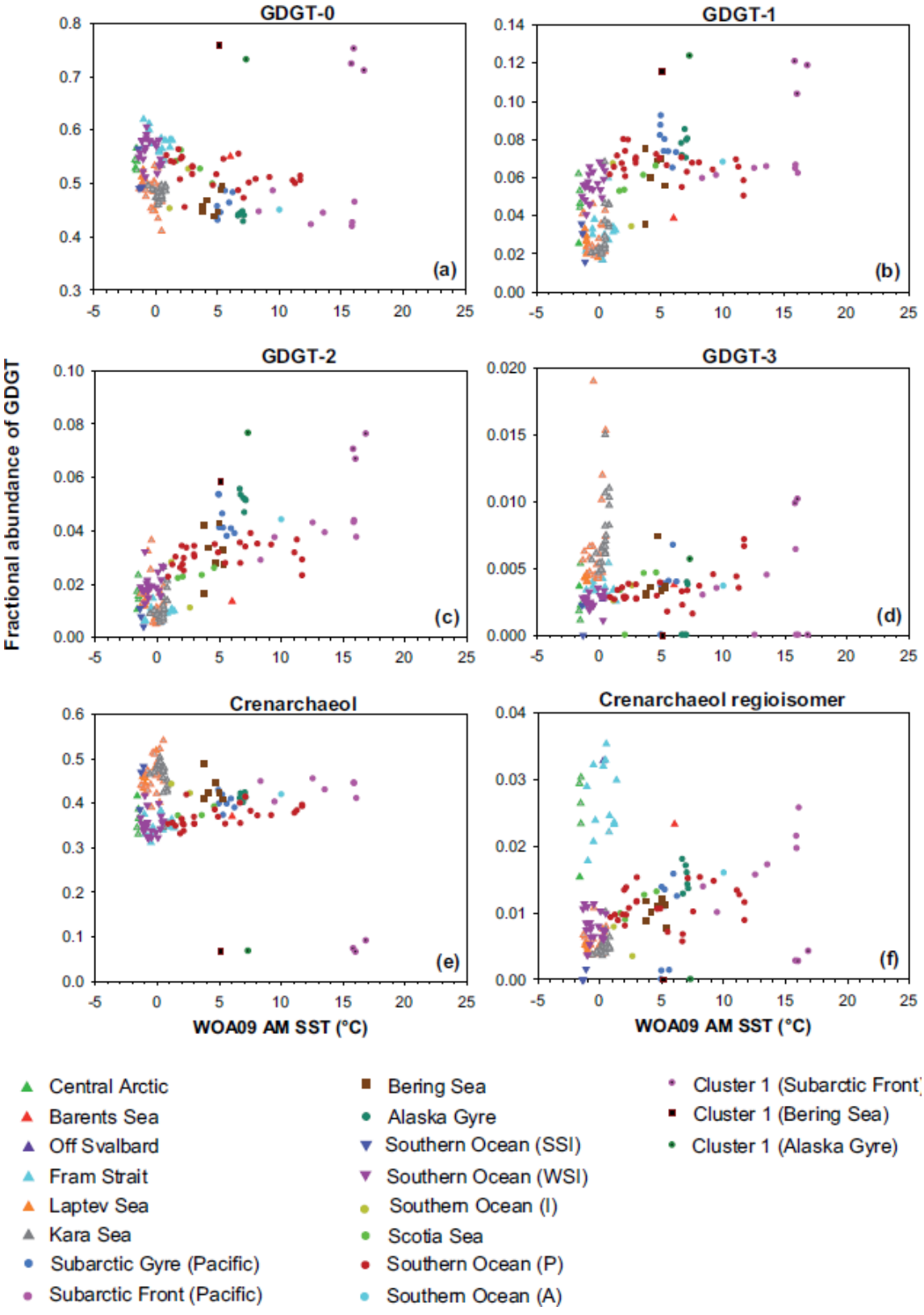

Figure 2.3: Relationship between the fractional abundance of individual GDGTs and the WOA09 annual mean SSTs, i.e., (a) GDGT-0, (b) GDGT-1, (c) GDGT-2, (d) GDGT-3, (e) Crenarchaeol, (f) Cren' (abbreviation for crenarchaeol regioisomer). Oceanic regions are marked by different symbols in different colors as explained in the legends.

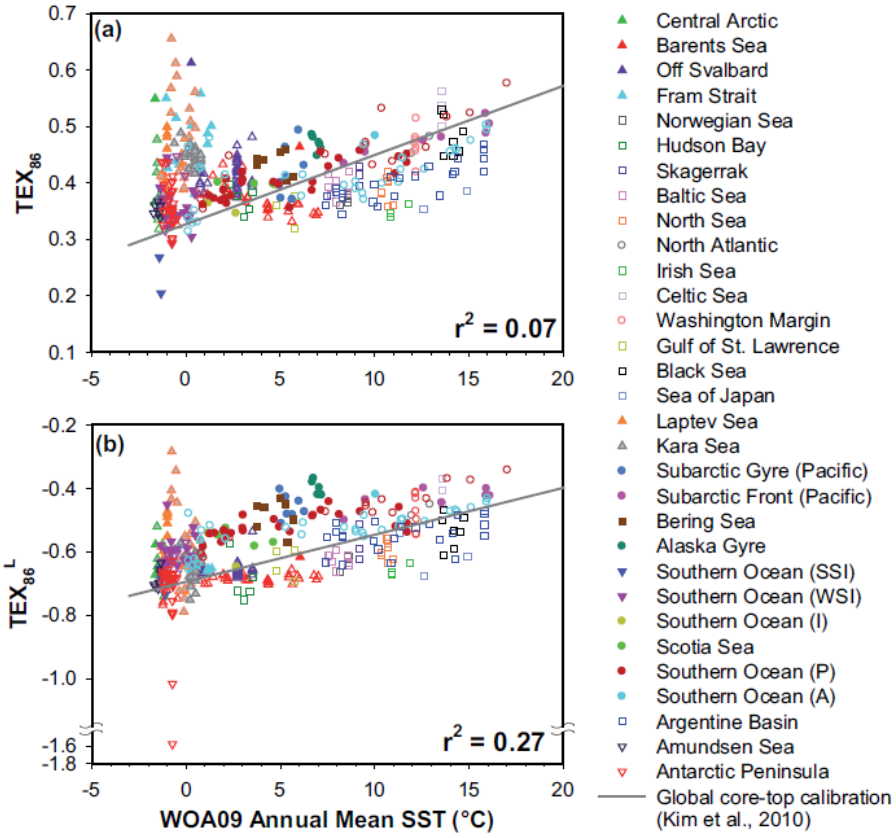

Figure 2.4: Correlation plots of TEX_{86} and TEX_{86}^{L} values with annual mean sea surface temperature derived from World Ocean Atlas 2009 (WOA09). Oceanic provinces are indicated by different symbols in different colors as explained in the legends. Filled symbols indicate data from this study, open symbols indicate published data, grey-filled symbols indicate data with BIT >0.3. Abbreviations: SSI – summer sea ice; WSI – winter sea ice, I – Indian, P – Pacific; A – Atlantic.

2.3.3.1. Correlation to temperature at various water depths

Overall, compared to its counterpart TEX_{86}, the TEX_{86}^{L} displays better correlation with the SST (**Figure 2.4**). There is considerable scatter in the TEX_{86} data, especially those from the Laptev Sea, the Fram Strait and the central Arctic, which form a separate cluster with relatively high TEX_{86} values at low temperatures. On the other hand, the most pronounced scatter in the TEX_{86}^{L} data set is attributable mainly to the data from the Laptev Sea with BIT values > 0.3 and two anomalous data from the Antarctic Peninsula. It is also notable that both the TEX_{86} and TEX_{86}^{L} values in the Barents Sea are invariant in spite of the large SST range (0 – 7 °C) encompassed by these sites.

In addition to the sea surface (0 m), we also examine the correlation of TEX_{86} and TEX_{86}^{L} values with the temperature at 3 different water depths (**Figure 2.5**), namely the base of the seasonal thermocline, the base of the oxycline (where the oxygen level is the lowest in

the water column), and the bottom waters (deepest datum available for a given site in the WOA data set). There is no strong linear relationship (low r^2 values below 0.05) between both the TEX_{86} and TEX_{86}^{L} values with the temperature of bottom waters and the base of the oxycline. On the contrary, a better correlation, comparable to that of the SST, is found for the temperature at the base of the seasonal thermocline.

2.3.3.2. Correlation to SST of various seasons

There is no difference between the correlation of TEX_{86} values with the annual mean SST (**Figure 2.4**) and that of the seasonal SSTs (**Figure 2.6a – 2.6d**). The same is true for the TEX_{86}^{L} data set (**Figure 2.6e – 2.6h**), with the exception of the correlation with the summer SST, which is slightly poorer than those of the other seasons and the annual mean.

2.3.4. Residuals of SST estimates

The residual of SST estimate is defined here as the difference between the estimated SST and the atlas SST. The residuals vary depending on the calibration used. Here we assess how the SST estimates derived from the global core-top calibrations compare to the climatological SSTs. The standard errors of estimates for the latest global core-top calibrations for TEX_{86} and TEX_{86}^{L} (*Kim et al.* [2010], n = 396) are 5.2°C and 4°C, respectively.

The standard deviation of the TEX_{86} derived SST estimates (relative to annual mean SST) is 6.1°C (**Figure 2.7a**). Although the residuals seem to become increasingly negative as SST increases, a large majority of the SST estimates are within the standard error of estimates. At the low temperature end, a separate cluster with deviant positive residuals ranging between ~5 to 30°C is apparent, consisting mostly of data from the Arctic regions and the Antarctic Peninsula. The global TEX_{86} calibration underestimates the SST at some marginal seas such as the Sea of Japan, the North Sea, and the Irish Sea, resulting in negative residuals.

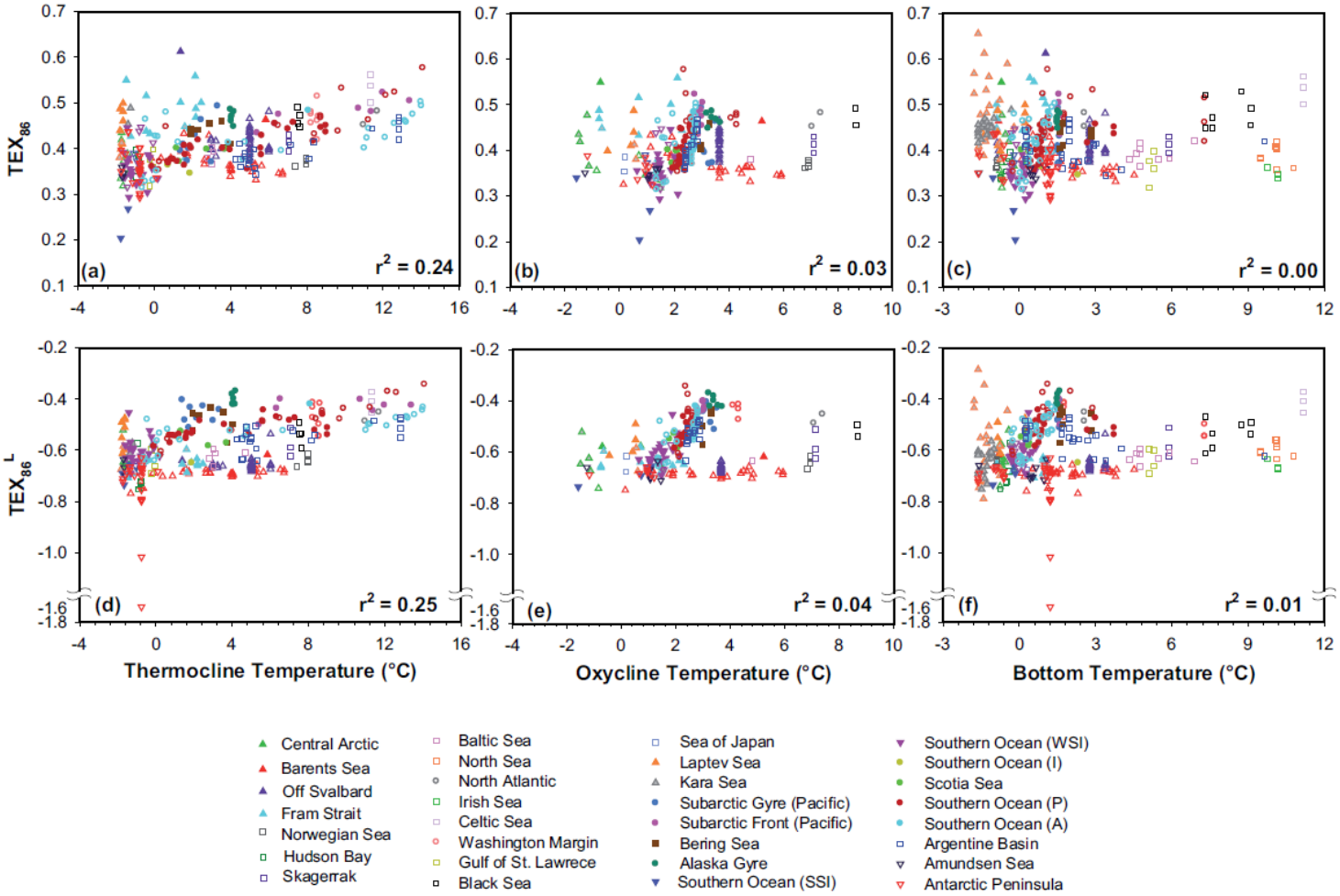

Figure 2.5: Correlation plots of TEX_{86} and TEX_{86}^{L} values with water temperatures derived from World Ocean Atlas 2009 (WOA09) at various depths. The water depths used in the plots are as follows: Thermocline – the base of seasonal thermocline, Oxycline – the base of the oxycline , Bottom – the deepest water depth datum available for the site. Oceanic provinces are indicated by different symbols in different colors as explained in the legends. Filled symbols indicate data from this study, open symbols indicate published data, grey-filled symbols indicate data with BIT >0.3. Abbreviations: SSI – summer sea ice; WSI – winter sea ice, I – Indian, P – Pacific; A – Atlantic.

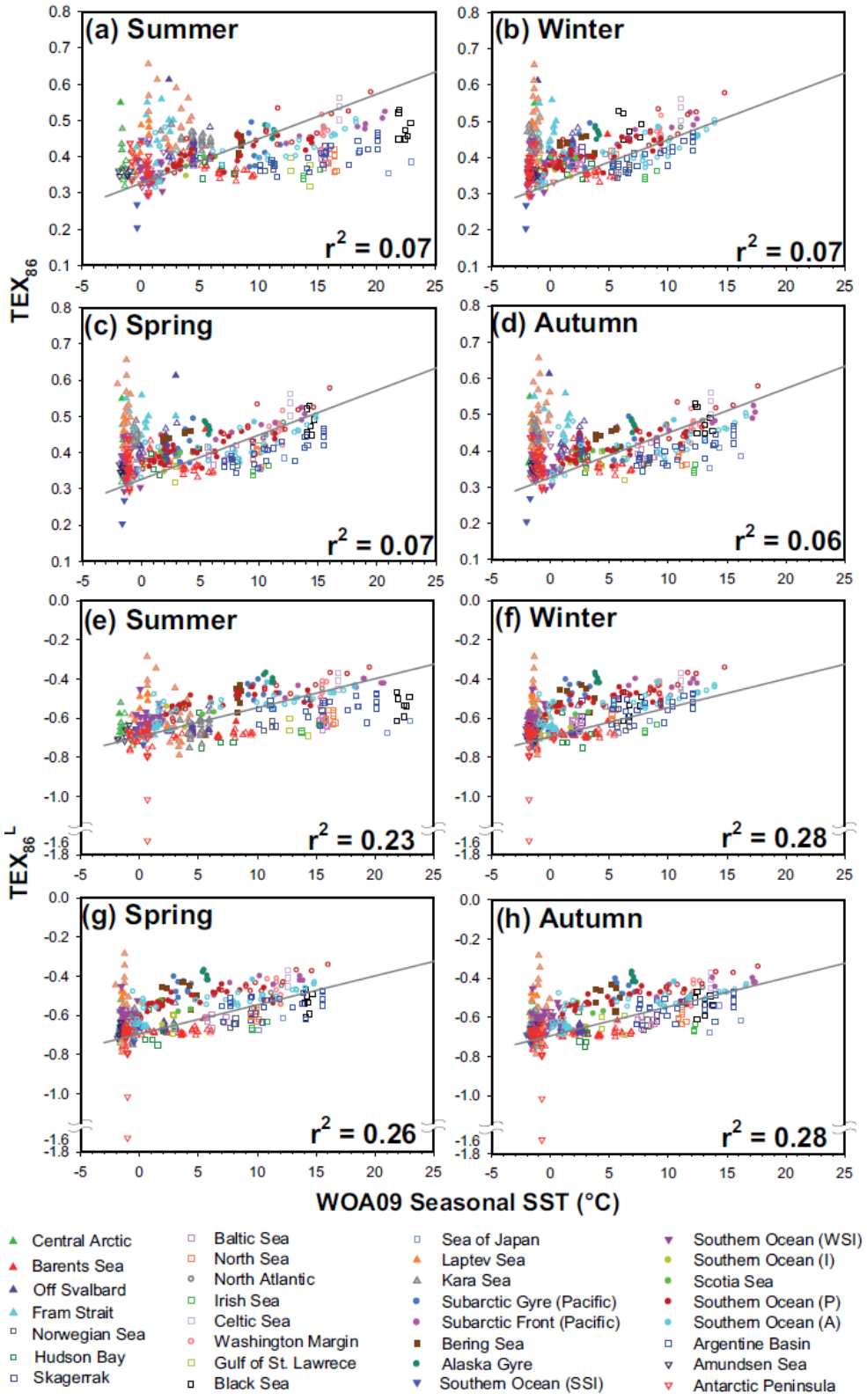

Figure 2.6: Correlation plots of TEX_{86} and TEX_{86}^{L} values with mean seasonal sea surface temperature derived from World Ocean Atlas 2009 (WOA09). Grey lines illustrate the latest global core-top calibrations [*Kim et al.*, 2010]. Oceanic provinces are indicated by different symbols in different colors as explained in the legends. Filled symbols indicate data from this study, open symbols indicate published data, grey-filled symbols indicate data with BIT >0.3. Abbreviations: SSI – summer sea ice; WSI – winter sea ice, I – Indian, P – Pacific; A – Atlantic.

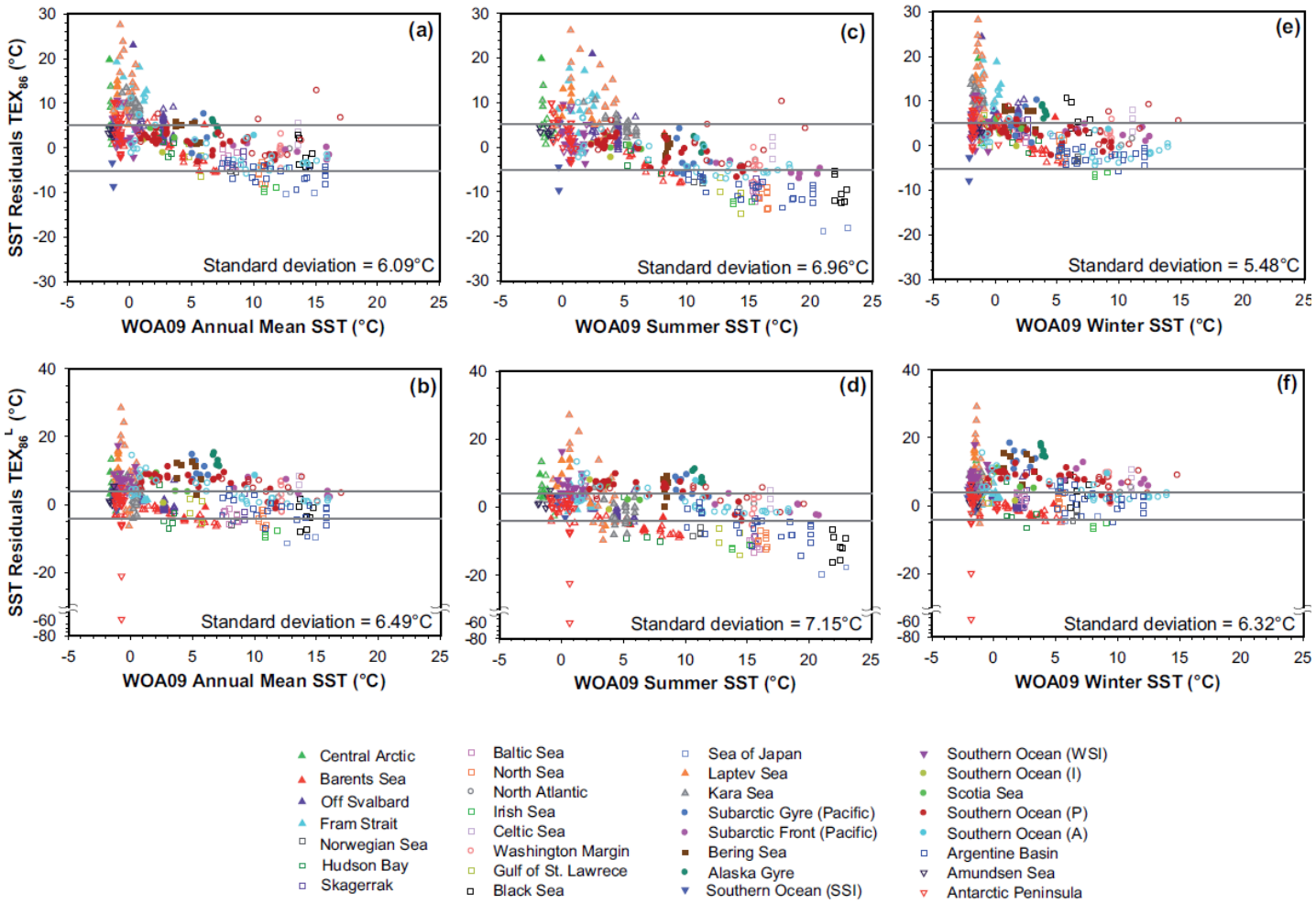

Figure 2.7: The residuals of temperature estimates derived from the latest global core-top calibrations for TEX_{86} and TEX_{86}^{L} [*Kim et al.*, 2010]. SST residuals are defined as the subtraction of World Ocean Atlas 2009 (WOA09) annual mean/summer/winter SST from the estimated SST. The grey lines represent the standard error of estimates for the calibrations. Oceanic provinces are indicated by different symbols in different colours as explained in the legends. Filled symbols indicate data from this study, open symbols indicate published data, grey-filled symbols indicate data with BIT >0.3. Abbreviations: SSI – summer sea ice; WSI – winter sea ice, I – Indian, P – Pacific; A – Atlantic.

On the other hand, the residuals of the TEX_{86}^{L} inferred SST estimates (relative to the annual mean SST) have a standard deviation of 6.5°C (**Figure 2.7b**). Some data from the Arctic form a separate cluster with large positive residuals, albeit to a smaller extent compared to the TEX_{86} temperature residuals. Two of the SST estimates at the Antarctic Peninsula are unrealistically low, with underestimation down to -60°C. Most of the SST estimates from the open ocean settings are overestimated beyond the standard error of estimates, including those from the Southern Ocean, the North Pacific and the Bering Sea. Meanwhile, underestimation mostly occurs in the marginal seas such as the Irish Sea, the Black Sea and the North Sea.

To detect any potential seasonal bias in the SST estimates, we also assess the residuals of the SST estimates relative to the summer and winter SST (**Figure 7c** to **7f**). The standard deviation of residuals relative to the winter SST are comparable to those of the annual mean, and are smaller than those of the summer SST. In general, the residuals of seasonal SST estimates display a similar data distribution as those of the annual mean SSTs, with amplification in the extent of underestimation, especially in the temperature range of 15 – 23°C.

2.4. Discussion

2.4.1. GDGT contribution from methanogenic archaea

The PCA on individual GDGTs reveals that 5 samples from the North Pacific (Subarctic Front and Alaska Gyre) and the Bering Sea have a distinctive GDGT signature (**Figure 2.2**). On a closer inspection, these samples contain elevated abundance of GDGT-0, and to a lesser extent also of the GDGT-1 and 2 (**Figure 2.3**), relative to crenarchaeol, the hallmark GDGT for marine Thaumarchaeota [*Sinninghe Damsté et al.*, 2002b]. The atypical GDGT distribution in these samples suggests a contribution from an archaeal community other than the pelagic Thaumarchaeota. Soil derived and fresh water related GDGTs are unlikely to be the cause, since these sites are far from the coast, hence receive insignificant riverine input of terrigenous GDGTs and are not in the vicinity of sea ice margin where fresh water could be generated via ice melting. The abundance ratio of GDGT-0/crenarchaeol at these sites ranges between 8 and 12, which are remarkably high compared to the values observed in typical marine sediment (0.2 – 2, *Schouten et al.* [2002]). It has been proposed that a ratio GDGT-0/crenarchaeol > 2 is indicative of significant methanogen archaeal input in

lake sediments [*Blaga et al.*, 2009], based on the assumption that the main contributors of GDGT-0 and crenarchaeol are the methanogens and the Thaumarchaeota, respectively. Therefore, the atypical GDGTs distribution observed at Cluster 1 sites in the North Pacific and the Bering Sea might be attributable to major contribution from the methanogens. Nevertheless, some of the SST estimates are within the standard error of estimates (three out of five for TEX_{86} and one out of five for TEX_{86}^{L}). At those sites with anomalously large residuals, there is an opposite trend in the TEX_{86} and TEX_{86}^{L} derived SST estimates, i.e., the TEX_{86} inferred estimates are warm-biased while those inferred from the TEX_{86}^{L} index are cold-biased. The warm-biased TEX_{86} derived estimates are in agreement with the finding of a study in Lake Challa where the methanogenic archaeal GDGTs biased TEX_{86} values were anomalously high [*Sinninghe Damsté et al.*, 2009]. Nonetheless, we exclude the Cluster 1 data from further discussion to avoid undue bias.

2.4.2. Correlation of TEX_{86} / TEX_{86}^{L} indices to subsurface temperature

Since the GDGTs are found throughout the water column [e.g., *Karner et al.*, 2001], it is tempting to speculate that the lack of correlation with SST could be due to a substantial input of GDGTs from deeper waters, interfering with the surface water GDGT signals. However, we do not observe much improved correlations at deeper water depths, such as at the base of oxycline and the bottom waters at the site (**Figure 2.5**). The correlations with the seasonal thermocline (10-200 m), on the other hand, seem to be better than those with the SST, especially evident for the TEX_{86} index (**Figure 2.5a** and **Figure 2.5d**). However, this observation probably arises as an artifact of the reduced data set for the TEX_{86} – thermocline correlation, which does not include most of the deviant data from the Arctic shelf (due to the difficulty in identifying this hydrographic barrier in the poorly resolved WOA09 data set for shelf regions). Indeed, if the same reduced data set would be considered for the correlation of the GDGT indices with both the seasonal thermocline and SST, comparable or better r^2 values would be obtained for the SST (0.22 and 0.33 compared to 0.24 and 0.25 for the TEX_{86} and TEX_{86}^{L}, respectively). This finding attests to the fundamental principle of the TEX_{86} paleothermometry, i.e., the GDGTs that end up in the sediment are mainly those of the near-surface dwelling archaea, in spite of the fact that the archaea thrive throughout the water column. This assumption is based on several lines of evidence. For example, *Sinninghe Damsté et al*. [2002a] and *Wuchter et al*. [2005] found that the sedimentary TEX_{86} values

reflect the SST in spite of higher GDGT abundance in mid water depths owing to a more efficient export of GDGTs from the surface waters presumably via an active food web [*Wakeham et al.*, 2003]. In addition, *Huguet et al*. [2006a] reported that the TEX_{86} derived SST estimates in the gut of decapods, one group of zooplankton, are in good agreement with the SSTs, suggesting that the zooplanktons graze upon the archaea or on the particles the archaea are associated with in the surface waters. Furthermore, the archaeal cells are less than 1µm in size and are neutrally buoyant [*Könneke et al.*, 2005; *Margot et al.*, 2002] which prevents them from sinking efficiently on their own [*Wakeham et al*., 2003].

2.4.3. Deviant SST estimates in the Arctic

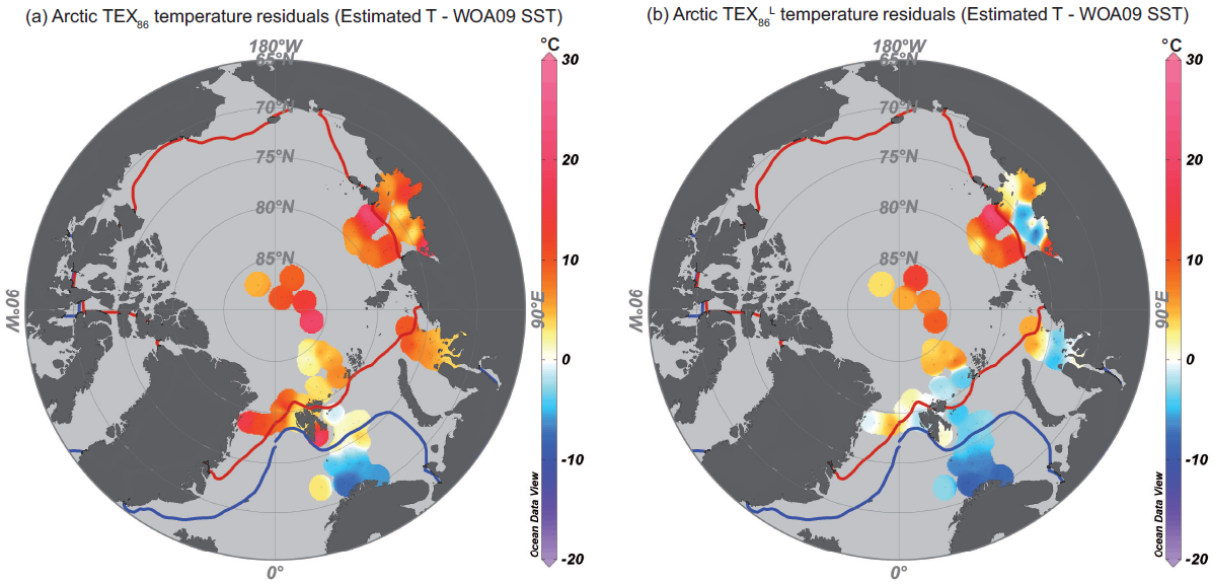

Figure 2.8: Close-up of the residuals of (a) TEX_{86} and (b) TEX_{86}^{L} derived SST estimates relative to World Ocean Atlas 2009 (WOA09) summer SST in the Arctic. The blue and red lines denote the maximum and minimum monthly sea ice extent respectively, incorporated in the ODV software [*Schlitzer*, 2011] based on data from *Walsh* [1978] and *Zwally et al*. [1983]. Color bar illustrates the residuals in blue-red color scheme: red indicates overestimation while blue indicates underestimation.

The TEX_{86} derived SST estimates for the Arctic are largely overestimated, to the extent of 28°C warmer than the summer SST at the sites (**Figure 2.7** and **Figure 2.8**). Some of the warm biased SST estimates near the coast, e.g., off Svalbard and off Siberia, are probably the consequence of a significant input of terrigenous GDGTs via river runoff, interfering with the marine signals. However, in the Arctic marginal seas especially the Laptev Sea, there is a seaward increase in the magnitude of the SST overestimation, peaking in the vicinity of the sea ice margin (**Figure 2.8**). This warm bias near the sea ice margin does

not occur in the Barents Sea, even though there is indeed a seaward increase in the temperature residuals. Interestingly, the extreme warm bias is also observed in the TEX_{86}^{L} derived SST estimates. In general, the warm TEX_{86}/ TEX_{86}^{L} SST estimates are associated with high fractional abundance of GDGT-3 or crenarchaeol regioisomer (**Figure 2.3**). Co-incidentally, a previous reconstruction work in the central Arctic during the PETM has also found anomalously high GDGT-3 [*Sluijs et al*., 2006] that resulted in high TEX_{86} values. The authors interpreted the deviant GDGT-3 as terrestrially originated, and discarded them from the TEX_{86} calculation. Nevertheless, since the warm bias in our core-top TEX_{86} inferred SST estimates is more pronounced near the sea ice margin than near the river mouth, we are more inclined to attribute the warm bias to the occurrence of the sea ice. It is plausibly due to a substantial input of GDGTs from sea-ice related archaeal communities with a different temperature adaptation mechanism in the lipids, which might have skewed the TEX_{86} values at the offshore Arctic sites. These archaea probably produce lipids with additional GDGT-3 (**Figure 2.3d**), resulting in anomalously high TEX_{86} values. Potential candidates for these archaeal communities may be associated with the Marine Group 1 Crenarchaeota in the Arctic [*Alonso-Sáez et al.*, 2008; *Bano et al.*, 2004], unspecified archaea in the sea ice [*Junge et al.*, 2004], or polar-specific Crenarchaeota dominant in the upper halocline of the Arctic waters [*Kalanetra et al.*, 2009]. Given that we do not observe such deviously warm SST estimates at the sea ice edges in the Southern Ocean and the coast off the Antarctica (**Figure 2.7**), it is possible that these sea ice archaea are limited to the Arctic. At this stage, however, it is impossible to unambiguously identify the group of archaea that contributes to the spuriously high TEX_{86} inferred SST estimates at our sites without further genomic work. Nevertheless, our results suggest that extreme caution should be used when interpreting TEX_{86} data in areas potentially influenced by sea ice.

2.4.4. Effect of sedimentation setting and/or seasonality

In addition to the spuriously warm Arctic SST estimates, there is also considerable scatter in the subpolar TEX_{86} / TEX_{86}^{L} data sets. A closer inspection of the scatter plots of TEX_{86} / TEX_{86}^{L} vs. SST (**Figure 2.4**) reveals two groups, congregating above and below the global calibration of *Kim et al*. [2010] respectively. In general, the data in the group above are mostly from the deep open ocean setting (depth > 2000 m), while the group below consists of mostly data from the marginal seas and/or continental shelves. The same trend could also be

observed in the TEX_{86} temperature residuals plots (**Figure 2.7**). Most of the warm-biased estimates (e.g., summer residuals within the standard error of estimates) are consisted of data from the open oceans, while the cold-biased estimates (e.g., winter residuals within the standard error of estimates) occur at the marginal seas and the continental shelves such as the Black Sea and the Gulf of St. Lawrence. The contrasting bias (warm bias vs. cold bias) in the SST estimates at open ocean and marginal seas might be the reason why we do not observe substantial difference in the correlation with seasonal SSTs (**Figure 2.6**), as the contradicting estimates might have canceled out the correlation to warm or cold seasons.

A combination of factors, including archaeal ecology, sedimentation regime and seasonality, might have contributed to the diverging TEX_{86} / TEX_{86}^{L} - SST relationship in different settings. The microbial communities are known to differ between coastal and open ocean regions, with latitude, and in regions where there is upwelling of mesopelagic waters to the surface [*Giovannoni and Vergin*, 2012]. For instance, the cold-biased TEX_{86} / TEX_{86}^{L} - derived SST estimates in marginal seas might arise as a consequence of higher archaeal cell / lipid abundances in winter, as reported for the North Sea [*Wuchter et al.*, 2005; *Wuchter et al.*, 2006] and the Antarctic coastal waters [*Church et al.*, 2003; *Murray et al.*, 1998]. On the other hand, the GDGT flux to the seafloor in open ocean setting (e.g., the Southern Ocean, the North Pacific) might be more tightly linked to the primary production export, which is heavily biased towards the warm seasons [*Honda et al.*, 2002; *Honjo et al.*, 2000] due to more availability of light, hence result in warm biased SST estimates. Similar findings, albeit on a regional scale, were observed previously in a seaward transect study in the Mediterranean [*Leider et al.*, 2010], in which the authors found that the TEX_{86}-derived SSTs were increasingly overestimated seaward. The authors invoked seasonality in the production of planktic archaea, the nutrient conditions and particle loading in surface waters to explain their findings. These mechanisms might be in play as well in the marginal seas and the open oceans in the subpolar and polar regions, causing the scatter in the low and mid temperature range in the data set. Furthermore, some of the underestimation at the continental margins may also be attributable to lateral transport, such as in the Argentine Basin, where previous studies suggested that the cold-biased alkenone-derived SSTs observed are due to the advection of allochthonous alkenones by vigorous surface currents [*Benthien and Müller*, 2000; *Conte et al.*, 2006; *Mollenhauer et al.*, 2006; *Rühlemann and Butzin*, 2006]. Nevertheless, it is beyond the scope of this study to reconcile the discrepancy in different sedimentation settings, hence

the confirmation of our hypotheses awaits future work, e.g., water column studies across different sedimentation settings.

2.4.5. Implications for global core-top calibrations

The compilation of our new data set, together with the global data set of *Kim et al.* [2010] (Red Sea data not included) and some recently published regional core-top data sets such as those from the Pacific [*Ho et al.*, 2011], the Antarctic Peninsula [*Shevenell et al.*, 2011] and the Mediterranean Sea [*Leider et al.*, 2010] results in an impressive data set of 630 data points (**Figure 2.9**). However, the linear regression through this data set yield mediocre r^2 values of 0.67 and 0.68 for TEX_{86} and TEX_{86}^{L}, respectively, which are inferior compared to those of the previously published global calibrations (0.77 and 0.86 for TEX_{86} and TEX_{86}^{L}). The poorer correlation in this compilation might be attributable to the large scatter in the low and mid temperature range. As discussed in **Section 2.4.2**, the SST estimates in the Arctic regions are spuriously warm, hence the addition of these data might potentially jeopardize the linear correlation of these index values with SST (**Figure 2.9**). Indeed, once all the data from the Arctic region (Central Arctic, Laptev Sea, Kara Sea, Fram Strait, Barents Sea, off Svalbard) are removed, the correlation of TEX_{86} with SST improves considerably, resulting in r^2 value of 0.8, which is slightly better than the r^2 value of the *Kim et al.* [2010] TEX_{86} calibration (0.77). The standard error of estimate for this calibration is 4.8°C, slightly smaller than that reported for *Kim et al.* [2010] TEX_{86} calibration (5.2°C). Interestingly, the scatter in the mid temperature range (~7 – 17°C) seem to be larger than that at the lower end of the temperature range (excluding the Arctic data), probably attributable to different sedimentation setting (open ocean vs. marginal sea / continental shelf, see **Section 2.4.4**). On the other hand, the removal of the Arctic data does not affect the correlation of TEX_{86}^{L} with SST. Even if the apparent outliers (see **Figure 2.9b**; two data from the Antarctic Peninsula with anomalously low TEX_{86}^{L} values) are removed, the r^2 value of TEX_{86}^{L} – SST correlation is only marginally improved to 0.73, compared to 0.86 of the *Kim et al.* [2010] TEX_{86}^{L} calibration. The deterioration in the TEX_{86}^{L} - SST correlation results in a larger standard error of estimates (5.6°C compared to 4°C reported for *Kim et al.* [2010] calibration).

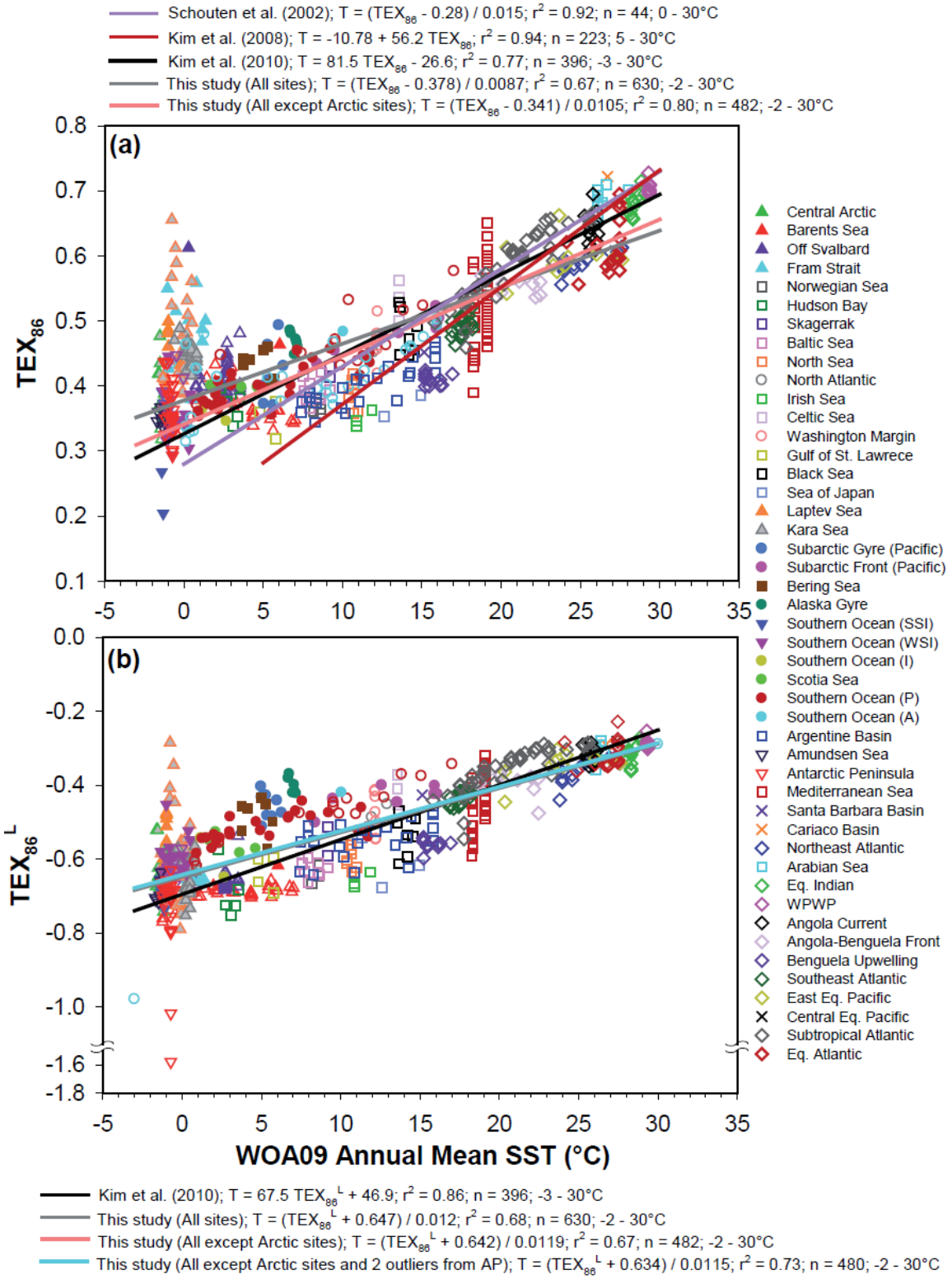

Figure 2.9: Compilation of the (a) TEX_{86} and (b) TEX_{86}^{L} data from this study and the published data set of *Kim et al*. [2010], *Kim et al*. [2008], *Leider et al.* [2010], *Ho et al*. [2011] and *Shevenell et al*. [2011], as a function of World Ocean Atlas 2009 (WOA09) annual mean SST. Oceanic provinces are indicated by different symbols in different colours as explained in the legends. Filled symbols indicate data from this study, open symbols indicate published data, grey-filled symbols indicate data with BIT>0.3. Published calibrations are marked by dashed lines while the calibrations derived from our compiled data set are marked by solid lines. Abbreviations: SSI – summer sea ice; WSI – winter sea ice, I – Indian, P – Pacific; A – Atlantic; Eq. – Equatorial; WPWP – West Pacific warm pool; AP – Antarctic Peninsula.

2.4.6. Applicability in (sub)polar regions and conclusions

Since its first proposal [*Schouten et al*., 2002], the TEX_{86} paleothermometry has been applied in several paleo reconstructions in the polar regions, such as in the Arctic during the PETM [*Sluijs et al*., 2006] and in the Antarctic Peninsula during the Holocene [*Shevenell et al*., 2011]. However, these studies employed modified versions of TEX_{86} calibrations due to the unsuitability of the global core-top calibrations at these sites. To shed more light on the validity of TEX_{86} thermometry in these regions, here we analyzed an extensive set of core-top samples to investigate the correlation of the TEX_{86} and TEX_{86}^{L} values to the SST and the predictive power of the presently available calibrations.

With regards to the global calibrations reported by *Kim et al.* [2010], the TEX_{86} calibration appears to be a better choice for the SST reconstruction in subpolar and polar regions. It yields better SST estimates (relative to WOA09 SST), especially in the Southern Ocean and the North Pacific, compared to the recommended proxy for sites with SST < 15°C [*Kim et al.*, 2010], i.e., the TEX_{86}^{L} calibration, which results in estimates that are warmer than the WOA09 summer SST in these regions (**Figure 2.7**). Moreover, the application of the TEX_{86}^{L} calibration on a sediment core in the Antarctic Peninsula resulted in large temperature variations during the Holocene [*Shevenell et al*., 2011 Supplementary information], with SSTs below freezing point (~-20°C) which are probably unrealistic for the site. Taken together, these findings argue against the applicability of the TEX_{86}^{L} paleothermometry in these regions.

We observed some regional differences in the TEX_{86} / TEX_{86}^{L} - SST relationships in the subpolar and polar regions. For instance, regardless of the indices or calibrations used, the SST estimates are cold- / warm-biased at some marginal seas (e.g., Irish Sea, North Sea) / most of the Arctic sites especially in the vicinity of the sea ice margin. Caution should thus be exercised in interpreting the TEX_{86} / TEX_{86}^{L} - derived SST estimates in these regions. In spite of these differences, the compilation of our data (excluding the Arctic data) with other published data sets (n = 482) resulted in linear regressions with reasonably good fit (r^2 values > 0.7). The addition of data yields contrasting consequences to the global calibrations, i.e., improving the TEX_{86} (r^2 = 0.8 and standard error = 4.8°C, compared to 0.77 and 5.2°C for *Kim et al*. [2010]) while worsening the TEX_{86}^{L} (r^2 = 0.73 and standard error = 5.6°C, compared to 0.86 and 4°C for *Kim et al*. [2010]). The contradictory findings in the TEX_{86} and TEX_{86}^{L} core-top data complicate the effort to disentangle the underlying causes contributing

to the scatter in the data set in subpolar and polar regions. Nevertheless, better TEX_{86}-SST correlation, together with smaller TEX_{86}-derived temperature residuals in the subpolar and polar regions, lead us to conclude that TEX_{86} is a better SST proxy for application in these regions.

2.5. Acknowledgements

We would like to express our gratitude to the chief scientists, scientists and crew members on board of R/V Polarstern, R/V Sonne, R/V Akademik Boris Petrov, and R/V Ivan Kireyev for samples retrieval during various expeditions. P. Masqué and P. Cámara are thanked for providing samples from the central Arctic (PS70 samples). Thanks also go to Carme Huguet for stimulating discussions that improved the data interpretation. A SCAR Fellowship 2010/2011 is acknowledged for financially supporting the scientific stay of S.L. Ho at the Universitat Autònoma de Barcelona. POLMAR Graduate School (Helmholtz Association) is acknowledged for funding S.L. Ho's PhD study at the Alfred Wegener Institute for Polar and Marine Research (Bremerhaven).

Chapter 3: Sea surface temperature variability in the Pacific sector of the Southern Ocean over the past 700 kyr

Sze Ling Ho[1*], Gesine Mollenhauer[1], Frank Lamy[1], Alfredo Martínez-Garcia[2], Mahyar Mohtadi[3], Rainer Gersonde[1], Dierk Hebbeln[3], Samuel Nunez-Ricardo[4,5], Antoni Rosell-Melé[6,7], Ralf Tiedemann[1]

[1]Alfred Wegener Institute for Polar and Marine Research, P.O.Box 12 01 61, 27515 Bremerhaven, Germany. [*Corresponding author: Sze.Ling.Ho@awi.de]
[2]Geological Institute, Swiss Federal Institute of Technology Zürich, NO G 55, Sonneggstrasse 5, CH-8092 Zürich, Switzerland.
[3]MARUM-Center for Marine Environmental Sciences, University of Bremen, Leobener Strasse, D-28359 Bremen, Germany.
[4]Department of Zoology, Facultad de Ciencias Naturales y Oceanográficas, Universidad de Concepción, Casilla 160-C, 4070386 Concepción, Chile.
[5]Presently at Programa de Biología, Facultad de Ciencias Básicas, Universidad del Magdalena, Cra. 32, No. 22-08, P.O.Box 2-121630, Santa Marta D.T.C.H., Colombia.
[6] Institució Catalana de Recerca i Estudis Avançats, Barcelona, Catalonia, Spain.
[7] Also at Institut de Ciència i Tecnologia Ambientals, Universitat Autònoma de Barcelona, 08193 Bellatera, Spain.

(In press in Paleoceanography)

3.0. Abstract

In spite of the important role played by the Southern Ocean in global climate, the few existing paleoceanographic records in the east Pacific sector do not extend beyond one glacial-interglacial cycle, hindering circumpolar comparison of past sea surface temperature (SST) evolution in the Southern Ocean. Here we present 3 alkenone-based Pleistocene SST records from the subantarctic and subtropical Pacific. We use a regional core-top calibration data set to constrain the choice of calibrations for paleo SST estimation. Our core-top data confirm that the alkenone-based U^{K}_{37} and $U^{K'}_{37}$ values correlate linearly with the SST, in a similar fashion as the most commonly used laboratory culture-based calibrations even at low temperatures (down to ~1°C), rendering these calibrations appropriate for application in the subantarctic Pacific. However, these alkenone indices yield diverging temporal trends in the Pleistocene SST records. Based on the better agreement with $\delta^{18}O$ records and other SST records in the subantarctic Southern Ocean, we propose that the U^{K}_{37} is a better index for SST reconstruction in this region than the more commonly used $U^{K'}_{37}$ index. The U^{K}_{37}-derived SST records suggest glacial cooling of ~8°C and ~4°C in the subantarctic and subtropical

Pacific, respectively. Such extent of subantarctic glacial cooling is comparable to that in other sectors of the Southern Ocean, indicating a uniform circumpolar cooling during the Pleistocene. Furthermore, our SST records also imply massive equatorward migrations of the Antarctic Circumpolar Current (ACC) frontal systems and an enhanced transport of ACC water to lower latitudes during glacials by the Peru-Chile Current.

3.1. Introduction

The Southern Ocean plays a key role in global climate via its influence in the meridional overturning circulation [*Marshall and Speer*, 2012] and the global carbon cycle [*Fischer et al.*, 2010]. Knowledge of past changes in this ocean is therefore essential for a better understanding of its mechanistic link to the global climate, and ultimately contributes to improving the prediction of future climate change via modeling efforts. In this regard, sea surface temperature (SST), as the interface between the ocean and the atmosphere, is an indispensable boundary parameter in driving global climate models. Our present understanding of Pleistocene SST evolution in the Southern Ocean is mostly derived from sediment records in the Atlantic sector [*Martínez-Garcia et al.*, 2009; *Schneider-Mor et al.*, 2008], the Indian sector [*Howard and Prell*, 1992] and the Southwest Pacific [*Pahnke et al.*, 2003; *Schaefer et al.*, 2005]. The eastern Pacific sector of the Southern Ocean, on the other hand, is a less studied region. The few existing high-resolution marine archives spanning one glacial cycle off Chile at ODP Site 1233 (41°S) indicate a dramatic equatorward shift (7-10°) of the Southern Ocean current systems [*Verleye and Louwye*, 2010] and substantial glacial cooling of 5 to 7°C based on a coccolithophorid transfer function and alkenones [*Kaiser et al.*, 2005; *Lamy et al.*, 2004; *Saavedra-Pellitero et al.*, 2011]. Further south at 53°S, an alkenone-based SST record off the Strait of Magellan [*Caniupán et al.*, 2011] displays glacial cooling of up to ~8°C. Meanwhile, a time-slice study of the LGM at the East Pacific Rise using a foraminiferal transfer function indicates a smaller amplitude of glacial-interglacial SST changes of 2 to 5°C between 48°S and 57°S [*Luz*, 1977]. The few South Pacific data in a circumpolar compilation from the subantarctic and the Antarctic zones of the Southern Ocean based on siliceous microfossil records [*Gersonde et al.*, 2005] suggest less severe glacial cooling (~1.5°C) in the Pacific compared to the other sectors during the Last Glacial Maximum (LGM). Notably, all these records do not extend beyond the last two glacial-interglacial cycles, hindering the comparison of temperature evolution in different sectors of

the Southern Ocean and Antarctica on orbital time-scales. The lack of paleo SST records in the subantarctic Pacific also precludes the examination of the SST gradients between low and high latitudes, from which the latitudinal migration of the oceanic frontal systems and the advection of the vigorous eastern boundary current, i.e., the Peru-Chile Current (PCC), could be inferred. The transport of subantarctic cold water by the PCC to the tropics could influence the SST in the cold tongue especially during glacial periods, as demonstrated by foraminiferal census data and a simple heat model [*Feldberg and Mix*, 2002, 2003].

For the evaluation of the SST gradient, it would be ideal if the individual SST records were derived from the same proxy and calibration in order to minimize the discrepancy that might arise from dissimilar habitat depth and/or sensitivity of biological proxies to environmental changes. In this work, we employ the most commonly applied organic geochemical SST proxy, i.e., the alkenone paleothermometry. It is based on the relative distribution of di-, tri- and tetra-unsaturated long-chain alkenones consisting of 37 carbon atoms, generally known as $C_{37:2}$, $C_{37:3}$ and $C_{37:4}$, respectively. The degree of alkenone unsaturation is a function of growth temperature of the precursor, i.e., haptophyte algae. An index known as U^{K}_{37} (= [$C_{37:2} - C_{37:4}$] / [$C_{37:2} + C_{37:3} + C_{37:4}$]) has been proposed to quantify the degree of unsaturation [*Brassell et al.*, 1986], and it was later simplified to $U^{K'}_{37}$ (= [$C_{37:2}$] / [$C_{37:2} + C_{37:3}$]) since the $C_{37:4}$ alkenones are often absent in open ocean sediments where overlaying SSTs are higher than 12°C [*Prahl and Wakeham*, 1987]. Over the years, work has been mainly focused on the simplified $U^{K'}_{37}$ index, which is applicable to most parts of the global ocean. However, alkenone-derived glacial SSTs that are warmer than those of the interglacial have been observed in the Sea of Okhotsk [*Harada et al.*, 2006] and the Northeast Atlantic [*de Vernal et al.*, 2006; *Rosell-Melé and Comes*, 1999], raising doubts about the applicability of alkenone paleothermometry at high latitudes. Another potential caveat, i.e., the non-linearity of the relationship of $U^{K'}_{37}$ index and SST at low temperatures (<6°C), has also been suggested [*Conte et al.*, 2006; *Rosell-Melé*, 1998; *Rosell-Melé et al.*, 1994; *Sikes and Volkman*, 1993]. It is still debatable whether U^{K}_{37} or $U^{K'}_{37}$ is the more appropriate SST proxy at high latitudes due to the lack of data in this region, especially in the Southern Ocean.

In this study we revisit the alkenone paleothermometry at the lower end of the temperature range and assess the applicability of the alkenone indices by using regional surface sediments. We present three SST records to investigate the temporal pattern and the amplitude of the paleo SST evolution in the South Pacific along the latitudinal range of the PCC spanning both subtropical and subantarctic oceanic zones. Based on our SST

reconstruction, we infer the latitudinal migration of the oceanic fronts and discuss their paleoclimatic implications.

3.2. Oceanographic setting

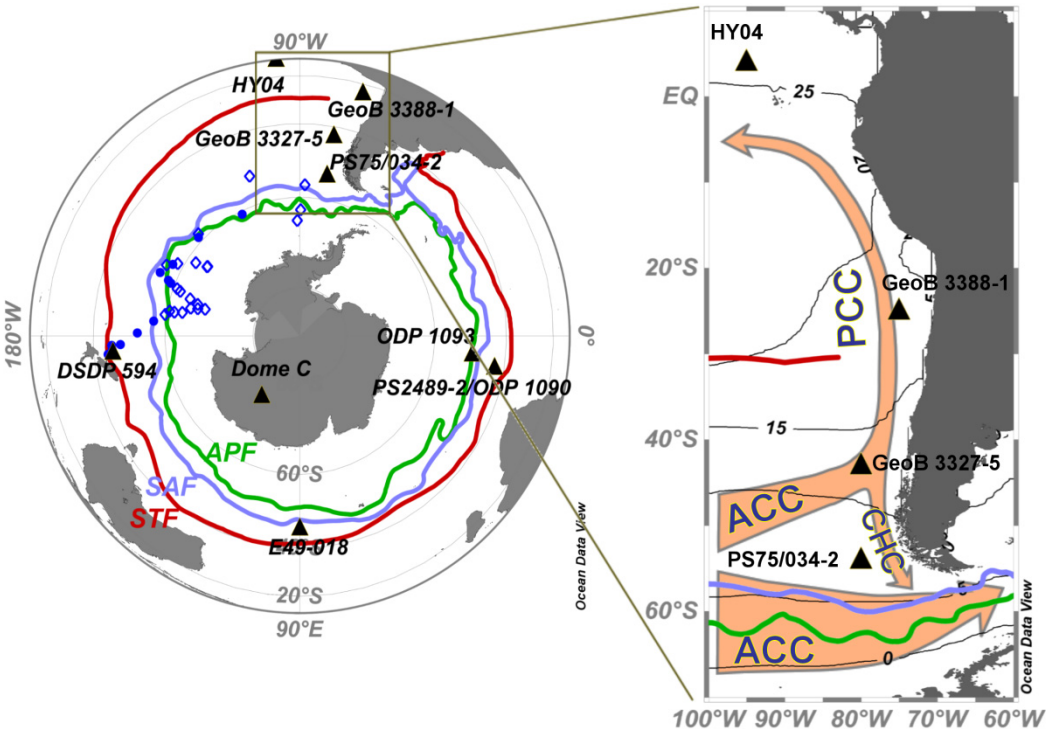

Figure 3.1: Location of sites and major oceanic currents discussed in this work. For the purpose of this study, the subantarctic region is defined as the waters between the Subtropical Front and the Subantarctic Front. Blue circles denote the sites of the core-top data in the regional alkenone unsaturation calibration, while blue open diamonds denote the sites where alkenones were below detection limit. Black triangles denote the sites of SST records used for discussion. In addition to the newly presented records (GeoB 3388-1, GeoB 3327-5 and PS75/034-2), we also include several previously published SST records from the tropics (HY04 [*Horikawa et al*., 2010] and the Southern Ocean (DSDP 594 [*Schaefer et al*., 2005], E47-018 [*Howard and Prell*, 1992], PS2489-ODP Site 1090 [*Martínez-Garcia et al.*, 2009] and ODP Site 1093 [*Schneider-Mor et al.*, 2008]), in addition to the Antarctic temperature record at EPICA Dome C [*Jouzel et al*., 2007]. Thin black lines indicate the annual mean isotherms in degree Celsius (°C) derived from the World Ocean Atlas 2009 (WOA09). Orange arrows indicate major surface currents, and colored lines illustrate the oceanic frontal system [after *Orsi et al.*, 1995]. Abbreviations: WSI = winter sea ice extent; APF = Antarctic Polar Front; SAF = Subantarctic Front; STF = Subtropical Front; PCC = Peru-Chile Current; ACC = Antarctic Circumpolar Current; CHC = Cape Horn Current.

The Peru-Chile Current (PCC; also known as Peru Current, Chile-Peru Current, and Humboldt Current) and the Antarctic Circumpolar Current (ACC) are the main features of the surface circulation in the Southeast Pacific (Figure 3.1). The eastward flowing ACC is driven

by the intense mid-latitude Southern hemisphere westerly winds (Westerlies). Thus, its latitudinal migration is closely related to the wind forcing [*Orsi et al.*, 1995]. The circumpolar transport of the ACC is approximately 107 Sv, with most of the transport occurring in the Subantarctic Front (SAF) and the Antarctic Polar Front (APF) [*Cunningham et al.*, 2003]. The impingement of the northern part of the ACC onto the South American continent leads to a bifurcation around 43°S, yielding a vigorous equatorward branch (PCC) and a weaker poleward branch (Cape Horn Current, CHC) [*Strub et al.*, 1998]. The PCC flows northward along South America and is deflected away from the coast at around 5°S, feeding the cold PCC water into the South Equatorial Current which flows westward as the equatorial cold tongue between 10°S and 4°N [*Wyrtki*, 1965]. Meanwhile, the CHC moves along the coastal region of southernmost Chile, mixing the subantarctic water with low salinity regional water and transporting this modified ACC water to the Atlantic Ocean via the Drake Passage [*Chaigneau and Pizarro*, 2005]. The Westerlies shift northward in the winter as a result of seasonal fluctuations of sea ice around Antarctica [*Kidston et al.*, 2011]. Modern day austral winter is also marked by more vigorous advection of cold water towards the tropics and a larger temperature gradient between low and high latitudes.

Our South Pacific core-top sites are located between the Subtropical Front (STF) and the APF, where the modern day annual mean temperatures of the overlaying surface waters are in the range of ~1 to ~12°C. Our long piston core sites are well suited for studying the open ocean PCC, as they are beyond the direct influence of the intense coastal upwelling that is confined within 50-60 km of the shoreline [*Strub et al.*, 1998]. Sites GeoB 3327-5 and PS75/034-2 are located at the northern extent of the ACC, in sensitive regions where the latitudinal movement of the ACC is expected to be registered. The southernmost site PS75/034-2 is located ~7° and ~9° north of the modern day mean location of the SAF and the APF, respectively. Site GeoB 3388-1 lies within the flowpath of the PCC, thus the SST changes here reflect the extent of the cold water advection by the PCC.

3.3. Materials and Methods

3.3.1. Materials

We analyzed 34 core-top samples (**Figure 3.1**) recovered by multicorer from the Pacific sector of the Southern Ocean between the STF and the APF, but alkenones were

detected at only 13 sites (see **Table 3.1** for coordinates). Two piston cores in the subantarctic Pacific sector of the Southern Ocean and one piston core from the subtropical South Pacific were analyzed in this study (**Figure 3.1**). Core GeoB 3327-5 (43°14'S, 79°59'W, 3534 m water depth, 900 cm length) and core GeoB 3388-1 (25°13'S, 75°31'W, 3558 m water depth, 710 cm length) were retrieved during the R/V Sonne cruise 102 [*Hebbeln et al.*, 1995], while core PS75/034-2 (54°22'S, 80°05'W, 4425 m water depth, 1808 cm length) was collected during the Alfred Wegener Institute expedition ANT XXVI/2 with R/V Polarstern [*Gersonde*, 2011]. The sediments of core GeoB 3327-5 alternate between clayey foraminifera and clayey foraminifera nannofossil ooze, while core GeoB 3388-1 consists of mainly nannofossil ooze. Core PS75/034-2, on the other hand, due to its location below the carbonate compensation depth, consists of mainly siliceous clay and is barren of foraminifera. The sampling intervals for core GeoB 3327-5 and GeoB 3388-1 were 5 cm throughout the core. Core PS75/034-2 was sampled every 10 cm throughout the core and every 5 cm in the section between 200 cm and 310 cm.

Table 3.1: Site information and alkenone index values of the Southern Ocean core-top samples retrieved via multicoring.

Site	Longitude	Latitude	WOA09 Annual mean SST (°C)	U^{K}_{37}	$U^{K'}_{37}$
PS75/034-1	80.09 °W	54.37 °S	6.71	0.213	0.256
PS75/104-2	174.53 °E	44.77 °S	11.74	0.371	0.411
PS75/099-1	177.27 °E	48.26 °S	9.24	0.294	0.294
PS75/072-3	151.22 °W	57.56 °S	1.89	0.007	0.086
PS75/082-2	158.36 °W	59.04 °S	1.52	-0.012	0.081
PS75/098-6	179.01 °W	52.97 °S	7.47	0.217	0.275
PS75/105-1	174.62 °E	44.41 °S	11.74	0.486	0.486
PS75/095-6	174.43 °W	57.02 °S	4.95	0.178	0.214
PS75/101-2	175.88 °E	45.81 °S	11.12	0.296	0.324
PS75/080-2	157.64 °W	58.18 °S	2.08	-0.021	0.084
PS75/053-1	115.98 °W	60.77 °S	3.01	0.016	0.085
PS75/076-1	156.14 °W	55.53 °S	4.68	0.089	0.219
PS75/063-2	135.62 °W	58.90 °S	2.18	-0.007	0.093

3.3.2. $\delta^{18}O$ measurement on foraminifera

A Finnigan MAT 251 mass spectrometer coupled with a Kiel device inlet system was used to measure the $\delta^{18}O$ composition of planktic *Neogloboquadrina pachyderma* (dextral coiling) from the >150 µm size-fraction and benthic *Cibicides spp.* from the >212 µm size-fraction for core GeoB 3327-5. The measurements were performed on approximately 5-10

individual tests. For all stable isotope measurements a working standard was used, which was calibrated against VPDB (Vienna Pee Dee Belemnite) by using the NBS 19 standard. Consequently, all isotopic data are relative to the PDB standard. Long-term analytical standard deviation is ± 0.07 ‰ (Isotope Laboratory, Faculty of Geosciences, University of Bremen).

3.3.3. Alkenone analysis

Sample preparation and alkenone analysis of cores GeoB 3327-5 and GeoB 3388-1 were carried out according to the procedure described by *Müller et al* [1998]. About 3 – 14 g of freeze-dried and ground sediment samples were subjected to three times of sonication in mixtures of methanol and dichloromethane with decreasing polarity. The supernatant was then rinsed with deionized water and sodium sulfate, before being concentrated and passed through a short bed of silica (Bond-Elut silica cartridge, Varian) to purify the fraction that contained the alkenones. The fraction was then saponified to remove esters. The quantification of alkenones was achieved using gas chromatography on an HP 5890, equipped with a 60 m fused silica capillary column (DB-5 MS, Agilent) and a flame ionization detector. The oven temperature was programmed to rise from 50 to 250°C at a rate of 25°C/min, then to 290°C at a rate of 1°C/min, followed by 26 min of isothermal period, before being ramped up to 310°C at a rate of 30°C/min and held constant for 10 min. Replicate analyses of laboratory internal reference sediment suggest analytical errors of ~0.5°C for both alkenone indices (U^{K}_{37} and $U^{K'}_{37}$).

Piston core PS75/034-2 was analyzed at the Alfred Wegener Institute (Bremerhaven). The extraction of organic compounds was accomplished using a Dionex ASE-200 pressurized solvent extractor, with a mixture of methanol and dichloromethane in the ratio of 1:9. Similar to the treatment for the GeoB cores, the total extract was separated into 3 fractions via silica gel fractionation using hexane, DCM and methanol, respectively. The fraction (eluted with DCM) containing the alkenones was then concentrated and analyzed by gas chromatography on an HP 6890 fitted with a flame ionization detector and a 60 m DB-1 MS column (Agilent). The initial temperature in the oven was set to 60°C. After the injection of samples, the temperature in the oven was ramped up to 150°C at a rate of 20°C/min, followed by a reduced rate of heating at 6°C/min until the final temperature of 320°C was achieved and held constant for 40 min. The alkenone fraction of this sediment core was pure enough for

quantification without saponification. We did not observe any systematic differences in the alkenone index values between saponified and untreated extracts in the six samples we tested. They agreed within ±0.015 units and ±0.012 units for U^{K}_{37} and $U^{K'}_{37}$, respectively, corresponding to ±0.47°C and ±0.37°C using the culture calibrations of *Prahl et al.* [1998]. Reproducibility of the instrument is estimated to be 0.17°C based on replicate analysis of alaboratory *E. huxleyi* culture extract.

South Pacific core-top samples were subjected to microwave-assisted extraction, followed by compound class fractionation using a Thermo Surveyor HPLC system equipped with a Lichrosphere Silicon dioxide column, according to the methods described by *Fietz et al.* [2011]. The fraction containing alkenones (eluted with DCM) was saponified to remove co-eluting esters, prior to analysis by gas chromatography (same GC system used for the alkenone analysis of piston core PS75/034-2 described above).

The concentrations of sediment extracts were adjusted such that the amounts of alkenones injected for each measurement were above threshold values (>5-10 ng) to avoid unjust bias due to low concentrations. The threshold values were previously suggested by *Rosell-Melé et al.* [1995], *Sonzogni et al.* [1997] and *Villanueva and Grimalt* [1996].

3.3.4. Alkenone-based indices and calibrations

The identification of alkenones was achieved by comparing chromatographic retention times of the samples with those of standards. The alkenone-based index (U^{K}_{37} and $U^{K'}_{37}$) values were calculated according to the previously proposed equations given in **Section 3.1**. In order to compare these two alkenone indices in downcore reconstructions and to compare SST records spanning the tropics and the subantarctic Pacific, we need U^{K}_{37} and $U^{K'}_{37}$ calibrations that are based on a common data set and covering the largest possible temperature range. For this purpose, we opted to convert the index values into sea surface temperature using the widely used *E. huxleyi* culture-based calibrations proposed by *Prahl et al.* [1988], i.e., $U^{K}_{37} = 0.04\ T - 0.104$ ($r^2 = 0.98$) and $U^{K'}_{37} = 0.034\ T + 0.039$ ($r^2 = 0.99$), the latter being statistically identical to those based on global core-top compilations [*Conte et al.*, 2006; *Müller et al.*, 1998].

3.3.5. SST gradient calculation

We calculated the SST gradient along the latitudinal range of the PCC using alkenone-derived SSTs. We preferred the U^{K}_{37} index over the commonly used simplified version that excludes the $C_{37:4}$ alkenone, i.e., $U^{K'}_{37}$ (see justification in **Section 3.5.1**). Considering the complexity of the hydrography in the eastern equatorial Pacific (EEP), we selected an open-ocean site HY04 (4°02'N 95°03'W, *Horikawa et al.* [2010]) that is beyond the influence of the east Pacific cold tongue and the Peru coastal upwelling to examine the equator-to-pole SST gradients. A recent core-top calibration study of *Kienast et al.* [2012] suggests that the alkenone unsaturation in the open ocean EEP conforms to the established global core-top calibrations. For the sake of consistency in the comparison, we recalculated the $U^{K'}_{37}$-derived SST estimates at site HY04 using the laboratory culture-based calibration of *Prahl et al.* [1988], assuming that $C_{37:4}$ alkenones are absent here. This results in similar U^{K}_{37} and $U^{K'}_{37}$ values. The assumption is justified by the fact that $C_{37:4}$ alkenones are numerically significant at growth temperatures below 15°C [*Prahl et al.*, 1988], and that the difference between U^{K}_{37} and $U^{K'}_{37}$ is only significant at ~10°C [*Rosell-Melé*, 1998]. Indeed, the recalculated SST estimates based on the U^{K}_{37} index are within ±0.5°C of the original $U^{K'}_{37}$-derived SST record reported in the literature (**Figure 3.6**) with exactly the same temporal trends. The SST records were re-sampled every 2 kyr for the calculation of the gradients between sites.

3.4. Results

3.4.1. Stratigraphy

In order to obtain a consistent stratigraphic framework for all records in the SST gradients calculation, we tuned all available benthic $\delta^{18}O$ records to the global benthic $\delta^{18}O$ stack LR04 [*Lisiecki and Raymo*, 2005] using the software package AnalySeries 2.0 [*Paillard et al.*, 1996]. For this purpose, we revised the published age model of GeoB 3388-1 [*Mohtadi et al.*, 2006] which was previously aligned to the orbitally-tuned ODP Site 677 [*Shackleton et al.*, 1990]. Overall, the differences between the revised and the original age models are minimal, with one exception during the time interval between 400 kyr and 500 kyr, especially at the termination of MIS 12. The linear sedimentation rates (LSR) at site GeoB 3388-1 fluctuate between 2.2 and 0.3 cm kyr^{-1}, with an average of less than 1 cm kyr^{-1} over the past 700 kyr (**Figure 3.2**).

The age model of core GeoB 3327-5 was similarly generated via graphical tuning of the *Cibicides spp.* benthic $\delta^{18}O$ record to the LR04 global benthic stack. According to the age model, the record extends back to 513 kyr and spans the past five glacial-interglacial cycles (**Figure 3.2**). Average sedimentation rate is 2.6 cm kyr^{-1} and the values range between 0.7 cm kyr^{-1} and 4.4 cm kyr^{-1} without any drastic fluctuation. The only exception is a brief interval during MIS 7, where sedimentation rates reach about 10 cm kyr^{-1}, which may suggest redeposition. However, there is no lithological indication for, e.g., turbidites during this interval. A lack of chronological tie points for MIS 9 and part of MIS 8 arises as a result of poor carbonate preservation.

In core PS75/034-2 carbonate preservation is poor, thus a benthic foraminifera-based $\delta^{18}O$ record could not be obtained. The attempt to use radiolarian biofluctuation for chronological control [*Hays et al.*, 1976] has also failed due to low abundance of *Cycladophora davisiana* (0 – 2.5% throughout the core) [*Cortese*, unpublished data]. There are no well-dated marine records in the subantarctic Pacific that would provide a reference chronology for graphical tuning of the downcore oscillations in the physical properties (e.g., lightness, major elements, magnetic susceptibility). In the absence of other alternatives, we graphically tuned the PS75/034-2 U^{K}_{37} record to the temperature evolution registered in the EPICA ice core at Dome C, Antarctica [*Jouzel et al.*, 2007], based on the updated chronology EDC3 [*Parrenin et al.*, 2007]. Justification for the preference of the U^{K}_{37} index over the $U^{K'}_{37}$ index is outlined in **Section 3.5.2**. The EPICA ΔT record was adjusted by a 15-point moving average smoothing prior to the graphical alignment to accommodate the much lower temporal resolution in core PS75/034-2. Our EDC3-derived age model is supported by the shipboard biostratigraphy based on diatom zonation (*Thalassiosira lentiginosa*) [*Zielinski and Gersonde*, 2002], i.e., ~178 kyr and ~350 kyr in our EDC3-based chronology correspond to the boundaries of MIS 6/7 and 9/10 as indicated by the biostratigraphy. The fairly uniform linear sedimentation rate throughout the core (1.4 – 3.5 cm kyr^{-1}) (**Figure 3.2**) and the resemblance in the general patterns between core PS75/034-2 and other Southern Ocean records (**Figure 3.5**) provide additional confidence in the stratigraphic framework. We adopted the original age model of core HY04 [*Horikawa et al.*, 2010], which is based on visual alignment of the benthic foraminiferal $\delta^{18}O$ to the orbitally-tuned ODP Site 677 [*Shackleton et al.*, 1990] for the upper 420 kyr, and the lower part of the record to the LR04 global stack. There is no significant temporal offset between the upper 420 kyr of this $\delta^{18}O$ record (on current time scale) and the LR04 benthic stack.

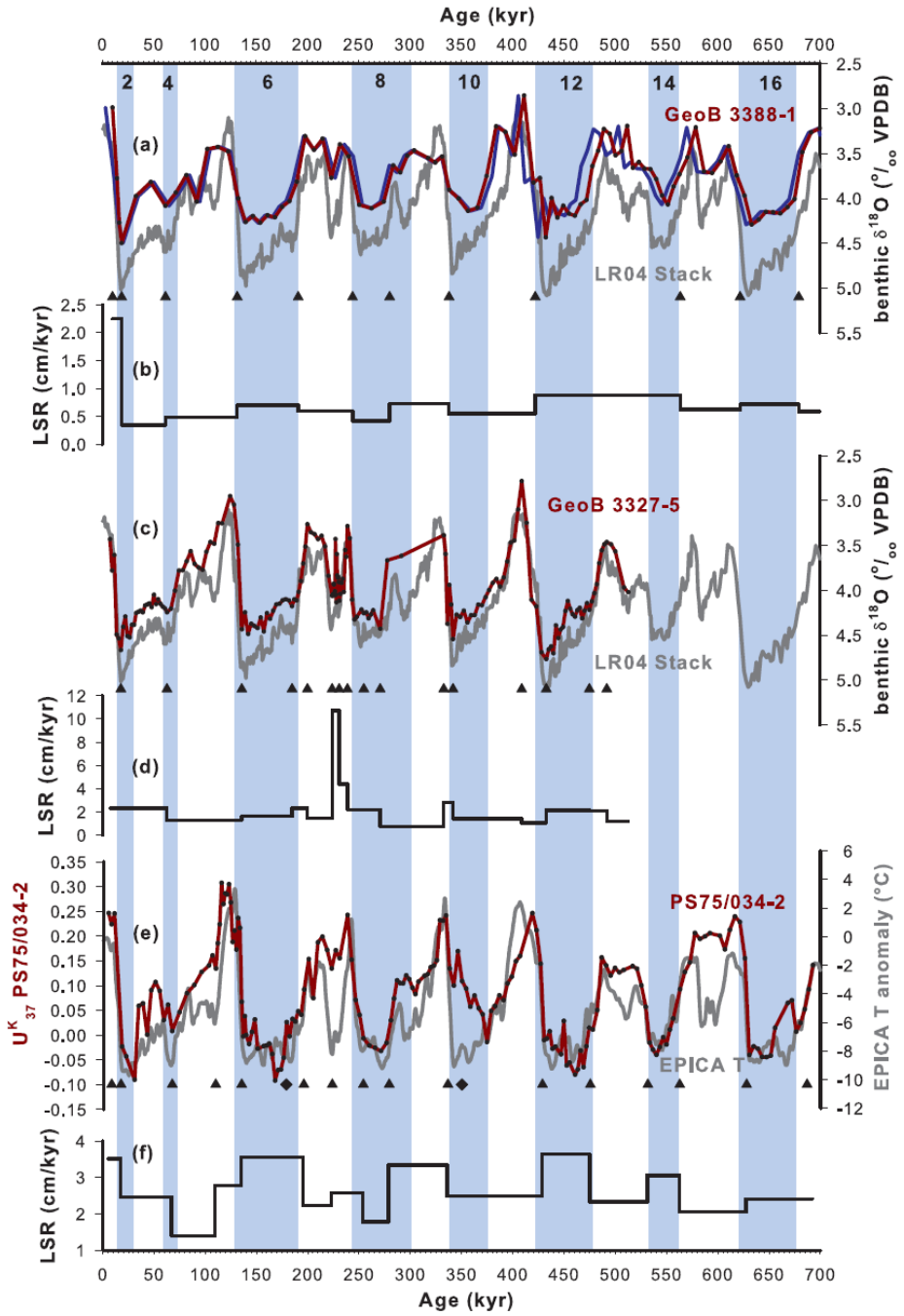

Figure 3.2: Age models and linear sedimentation rates at core sites GeoB 3388-1, GeoB 3327-5 and PS75/034-2. Shaded bars indicate glacial intervals, and the black numbers in the bars represent the marine isotope stages. Black triangles illustrate the stratigraphic tie points while the black diamonds mark the shipboard biostratigraphic points based on diatom zonation. (a) Stratigraphic framework for core GeoB 3388-1 was revised by graphical tuning of the benthic foraminiferal $\delta^{18}O$ record (red curve) to the benthic $\delta^{18}O$ stack LR04 (grey curve) [*Lisiecki and Raymo*, 2005]. The previously published age model [*Mohtadi et al*., 2006] is represented by the blue curve. (b) Linear sedimentation rate at site GeoB 3388-1 derived using the stratigraphic tie points based on the benthic $\delta^{18}O$ record. (c) Stratigraphic framework for core GeoB 3327-5 was established by graphical tuning of the benthic foraminiferal (*Cibicides spp*.) $\delta^{18}O$ record (red curve) to the benthic $\delta^{18}O$ stack LR04 (gray curve) [*Lisiecki and Raymo*, 2005]. (d) Linear sedimentation rate at site GeoB 3327-5 based on the tuned benthic $\delta^{18}O$ record. (e) Stratigraphic framework for core PS75/034-2 was established by graphical tuning of the U^{K}_{37} record (red curve) to the smoothed (15-points running average) EPICA ΔT record at Dome C, Antarctica [*Jouzel et al.*, 2007; *Parrenin et al.*, 2007] (gray curve). (f) Linear sedimentation rate at site PS75/034-2 based on tuning to the EPICA ΔT record.

3.4.2. South Pacific core-top alkenone calibrations

As shown in **Figure 3.3**, both U^{K}_{37} and $U^{K'}_{37}$ indices correlate linearly to annual mean WOA09 SST (with r^2 values of 0.94 and 0.93, respectively) for the temperature range of 1.5 to 11.7°C. These regressions are identical within estimation error to the extrapolated *Prahl et al*. [1988] calibrations below 8°C.

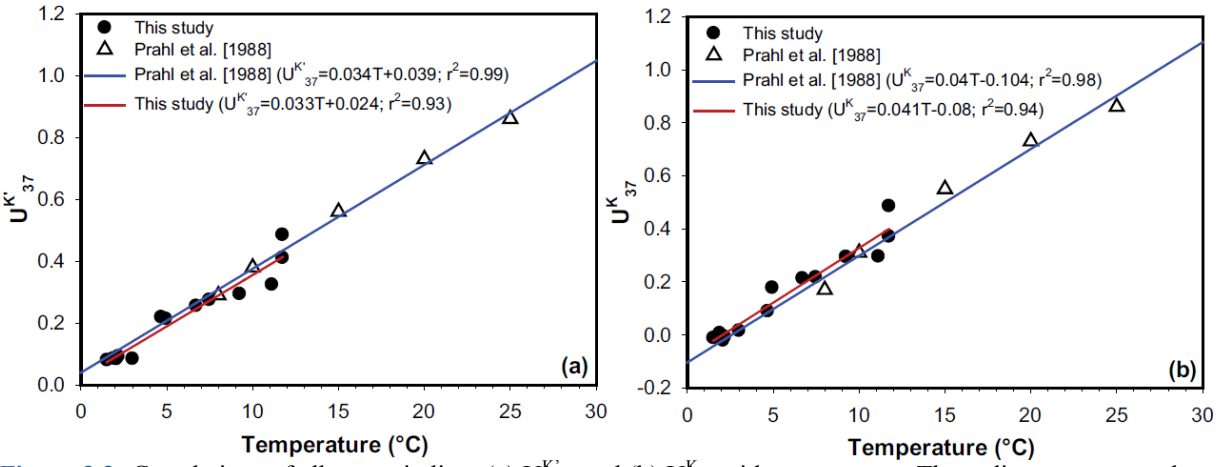

Figure 3.3: Correlations of alkenone indices (a) $U^{K'}_{37}$ and (b) U^{K}_{37} with temperature. The sediment core-top data were calibrated against the WOA09 annual mean SST, while the *E. huxleyi* culture data of *Prahl et al*. [1988] plotted against the growth temperature as reported in the original publication. Blue line illustrates the linear regressions proposed by *Prahl et al*. [1988], with extrapolation for temperatures below 8°C. Red line denotes our South Pacific core-top calibration (through the black circles).

3.4.3. Downcore SST estimates and planktic $\delta^{18}O$ values

3.4.3.1. Core GeoB 3388-1

At subtropical site GeoB 3388-1, the $U^{K'}_{37}$-derived SSTs for the past 700 kyr range between 15°C and 21°C (**Figure 3.4a**). The index suggests that SST during MIS 12 is slightly colder (~2°C) than the average glacial SST, while MIS 13 is the coolest interglacial. Meanwhile, the U^{K}_{37}-inferred SSTs at site GeoB 3388-1 are in the range of 16°C to 22°C. The amplitudes of glacial/interglacial SST variations in both U^{K}_{37}- and $U^{K'}_{37}$-derived records are ~6°C.

3.4.3.2. Core GeoB 3327-5

The $U^{K'}_{37}$-SST estimates are between ~5°C and ~14°C over the past 513 kyr at site

GeoB 3327-5 (**Figure 3.4c**). While there is not much difference in the warmth of interglacials, the $U^{K'}_{37}$-inferred estimates suggest strong variability in the severity of glacials, with SSTs from ~5°C during MIS 10 to ~10°C during MIS 6. On the other hand, the U^{K}_{37}-derived glacial-interglacial SST oscillations at site GeoB 3327-5 range between ~8°C and ~16°C, without any substantial long-term trend in glacial cooling and interglacial warming. Alkenones in the top of a multicore at this site register U^{K}_{37}- and $U^{K'}_{37}$-inferred SST estimates of 15.4°C and 13.9°C, respectively.

The $\delta^{18}O$ values of planktic dextral-coiling *N. pachyderma* range between 1.1 to 3.1‰ (**Figure 3.4b**). There is a data gap between MIS 8 and MIS 10 because of carbonate dissolution. The $\delta^{18}O$ values during MIS 11 are more enriched than those in other interglacials. Some abrupt shifts towards more depleted values are recorded during MIS 11 and 12.

3.4.3.3. Core PS75/034-2

The overall SST variability suggested by the $U^{K'}_{37}$ index at site PS75/034-2 is between ~1ºC and ~8ºC, resulting in a glacial-interglacial amplitude of up to ~7°C (**Figure 3.4d**). The $U^{K'}_{37}$ index indicates that MIS 10 is the coldest glacial, while MIS 5 is the warmest interglacial. During the interval between MIS 16 and MIS 12, the $U^{K'}_{37}$-inferred glacial-interglacial cycles are not pronounced due to substantially smaller amplitude of SST oscillations (~2°C compared to ~7°C after MIS 12). The $U^{K'}_{37}$-derived SST estimates for these glacial intervals (especially MIS 16) are as warm as the SST estimates for the subsequent interglacial intervals. The $U^{K'}_{37}$ index suggests a pervasive long-term trend in the glacial cooling, i.e., the glacial SSTs decrease from MIS 16 to MIS 10, and increase thereafter to MIS 6, followed by a colder MIS 2. On the other hand, the U^{K}_{37}-derived SSTs at site PS75/034-2 range between ~1°C and ~10°C over the past 700 kyr (**Figure 3.4d**). According to the U^{K}_{37}-derived SST estimates, the severity of glacial SSTs does not vary substantially at site PS75/034-2. MIS 10 is slightly warmer (~2°C) than the other glacial periods, while MIS 5 and MIS 13 stand out as the warmest and coolest interglacials, respectively. The SST estimates inferred from the $U^{K'}_{37}$ and the U^{K}_{37} indices for the top of a multicore at this site are 6.4°C and 7.9°C, respectively.

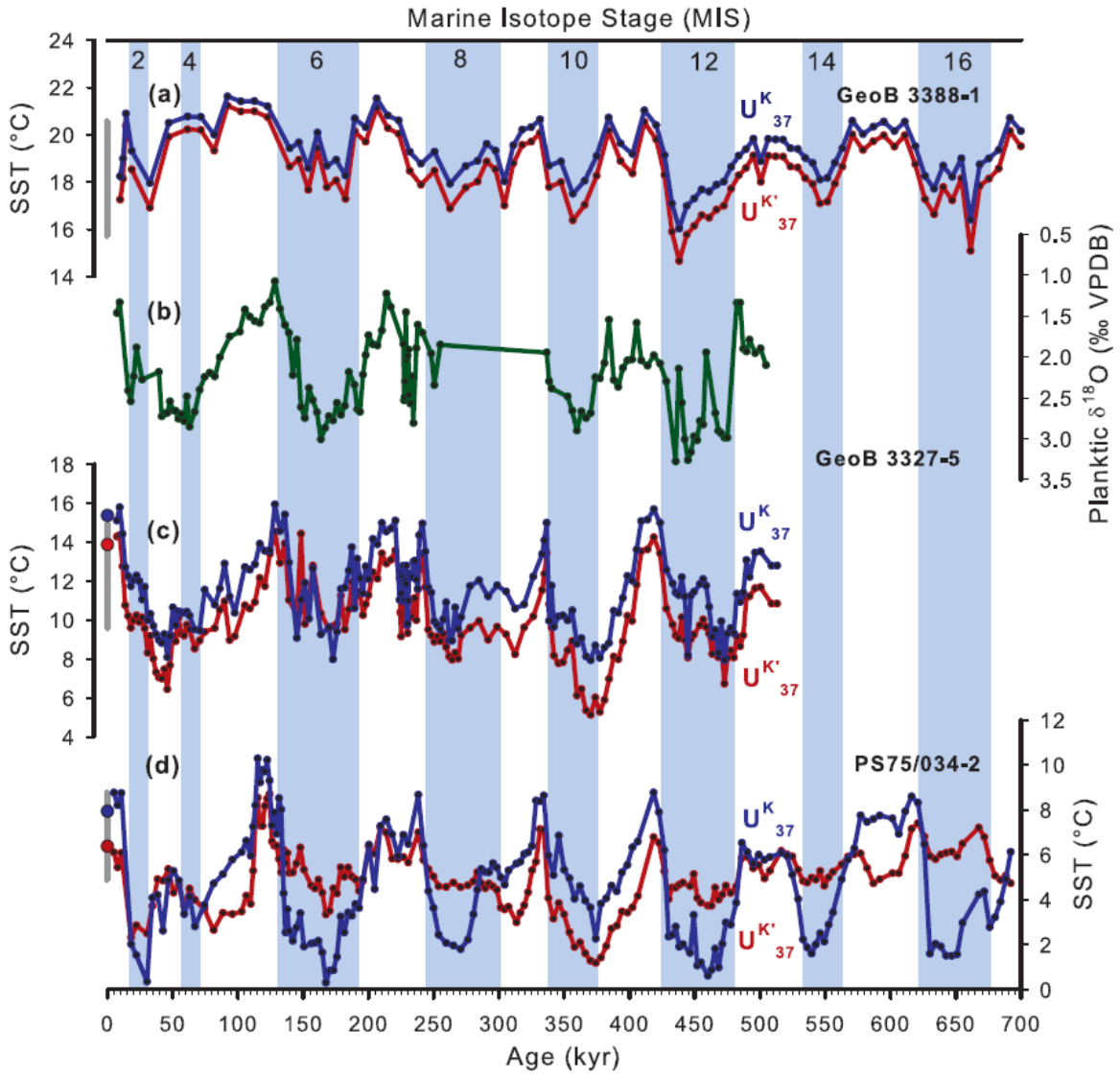

Figure 3.4: Planktic $\delta^{18}O$ and alkenone-based SST records. Shaded bars indicate glacial intervals and the black numbers in the bars represent the marine isotope stages. Gray bars denote modern day maximum and minimum SSTs derived from WOA09. (a) SST records derived from alkenone based indices, i.e., U^{K}_{37} (blue) and $U^{K'}_{37}$ (red) at site GeoB 3388-1. (b) Planktic $\delta^{18}O$ of dextral-coiling *N. pachyderma* at site GeoB 3327-5. Poor carbonate preservation result in a data gap from MIS 8 to MIS 9. (c) SST records derived from alkenone based indices, i.e., U^{K}_{37} (blue) and $U^{K'}_{37}$ (red) at site GeoB 3327-5. Filled circles indicate core-top data at the same site. (d) SST records derived from alkenone based indices, i.e., U^{K}_{37} (blue) and $U^{K'}_{37}$ (red) at site PS75/034-2. Filled circles indicate core-top data at the same site.

3.5. Discussion

3.5.1. Alkenone-based calibrations for application in the subantarctic Pacific

Here we use the *E. huxleyi* culture-based alkenone calibrations from *Prahl et al.* [1988] for SST reconstruction. While the $U^{K'}_{37}$-SST relationship of this calibration has been confirmed by global core-top calibrations [*Conte et al.*, 2006; *Müller et al.*, 1998] with

extensive data sets encompassing diverse biogeographic provinces and a wide temperature range, the U^{K}_{37}-SST correlation has not been calibrated globally. Thus, the U^{K}_{37}-SST relationship outside the calibration range (T<8°C) is unknown except for the North Atlantic and the Nordic Sea [*Bendle and Rosell-Melé*, 2004; *Bendle et al.*, 2005; *Rosell-Melé et al.*, 1994; *Rosell-Melé et al.*, 1995]. Considering the low modern SST at our southern site PS75/034-2 (WOA09 annual mean SST of 6.7°C), the paleo SST here, especially during glacials, are likely to be well below the calibrated temperature range of the culture calibration (8-25°C). To better constrain our choice of calibrations, we examine the alkenone index values in the South Pacific surface sediments and find that firstly, the linearity of both U^{K}_{37}- and $U^{K'}_{37}$-SST correlations holds even at low temperatures in the South Pacific, indicating that both indices faithfully record modern SSTs in this temperature range. Secondly, the sedimentary alkenone unsaturation-SST relationships in the South Pacific are comparable to those observed in the *E. huxleyi* culture of *Prahl et al*. [1988], rendering these culture calibrations suitable for application in this region. Indeed, the U^{K}_{37} and the $U^{K'}_{37}$ calibrations resulted in core-top SST estimates (8°C and 6°C at PS75/034-2; 15°C and 14°C at GeoB 3327-5) that are within the range of modern seasonal SSTs (see grey bars in **Figure 3.4**; 5 – 9°C at PS75/034-2 and 10 – 15°C at GeoB 3327-5). We refrain from using our own core-top calibrations for downcore reconstruction because of their limited calibration range (~1-12°C) which makes them inappropriate for the application in the subtropics for calculating the meridional SST gradients.

We note that our finding is in contrast to that of the Southern Ocean core-top calibration study of *Sikes et al*. [1997]. The better correlation in the $U^{K'}_{37}$-SST relationship (r^2 value of 0.92 compared to r^2 value of 0.76 for U^{K}_{37}-SST) led the authors to suggest that the $U^{K'}_{37}$ is the better index for paleo SST reconstruction in the Southern Ocean. Application of their calibrations at our sites yields core-top SST estimates (U^{K}_{37} and $U^{K'}_{37}$: 14°C and 9°C at PS75/034-2; 21°C and 16°C at GeoB 3327-5) that are warmer than those inferred from the *Prahl et al*. [1988] calibrations. The warm bias is especially pronounced in the U^{K}_{37}-derived estimates, which are substantially warmer than the modern day warmest month SST in WOA09 (see grey bars in **Figure 3.4**; ~9°C at PS75/034-2; ~15°C at GeoB 3327-5). These anomalously warm estimates produced by the core-top calibrations of *Sikes et al*. [1997], in addition to a good match between our South Pacific core-top calibrations and the *Prahl et al.* [1988] culture calibrations, led us to choose the latter calibrations to estimate paleo SSTs at our study sites in the subantarctic Pacific.

3.5.2. Assessing contrasting temporal trends in U^{K}_{37}- and $U^{K'}_{37}$-derived SST records

In alkenone-based SST records, the temporal trend is governed by the definition of the index, while the amplitude of downcore variation and the absolute value are determined by the calibration employed. In the subtropics (GeoB 3388-1), the SST patterns inferred from both U^{K}_{37} and $U^{K'}_{37}$ indices are similar, and their values are in agreement within 1.5°C. As discussed in **section 3.5.1**, the strong linear relationship between both the U^{K}_{37} and the $U^{K'}_{37}$ indices in the subantarctic surface sediments with the overlaying SSTs (i.e., comparable r^2 values) imply that both indices may be used to obtain paleo SST estimates in the region (**Figure 3.3**). However, downcore reconstructions yield a different picture, i.e., the indices result in contrasting subantarctic SST patterns for cores GeoB 3327-5 and PS75/034-2 (**Figure 3.4**). For the past two glacial-interglacial cycles, the $U^{K'}_{37}$–derived SSTs display a so-called Type 1 [*Schneider et al.*, 1999] alkenone SST record which is typical for the tropics and the monsoon-influenced region, characterized by a relatively warm MIS 6 and the occurrence of the coldest glacial SST in the middle or the inception of glacials. There is also a warming trend of glacials from MIS 10 to MIS 6 in these subantarctic $U^{K'}_{37}$ records. On the other hand, the U^{K}_{37}-derived SST records suggest little fluctuation in the severity of glacial intervals and the MIS 6 is as cold as other glacial intervals (a Type 3 alkenone SST record according to the definition of *Schneider et al.* [1999]), which shows more resemblance to the global ice volume oscillations documented in the benthic $\delta^{18}O$ record. The differences in temporal trends are especially clear for the time interval MIS 16 – 12 at our southernmost site PS75/034-2, during which the $U^{K'}_{37}$-derived SSTs exhibit a reduced amplitude of glacial-interglacial SST variations due to relatively warm glacials, especially MIS 16 which is as warm as interglacial MIS 11. However, the U^{K}_{37} index record suggests that the glacial SSTs during this time interval are consistent with those from other glacial intervals. Interestingly, such observations are not limited to the South Pacific. As shown in **Figure 3.5c**, dissimilar amplitudes of glacial-interglacial SST oscillations during MIS 12 – 16 are also evident in the alkenone-derived SST records at PS2489-2/ODP Site 1090 in the mid-latitudes of the South Atlantic [*Martínez-Garcia et al.*, 2009; *Martínez-Garcia et al.*, 2010], suggesting that this divergene can be found throughout the Southern Ocean south of the Subtropical Front. To determine which pattern is more realistic, we further compare our alkenone records with the planktic $\delta^{18}O$ record at the same site, and with other subantarctic SST records from other sectors of the Southern Ocean (**Figure 3.5**). Since the most outstanding divergence in the two

different alkenone SST patterns is in the long-term trend of the glacial severity (interglacial warmth is consistent), we focus our discussion on the cold intervals.

Contrary to the $U^{K'}_{37}$–based SST records, the planktic $\delta^{18}O$ records in the South Pacific (GeoB 3327-5) and the South Atlantic (PS2489-2 / ODP Site 1090, see *Venz and Hodell* [2002]) suggest minor oscillations in glacial severity. Apart from global ice volume and SST, the planktic $\delta^{18}O$ records are also influenced by changes in sea surface salinity (SSS). However, given the lack of any major freshwater sources in the vicinity of sites GeoB 3327-5 and PS2489-2 / ODP Site 1090, large perturbations to the SSS at these sites over the past 700 kyr are unlikely. SSS here might be driven by an enhanced influence of low SST and low SSS polar water mass during glacials. However, in such a scenario, the SSS variations would be accompanied by concurrent changes in SST. Therefore we believe that SSS variations are not the reason for the diverging trends between the planktic $\delta^{18}O$ and the $U^{K'}_{37}$ records.

In addition to a warming trend in glacial severity from MIS 10 to MIS 6, the $U^{K'}_{37}$ SST estimates for MIS 12, 14 and 16 are relatively warm at sites PS75/034-2 and PS2489 / ODP Site 1090, even though MIS 12 and MIS 16 are known to be among the most severe glacial stages during the Pleistocene [*Lang and Wolff*, 2011; *Shackleton*, 1987]. We note that varying Pleistocene glacial severity is not physically impossible. Indeed, a SST record in the subtropical Agulhas region suggested its occurrence [*Bard and Rickaby*, 2009]. Here, MIS 10 and 12 are substantially colder than other glacials in the past 800 kyr; but the glacial-interglacial cycles before MIS 12 are well-defined – unlike in the subantarctic $U^{K'}_{37}$ records. Furthermore, the Agulhas core site is located north of the Subtropical Front, under the influence of a completely different hydrographic setting (e.g., warm Agulhas current and associated eddies) from that of the subantarctic Southern Ocean. These differences suggest that the varying glacial severity trends in *Bard and Rickaby* [2009]'s Agulhas SST record and the subantarctic $U^{K'}_{37}$ SST records are unrelated.

On the other hand, the glacial severity trends in U^{K}_{37}-derived SST records are in agreement with the planktic $\delta^{18}O$ records at site GeoB 3327-5 and PS2489-2 / ODP Site 1090. At the latter site, a summer SST record inferred from foraminiferal assemblages further supports this pattern [*Becquey and Gersonde*, 2002, 2003] (**Figure 3.5d**). Similar patterns in glacial severity over the past 700 kyr has been observed elsewhere in the subantarctic Southern Ocean and Antarctica, such as ODP Site 1093 and ODP Site 1094 in the South

Atlantic [*Schneider-Mor et al.*, 2008], DSDP Site 594 off New Zealand [*Schaefer et al.*, 2005], South Indian [*Howard and Prell*, 1992] and Antarctic atmospheric temperature records at EPICA Dome C [*Jouzel et al.*, 2007] and Dome Vostok [*Petit et al.*, 1999] (**Figure 3.5e – 3.5h**). These temperature records suggest that unvarying glacial severity is a pervasive Pleistocene climatic feature in the Southern Ocean.

The better agreement of the temporal trend of the U^{K}_{37} than the $U^{K'}_{37}$ SST records with other surface proxy records in the same oceanic region suggests that the U^{K}_{37}-derived SSTs are plausibly more realistic than the $U^{K'}_{37}$ estimates at these sites, even though the core-top values of both indices correlate equally well with modern SSTs. Our findings agree with a multi-proxy comparison study off the Iberian margin [*Bard*, 2001]. The author found that the U^{K}_{37}-derived glacial coolings were more comparable with those derived from other proxies, even though the core-top SST estimates inferred from both U^{K}_{37} and $U^{K'}_{37}$ indices were comparable with the observed annual average SST. These findings demonstrate that different alkenone indices could result in diverging paleo SST patterns during the cold intervals even if the core-top SST estimates suggested by both indices agree with the modern day SST. The discrepancy in paleo SST patterns stems from the higher relative abundance of the $C_{37:4}$ alkenones during the cold intervals. Having established that the U^{K}_{37} index is a more suitable SST proxy in the subantarctic Pacific (south of the Subtropical Front at ~30°S), we base our stratigraphic framework of PS75/034-2 and the following discussion on the SST variations and the meridional gradients on the U^{K}_{37}- derived SST records.

3.5.3. Southern Ocean SST evolution: circum-Antarctic comparison

High-resolution alkenone SST records off Chile (e.g., ODP Site 1233 and MD07-3128) suggest that the SST in the mid-latitude Southeast Pacific evolved in synchrony with the atmospheric temperature at Antarctica on millennial time-scales over the past 70 kyr [*Caniupán et al.*, 2011; *Kaiser et al.*, 2005; *Lamy et al.*, 2004]. Due to the coarser temporal resolution in our Pleistocene SST records, it is impossible to assess these millennial-scale patterns. Instead, our SST records, especially the southern site, share first-order patterns on glacial-interglacial timescale with the EPICA Dome C temperature record of *Jouzel et al.* [2007]. There are, however, some minor differences compared to the Antarctic temperature record, such as the absence of a luke-warm interglacial MIS 15 at site PS75/034-2, and a cooling during MIS 3 at site GeoB 3327-5. Besides, unlike in the Antarctic temperature

record, the Mid-Brunhes Event (~430 kyr) shift is not well expressed in our SST records from the Southeast Pacific (**Figure 3.5**). This suggests an overprint of regional climate in our subantarctic SST records on the background of glacial-interglacial climatic changes closely linked to Antarctica. Meanwhile, other features such as the coolest MIS 13 and the warmest MIS 5 in the past 700 kyr, and the smallest amplitude of termination during the MIS 14 – MIS 13 transition observed in our records are common in many marine and terrestrial records [*Lang and Wolff*, 2011]. With the exception of a warmer-than-today MIS 5 and a colder-than-today MIS13, the maximum SST estimates for other interglacials at sites GeoB 3327-5 and PS75/034-2 are similar to modern day summer SST (**Figure 3.4**).

The intensity of Pleistocene glacial cooling (~8°C) at our subantarctic Pacific sites is within the range of other subantarctic SST records derived from various proxies (**Figure 3.5**), i.e., ~5°C in the South Indian [*Howard and Prell*, 1992], ~7 to 10°C in the Southwest Pacific [*Pahnke et al.*, 2003; *Schaefer et al.*, 2005], and ~7 to 11°C in the South Atlantic [*Becquey and Gersonde*, 2003; *Martínez-Garcia et al.*, 2009], indicating that the Pleistocene glacial cooling in the Southeast Pacific is comparable, if not stronger, than in other sectors of the Southern Ocean. This is in contrast to the findings of *Gersonde et al*. [2005] in a circum-Antarctic LGM SST study using siliceous microfossil transfer functions. The authors reported a non-uniform glacial cooling in the Southern Ocean, with less cooling (~1°C) in the Pacific compared to the Atlantic and Indian sectors (4-5°C). The discrepancy between this study and our compilation may be due to the more climatically sensitive sites of the long Pleistocene records (i.e., DSDP 594, GeoB 3327-5, PS75/034-2, MD97-2021). Alternatively, it could also be due to the different sensitivity of proxies (siliceous microfossils vs. geochemical/carbonaceous microfossils) or the fact that the South Pacific is under-represented in their calibration database. Indeed, foraminiferal assemblage-based LGM time slice studies suggest cooling of ~5°C in the subantarctic Southeast Pacific (111-123°W) [*Luz*, 1977] and up to ~8°C in the Southwest Pacific [*Barrows and Juggins*, 2005], in better agreement with our alkenone-based estimates than those derived from the siliceous microfossil transfer functions.

If true, the substantial Pleistocene glacial cooling in the subantarctic Southeast Pacific suggested by the alkenone paleothermometry is plausibly due to an extensive equatorward migration of the Westerlies and the Southern Ocean frontal systems embedded within the

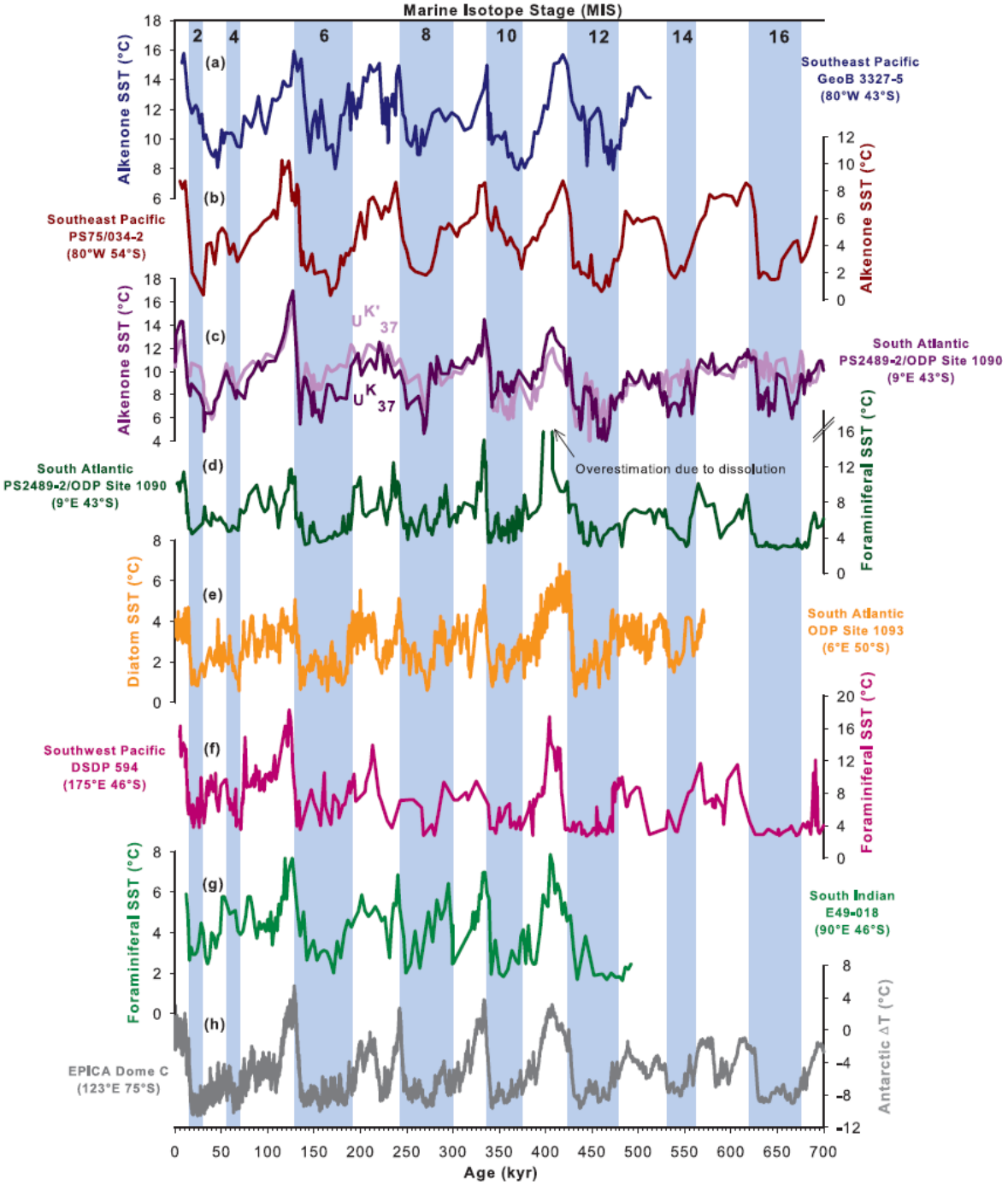

Figure 3.5: Comparison of temperature records from the Southern Ocean and Antarctica based on different proxies. Shaded bars indicate glacial intervals and the black numbers in the bars represent the marine isotope stages. (a) Alkenone U^{K}_{37}-derived sea surface temperature record at site GeoB 3327-5 in the Southeast Pacific. (b) Alkenone U^{K}_{37}-derived at site PS75/034-2 in the Southeast Pacific. (c) Alkenone-derived sea surface temperature records based on the $U^{K'}_{37}$ index (light purple curve) and the U^{K}_{37} index (dark purple curve) [*Martínez-Garcia et al.*, 2010; *Martínez-Garcia et al.*, 2009] at site PS2489-2 / ODP Site 1090 in the South Atlantic. (d) Foraminiferal transfer function-derived summer SST record [*Becquey and Gersonde*, 2002; 2003] at site PS2489/ ODP Site 1090. The authors regarded the estimates for MIS 11 as an overestimation due to preferential dissolution of cold-water species. (e) Diatom transfer function-derived summer sea surface temperature record [*Schneider-Mor et al.*, 2008] at ODP Site 1093 in the South Atlantic. (f) Foraminiferal transfer function-derived winter SST record [*Schaefer et al.*, 2005] at site DSDP 594 in the Southwest Pacific. (g) Foraminiferal transfer function-derived winter SST record [*Howard and Prell*, 1992] at site E49-018 in the South Indian. (h) Atmospheric temperature record registered in the EPICA ice core at Dome C, Antarctica [*Jouzel et al.*, 2007].

ACC, superimposed on the generally colder climate during glacials. Such equatorward shift of the oceanic systems might have occurred as a consequence of a massive northward sea ice expansion by 5° to 10°, as suggested previously by various faunal-based sea-ice and IRD records in the Southern Ocean [*Becquey and Gersonde*, 2002, 2003; *Crosta et al.*, 2004; *Gersonde et al.*, 2005]. By using the present as an analogue for the past and assuming that the SST ranges associated with the oceanic fronts during glacial intervals would remain the same as modern day (~5°C in the SAF and ~2°C in the APF as in **Figure 3.1**), the average glacial SST estimates for sites PS75/034-2 (~1°C) and GeoB 3327-5 (~9°C) imply that both the SAF and the APF were located between 43°S and 54°S in the Southeast Pacific during glacials. This suggests that these oceanic fronts underwent substantial equatorward migration of ~7° (SAF) and ~9° (APF) during glacials and resided northward of site PS75/034-2. Such frontal migrations are conceivable, considering that no shallow bathymetric feature stands between site PS75/034-2 and the modern average latitudes of these oceanic fronts. Thus, no topographic obstacle restricts the equatorward movement. In fact, frontal shifts (SAF and APF) of such magnitude during the Pleistocene have previously been proposed for the subantarctic Atlantic [*Becquey and Gersonde*, 2003] and the Southwest Pacific [*Schaefer et al.*, 2005; *Wells and Okada*, 1997].

Such massive equatorward shifts of the ACC and its associated fronts in the Southeast Pacific may have important implications for the water transport through the Drake Passage. If, for instance, the SAF and the APF, which transport the bulk of the water in the ACC system, would be deflected equatorward within the PCC instead of flowing through the Drake Passage as they do today, the transport to the South Atlantic would have been markedly reduced during glacials. In fact, such a scenario was invoked by *Gersonde et al.* [2003] to explain the intense cooling east of the Argentine basin during the LGM. The authors further hypothesized that such changes in the transport through the Drake Passage, which is one of the "Cold Water Routes" of the global thermohaline circulation, would have major implications for the global climate development. Our records corroborate their hypothesis and further suggest that the same mechanism might have occurred during all glacials prior to the LGM over the past 700 kyr.

3.5.4. Meridional SST gradients: equatorward cold water transport

Considering the large latitudinal range covered by the study sites, the alkenone-inferred SST records might be affected by different biogeographic patterns or seasonality. For instance, if the abundances of the alkenones or the source organisms (e.g., *E. huxleyi*) are skewed towards the warm / cold season at high / low latitudes [*Schneider et al.*, 2010], the resulting SST gradient would be artificially reduced. Thus, our estimation of meridional SST gradients is conservative and might be underestimated.

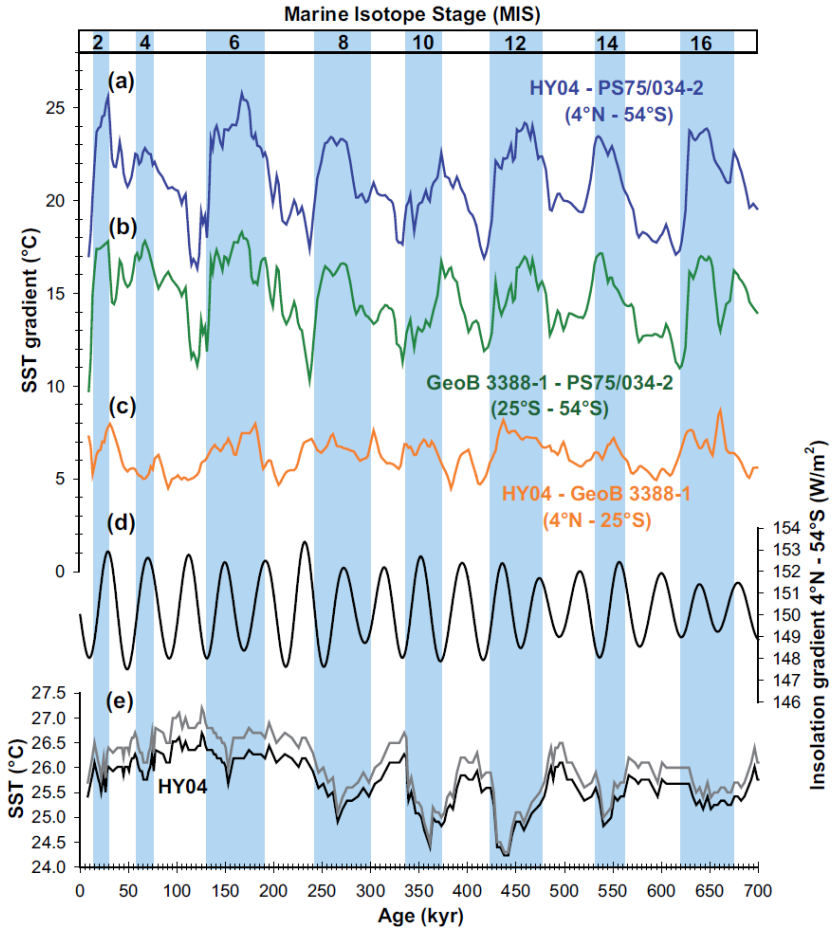

Figure 3.6: Meridional gradients of alkenone-inferred SSTs and mean annual insolation along the Southeast Pacific and SST evolution in the tropical Pacific. Shaded bars indicate glacial intervals, and the black numbers in the bars represent the marine isotope stages. The meridional SST gradients (a) between the tropics (HY04) and the subantarctic (PS75/034-2) (b) between the subtropics (GeoB 3388-1) and the subantartic (PS75/034-2) (c) between the tropics (HY04) and the subtropics (GeoB 3388-1) are derived from U^{K}_{37} SST estimates calculated using the *E. huxleyi* culture calibration of *Prahl et al.* [1988]. (d) Meridional mean annual insolation gradient between 4°N and 54°S [*Laskar*, 1990] (e) Alkenone-based SST records at site HY04 [*Horikawa et al.*, 2010]. For the SST gradient reconstruction, we recalculated the published SST using the U^{K}_{37} calibration of *Prahl et al.* [1988] (black curve) so that it is consistent with other SST records. The gray curve depicts the originally published SST record by *Horikawa et al.* [2010].

Our results show that in contrast to the pronounced glacial cooling in the subantarctic Pacific (~8°C), the amplitudes of glacial cooling decrease to ~4°C and ~1.5°C in the subtropics (GeoB 3388-1) and the tropics (HY04) (**Figure 3.6**), respectively. The glacial SST estimates in the subtropics (GeoB 3388-1) are 1-2°C colder than the modern SST associated with the STF in the Southeast Pacific (~19°C), suggesting that the STF might have also shifted equatorward along with the SAF and the APF, albeit to a smaller extent, and resided slightly northward of our study site. The SST gradients between low and high latitudes (4°N at HY04 and 54°S at PS75/034-2) are steeper during glacials than interglacials, and the overall pattern resembles a mirror image of the high latitude SST record (see **Figure 3.6**). The pattern holds even if other EEP SST records such as the ODP 846 (cold-tongue) and ODP 1239 (coastal upwelling) are used for gradient calculation. The more substantial glacial cooling at the higher latitudes leads to steeper SST gradients between the subantarctic and the subtropics, than those between the subtropics and the tropics. Notably, the smaller tropical-subantarctic SST gradient during MIS 4 is of the same magnitude as those of MIS 8, 10, 12, 14 and 16, while the SST gradients are larger during MIS 2 and MIS 6. The finding of steeper SST gradients between the tropics and mid-latitudes during glacials is consistent with the observation of *Kaiser et al.* [2005] over the past 70 kyr in the Southeast Pacific. However, their reconstruction suggested a slightly larger gradient (~1°C) during MIS 4 than during LGM, in contrast to ours. The discrepancy stems from the less intense cooling during MIS 4 at site GeoB 3388-1 relative to other glacials. Alternatively, it might also be due to a combination of other factors, including the lower temporal resolution in our records, records derived from different proxies (foraminiferal census count and Mg/Ca ratio) used in the gradient calculation of *Kaiser et al*. [2005], or different SST calibrations employed ($U^{K'}_{37}$ vs. U^{K}_{37}). Notwithstanding, our records indicate that steeper meridional SST gradients during glacials are a recurring feature in the Southeast Pacific over the past 700 kyr.

Several factors may contribute to the steeper high-to-low latitude gradients, including the insolation gradient and local hydrographic dynamics. The temporal resolution of our SST records is insufficient for determining the contribution of the local insolation gradient in shaping the meridional SST gradient, based on the wiggle-matching of the SST gradients to the insolation gradients (**Figure 3.6**). Besides, the subtropical site GeoB3388-1 might also be influenced by filaments advected from the coastal upwelling off Chile, if the upwelling was stronger in the past. This notion, however, cannot be rigorously tested by our SST records and awaits future work based on more conservative water mass tracers. Alternatively, the steeper

high-to-low latitude gradients during glacials might be linked to the vigor of the PCC. As readily observable in the modern day SST contour map (**Figure 3.1**), site GeoB 3388-1 is characterized by the advection of cold water from the south. It is conceivable that the steeper gradients between this site and the tropics (site HY 04 is beyond the influence of the east Pacific cold tongue) during the glacial periods are a result of enhanced cold water transport via an intensified PCC. Increased influence of ACC-sourced water in the subtropical Southeast Pacific has been inferred from enhanced glacial paleoproductivity, assuming that the main nutrient source was supplied from the south via the PCC [*Mohtadi and Hebbeln*, 2004; *Romero et al.*, 2006]. Increased transport by the PCC during glacials was invoked to explain the higher abundance of ACC cold-water coccolithophorid and dinoflagellate species at the mid-latitudes Southeast Pacific [*Saavedra-Pellitero et al.,* 2011; *Verleye and Louwye*, 2010] and the increased cold-water foraminiferal abundance in the equatorial Pacific [*Feldberg and Mix*, 2002; 2003]. In addition, it has also been proposed on the basis of a steeper glacial meridional SST gradient at the equator, which suggested a northward shift of the Equator Front - Intertropical Convergence Zone (ITCZ) during glacial periods [*Rincón-Martínez et al.*, 2010]. Stronger cooling and intensification in the PCC transport (an eastern boundary current) during the glacial periods might have resulted from enhanced Ekman pumping from the subantarctic zone, as a response to an increase in wind strength and/or northward migration of the Westerlies. Such changes in the southern Westerlies have been inferred from some marine records [e.g., *Mohtadi and Hebbeln*, 2004; *Stuut and Lamy*, 2004]. Indeed, based on the conservation of energy, a stronger zonal circulation north of the subantarctic zone could be deduced from steeper meridional gradients and an equatorward contraction of the subtropical realm. Moreover, as mentioned in **Section 3.5.3**, an equatorward deflection of the major ACC fronts (the SAF and the APF) would also contribute to increased cold water transport via the PCC.

3.6. Conclusions

The empirical relationship of U^{K}_{37}- and $U^{K'}_{37}$ with SST in our South Pacific regional core-top data set is similar to the commonly used calibrations derived from the laboratory *E. huxleyi* culture of *Prahl et al*. [1988]. These linear relationships hold even at low temperatures (down to ~1°C), suggesting that the temperature dependence of the alkenone indices is not lost at low temperatures in the Southern Ocean. This finding indicates that both alkenone

indices are suitable for reconstructing SST at our cold subantarctic sites. However, these indices result in dissimilar SST patterns over the past 700 kyr in the subantarctic Pacific. The $U^{K'}_{37}$-derived SST records display varying glacial severity, as opposed to the more uniform relative glacial/interglacial change in the U^{K}_{37}-inferred SST records. Based on the better agreement of the glacial severity patterns of the U^{K}_{37} records with that of the planktic $\delta^{18}O$ at the same sites and other subantarctic SST records, we conclude that the U^{K}_{37} is a more suitable index for paleo SST reconstruction in the subantarctic Pacific. The U^{K}_{37}-derived SST records suggest pronounced glacial cooling of ~8°C and ~4°C in the subantarctic and the subtropical regions, respectively. The magnitude of subantarctic glacial cooling is comparable to that reported for other sectors of the Southern Ocean. The SST estimates also suggest that the ACC and its associated fronts migrated equatorward by 7° to 9° during glacials over the past 700 kyr, which might have reduced the water transport through the Drake Passage to the South Atlantic. Conversely, the deflection of more ACC waters equatorward during glacials probably enhanced the cold water advection via the PCC, resulting in colder subtropical SSTs and, thus, larger meridional SST gradients between the tropics and the subtropics.

3.7. Acknowledgements

Constructive comments from three anonymous reviewers and the editor Rainer Zahn have improved the manuscript tremendously. We are grateful to Giuseppe Cortese for sharing his unpublished data. Thanks also go to Gemma Rueda, Susanne Fietz, Nicole Meyer and Hendrik Grotheer for assisting in the alkenone analysis. Technical support from Walter Luttmer and Ralph Kreutz in the laboratories is also highly appreciated. We acknowledge the POLMAR Graduate School for funding S.L.H's PhD study at the Alfred Wegener Institute and a SCAR Fellowship 2010/2011 for funding S.L.H's short stay at the Autonomous University of Barcelona during the preparation of PS75 core-top samples.

Chapter 4: Diverging Pleistocene SST trends revealed by U^{K}_{37} and TEX_{86}^{H} in the Southeast Pacific

Sze Ling Ho[1*], Gesine Mollenhauer[1], Frank Lamy[1], Mahyar Mohtadi[2], Ralf Tiedemann[1]

[1]Alfred Wegener Institute for Polar and Marine Research, P.O.Box 12 01 61, 27515 Bremerhaven, Germany.
[*Corresponding author: Sze.Ling.Ho@awi.de]
[2]MARUM-Center for Marine Environmental Sciences, University of Bremen, Leobener Strasse, D-28359 Bremen, Germany.

(Manuscript in preparation)

4.0. Abstract

Multi-proxy approach is essential for constraining sea surface temperature (SST) reconstruction. Organic SST proxies based on the alkenones (of haptophyte) and the archaeal glycerol dialkyl glycerol tetraether (GDGT) are useful in this regard. Here we present a new GDGT-inferred SST record and compare it to a previously published alkenone-derived SST record from the same site. The comparison reveals different temporal patterns and values in both records. The GDGT-based SST estimates are generally colder. To explain the differences between these proxies, we assess both seasonality and habitat depth of the source organisms, and conclude that the latter is a more likely reason. Based on previous findings of maximum archaeal abundance at the oxycline in this region, we hypothesize that the colder GDGT-inferred estimates reflect the water temperature at this hydrographic boundary instead of the sea surface, as in the alkenone record. The only exception to this pattern occurs during MIS 11 and 13, when the GDGT-based temperatures are considerably warmer than other interglacials, leading to a convergence of temperature values inferred from both proxies. This phenomenon is probably attributable to variability in the water column structure in the Southeast Pacific. One plausible mechanism is a more drastic deepening in the thermocline relative to the oxycline. In this scenario, the oxycline corresponds to the warmer upper part of the thermocline instead of the base of thermocline as observed in the modern day climatological data.

4.1. Introduction

Given the importance of the ocean in climate system, knowledge of past variability in sea surface temperature (SST) is essential for understanding the mechanism involved in climate changes and for validating the numerical models that are widely used for projection of future climate. A large array of proxies have been developed to reconstruct past SST changes, such as the foraminiferal $\delta^{18}O$ and Mg/Ca, the alkenone unsaturation index and the transfer functions of various microfossils. Very often these proxies result in dissimilar reconstructed SST patterns, due to differences in the sensitivity of their response to environmental change, the habitat depth and the production seasonality of the source organisms, or other secondary non-thermal effects. Therefore, it is important to constrain SST reconstructions with multiple proxies. In this regard, organic geochemical proxies based on alkenones and glycerol dialkyl glycerol tetraethers (GDGT) are good options for carrying out a multi-proxy approach, since they can be extracted simultaneously from marine sediments, rendering this approach less labor intensive than comparing organic-inorganic proxies. The alkenones unsaturation index, i.e., the U^{K}_{37} is based on the lipids of haptophyte algae, including the cosmopolitan coccolithophores *Emiliania huxleyi* [*Brassell et al.*, 1986; *Prahl and Wakeham*, 1987]. The GDGT-based proxy, termed TetraEther index with 86 carbon atoms (abbreviated as TEX_{86}) [*Schouten et al.*, 2002], is based on the membrane lipids of mesophilic marine archaea from group Thaumarchaeota (formerly known as Marine Group 1 Crenarchaeota). Recent development has seen increasing numbers of publications based on this organic multi-proxy approach, including studies in the Arabian Sea [*Huguet et al.*, 2006b], the Mediterranean [*Castañeda et al.*, 2010; *Huguet et al.*, 2011], the equatorial Atlantic [*Lopes dos Santos et al.*, 2010], the Gulf of California [*McClymont et al.*, 2012] and the Agulhas system [*Caley et al.*, 2011]. While some of these studies showed similar SST patterns derived from both proxies [e.g., *Castañeda et al.*, 2010], others not [*Huguet et al.*, 2006b; *Lopes dos Santos et al.*, 2010]. These authors attributed the differences between alkenone and GDGT proxies to several possibilities, e.g., the GDGTs record subsurface temperature instead of SST [e.g., *Lopes dos Santos et al.*, 2010; *McClymont et al.*, 2012], or these lipids are produced in different seasons, thus are not controlled by the same climatic systems [*Huguet et al.*, 2006b]. Given that the isoprenoid GDGTs used in TEX_{86} are also found in soil, it is important to assess whether the GDGT-derived SST estimates are biased by terrestrial input. *Hopmans et al.* [2004] proposed an index known as Branched and Isoprenoid Tetraether (BIT) index as a qualitative parameter to gauge the influence of terrestrial end-member on the sedimentary GDGT pool. A threshold

value of 0.3 (above which the SST estimates might be biased) was suggested by *Weijers et al.* [2006]. However, recent studies [e.g., *Fietz et al.*, 2011; *Smith et al.*, 2012] questioned its usefulness in tracing the changes in fluvial input as the ratio could be overwhelmed by the marine end member.

Here we present a GDGT-inferred SST record over the past 700 kyr in the relatively under-studied Southeast Pacific, and compare it with a previously published alkenone SST record at the same study site [*Ho et al.*, in press]. We use BIT values and the concentration of GDGTs to evaluate potential bias introduced by terrestrial GDGTs on the GDGT-inferred SST estimates, before discussing the patterns in both SST records.

4.2. Study site

Core GeoB 3388-1 (25°13'S 75°31'W, 3558 m water depth) was retrieved from the Iquique Ridge approximately 500 km off Chilean coast during the R/V Sonne cruise 102 [*Hebbeln et al.*, 1995]. The site lies underneath a vigorous eastern boundary current, i.e., the oceanic Peru-Chile Current (PCC, also known as the Humboldt Current). The PCC carries cold, nutrient-rich water originates from the Antarctic Circumpolar Current (ACC) equatorward, feeding into the South Equatorial Current (SEC). The nutrients upwelled in the coastal PCC zone result in high productivity, which in turn leads to high consumption of dissolved oxygen for organic matter decomposition. This high oxygen demand, along with sluggish ventilation in the region, produce a subsurface oxygen minimum zone (OMZ; <0.5 mL/L oxygen concentration) [*Helly and Levin*, 2004] as thick as 500 m [*Fuenzalida et al.*, 2009]. The upper boundary of the OMZ deepens and the intensity diminishes further offshore (**Figure 4.1**). The thickness, the position and the intensity of the OMZ could be influenced by the El Niño Southern Oscillation (ENSO) [*Morales et al.*, 1999; reference therein]. The depth of the upper boundary of the OMZ (referred to as the oxycline in the text), is generally deeper than the thermocline (see also **Figure 4.6**), and both deepen considerably during the warm ENSO phase, i.e., the El Niño. The coastal OMZ water is advected poleward by the Peru-Chile Undercurrent (PUC, also known as the Poleward Undercurrent and the Gunther Current). The PUC is the poleward branch formed after the bifurcation of the Equatorial Undercurrent (EUC) as it approaches the Galapagos Islands[*Strub et al.*, 1998].

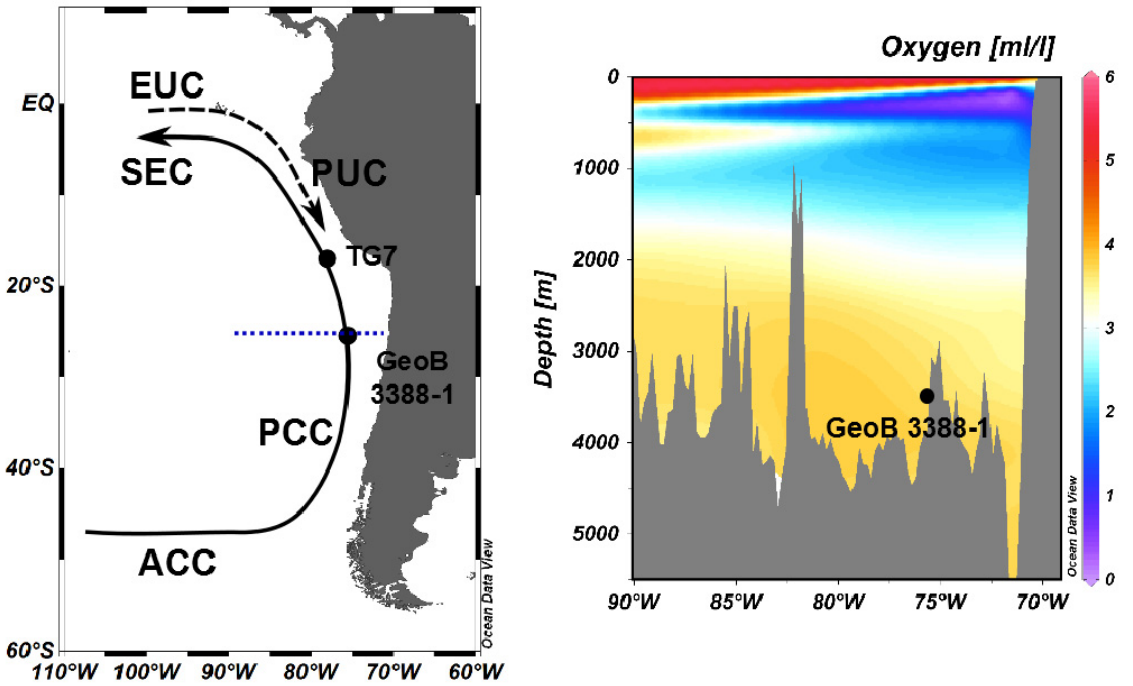

Figure 4.1: Core locations of GeoB 3388-1 and TG7 [*Calvo et al.*, 2001], and major hydrographic features in the Southeast Pacific. Black full line denotes surface currents while black dashed line denotes subsurface currents. Right panel illustrate the oxygen concentration along a section at 25°S between the Chilean coast and subtropical gyre (illustrated by the blue dotted line in the left panel). Abbreviations: ACC – Antarctic Circumpolar Current; PCC- Peru-Chile Current; SEC – South Equatorial Current; EUC – Equatorial Undercurrent Current; PUC – Peru-Chile Undercurrent.

4.3. Materials and methods

Piston core GeoB 3388-1 was previously described by *Mohtadi et al.* [2006] and *Ho et al.* [in press]. Here we opt for the age model revised by *Ho et al*. [in press], which is based on the visual tuning of the benthic $\delta^{18}O$ record to the global benthic $\delta^{18}O$ stack of *Lisiecki and Raymo* [2005]. According to this age model, the average sedimentation rate at the site is 0.7 cm/kyr. Lipids were extracted from freeze-dried, homogenized sediments, via sonication with successively less polar solvent mixture (dichloromethane and methanol), as described by *Müller et al.* [1997]. Total lipid extracts were separated into two fractions (alkenones and GDGTs) using column chromatography (silica cartridge) prior to analysis of individual compounds. GDGTs were eluted using methanol and passed through PTFE filters before they were analyzed using a High Performance Liquid Chromatography system coupled to a mass spectrometer with an atmospheric pressure chemical ionization interface (HPLC-APCI-MS). The setting of the instrumental condition was modified from the method of *Hopmans et al.*

[2000] as reported previously by *Ho et al*. [submitted to GCA]. GDGTs were quantified using internal standard, i.e., C_{46} GDGT.

SST estimates were calculated using a modified version of the TEX_{86}, known as TEX_{86}^{H}, following *Kim et al.* [2010]:

$$TEX_{86}^{H}=\mathrm{Log}\left(\frac{[GDGT\text{-}2+GDGT\text{-}3+Cren']}{[GDGT\text{-}1+GDGT\text{-}2+GDGT\text{-}3+Cren']}\right)$$

$$SST=68.4\times TEX_{86}^{H}+46.9$$

where Cren' denotes crenarchaeol regio-isomer.

We also calculated the BIT index values to assess the relative abundance of marine to soil GDGTs, as proposed by *Hopmans et al.* [2004]:

$$BIT=\frac{[GDGT-I+GDGT-II+GDGT-III]}{[GDGT-I+GDGT-II+GDGT-III+Crenarchaeol]}$$

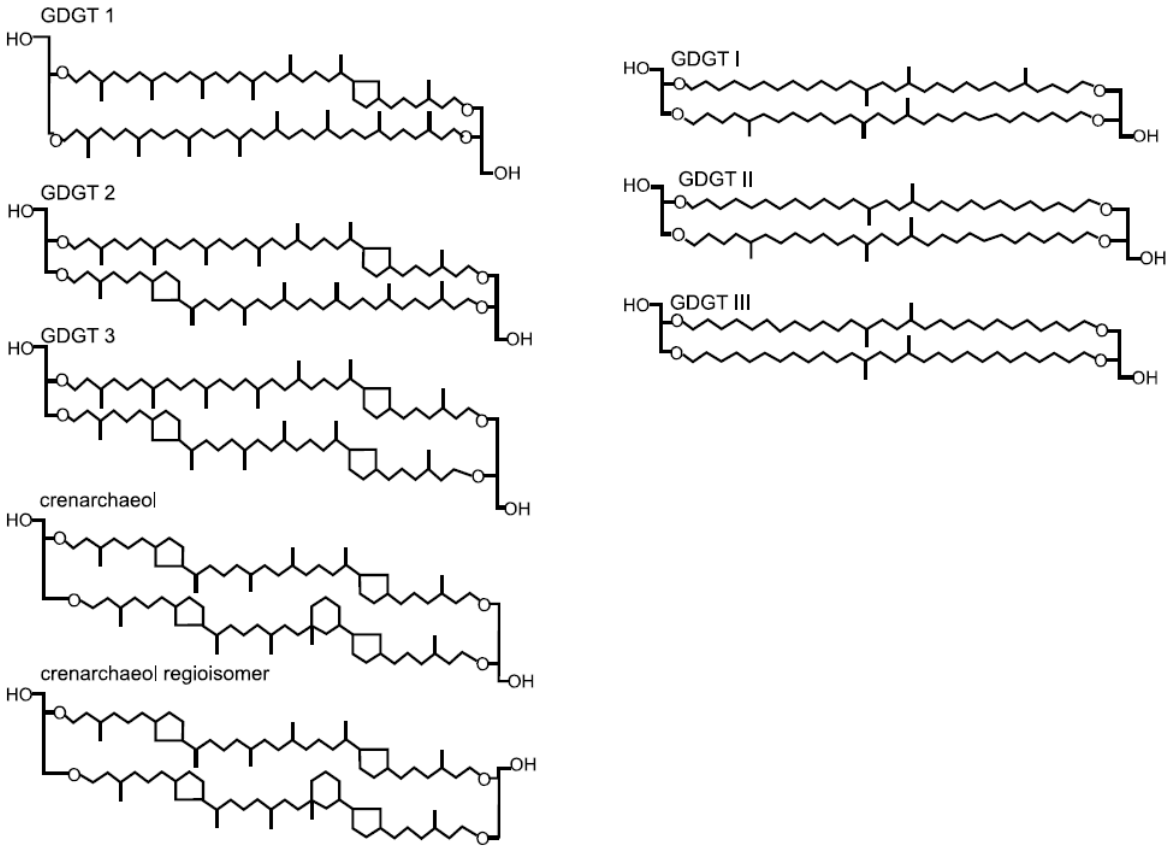

Figure 4.2: Molecular structures of glycerol dialkyl glycerol tetraethers (GDGTs) used for the calculation of the TEX_{86}^{H} and BIT indices [*Castañeda et al.*, 2010].

4.4. Results and discussion

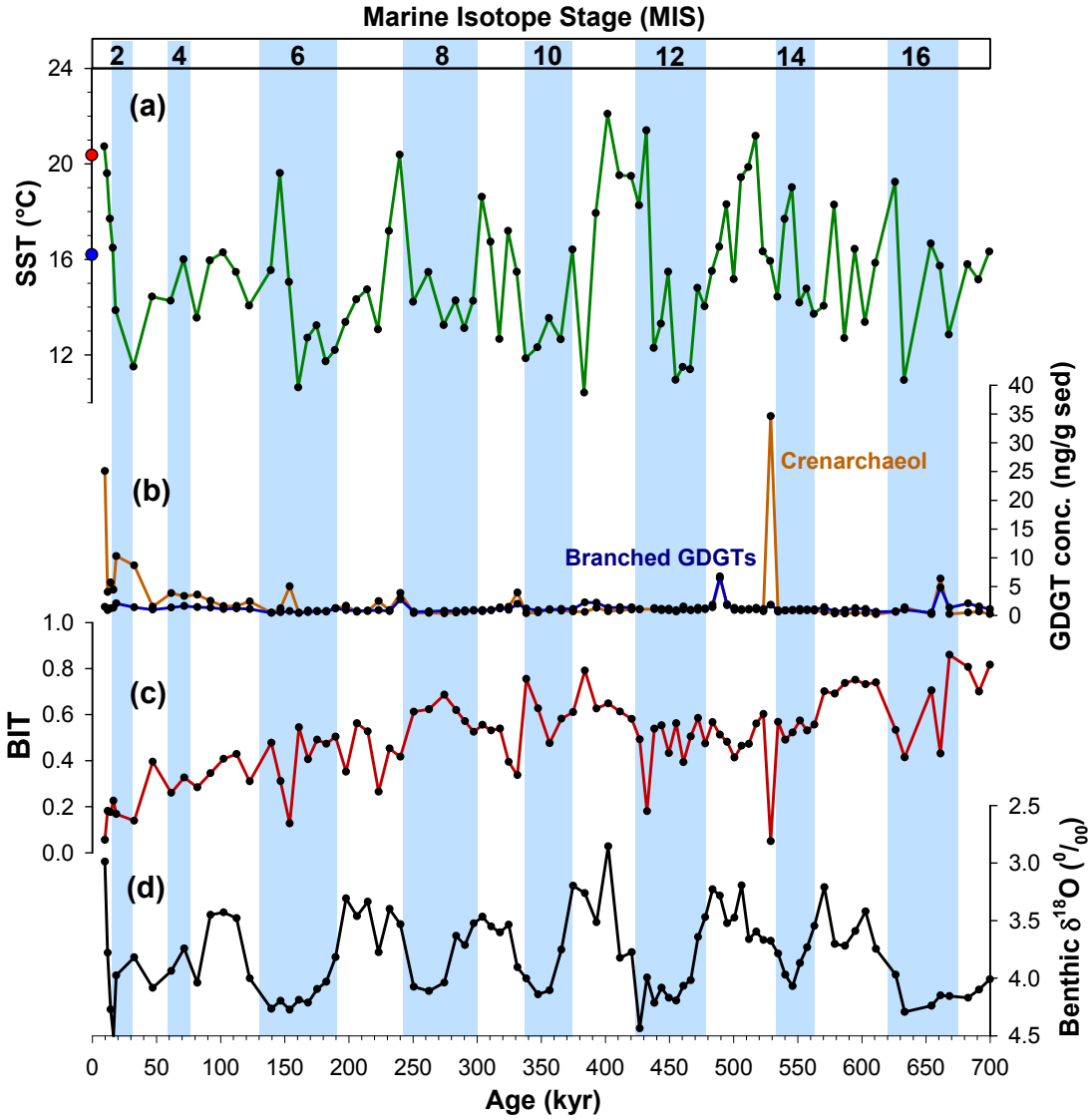

Figure 4.3: Glycerol dialkyl glycerol tetraether (GDGT) parameters and benthic $\delta^{18}O$ record of core GeoB 3388-1. Blue shaded bars represent glacial intervals while the black numbers on top denote the marine isotope stages (a) TEX_{86}^{H}-derived SST estimates computed using the global core-top calibration of *Kim et al.* [2010]. The blue and red circles denote the present day WOA09 coldest and warmest months, respectively. (b) Concentration of branched GDGTs and creanarchaeol used in the calculation of the BIT values. (c) Branched and Isoprenoid Tetraether (BIT) index values. (d) Benthic $\delta^{18}O$ values of *Cibicidoides wuellerstorfi* previously published by *Mohtadi et al.* [2006].

The TEX_{86}^{H}-derived SST record displays glacial-interglacial (G-IG) fluctuations with values ranging between 22°C and 10°C over the past 700 kyr at site GeoB 3388-1. The record is rather noisy with some drastic jumps especially at the lower part of the record. There also seems to be some G-IG temporal offsets between the TEX_{86}^{H} record with the foraminiferal benthic $\delta^{18}O$ values, where warm peaks appear in glacial intervals, e.g., MIS 6 and MIS 14.

TEX_{86}^{H} suggests Holocene warmth (~9 kyr) of around 20.7°C (the top of the piston core) that is comparable to modern day warmest month SST (20.2°C from WOA09). The average glacial SST values are colder than the present day winter SST.

4.4.1. High BIT values: potential terrestrial bias on TEX_{86}^{H} SST?

Before making any climatic interpretation of the TEX_{86}^{H}-derived record, it is necessary to assess whether the record has been compromised by terrestrial GDGTs, in light of the high BIT values (>0.3) at our study site for most part of the past 700 kyr. The BIT index was initially proposed as a proxy to monitor the fluvial input to marine sediment. *Weijers et al.* [2006] found that soil GDGTs caused an artificial warming in TEX_{86}-derived SSTs and suggested a cut-off value of 0.3, above which the temperature estimates might become unreliable. The BIT values at our site are in the range of 0 and 0.8, with a decreasing trend towards the Holocene. The trend in the BIT record is clearly governed by the variations in the crenarchaeol concentrations, as the concentrations of branched GDGTs are invariant throughout the record (**Figure 4.3**). Given the considerable distance from land (~500km) and the absence of major rivers on land around the latitude of our core site, substantial fluvial input of branched GDGTs to site GeoB 3388-1 is unlikely. Furthermore, the little fluvial sediments that end up in the ocean are probably caught in the Peru-Chile Trench, which lies between the coast and our study site. Previous sedimentological evidences suggest that the terrigenous components west of the trench are eolian-derived [*Lamy et al.*, 1998; *Saukel et al.*, 2011]. To-date it is still unclear whether the GDGTs could be transported by winds. However, if indeed such massive amount of dust-entrained GDGTs are blown to our study site and interfere with the marine GDGT signal, one would expect to see an overall "warm" TEX_{86}^{H}-derived SST throughout the record consistent with the invariant concentration of branched GDGTs. Warm bias on TEX_{86}-derived temperature estimates by terrestrial GDGTs is suggested by *Weijers et al.* [2006] and the TEX_{86}^{H}-inferred temperature values (approx. 29°C) in three soil samples from the Atacama Desert at subtropical latitudes (see **Section 4.7**). Since the interglacial TEX_{86}^{H} SSTs at site GeoB 3388-1 are comparable with modern day SSTs and not anomalously warm, it is likely that a terrigenous overprint on this record is negligible. Furthermore, there is no apparent correlation between the BIT index values and the SST estimates (**Figure 4.4**). The branched GDGTs in our sediment record are probably produced in situ, e.g., in the water column or the sediment by bacteria, as previously invoked by *Peterse*

et al. [2009] and *Zhu et al.* [2011] to explain the occurrence of branched GDGTs in the marine sediments off Svalbard and the South China Sea, respectively. High relative abundances of branched GDGTs (hence BIT values) have also been observed in marine sediments from the Southern Ocean [*Fietz et al.*, 2011] and the equatorial Atlantic [*Fietz et al.*, 2012] far from any apparent fluvial sources (e.g., major rivers), further support the plausibility of in-situ production of branched GDGTs in open ocean settings. Since the branched GDGTs-producing bacteria are not known to produce isoprenoid GDGTs, we contend that high BIT values do not compromise the validity of the TEX_{86}^{H}-inferred SST estimates at our study site.

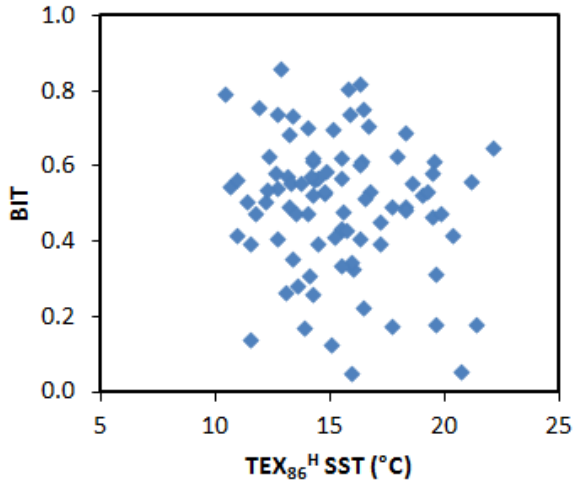

Figure 4.4: Correlation between the Branched and Isoprenoid Tetraether (BIT) index values and the TEX_{86}^{H}-derived SST estimates calculated with the global core-top calibration of *Kim et al.* [2010].

4.4.2. Comparison with alkenone-derived SSTs

In spite of lower temporal resolutions, the alkenone-inferred SST record at site GeoB 3388-1 resembles the subtropical TG7 alkenone SST record [*Calvo et al.*, 2001] which lies a few degrees northward (see **Figure 4.1** for location), suggesting that both records likely reflect the regional SST pattern. Comparison of the alkenone-derived and the smoothed TEX_{86}^{H}-derived SST records suggests that for most part of the past 700 kyr, the G-IG amplitude of SST oscillation is ~4°C. The only exception was during MIS 11 and 13, where the TEX_{86}^{H} suggests larger amplitudes of up to 8°C. In general, the alkenone-derived SST estimates are warmer by approximately 5°C than those inferred from the TEX_{86}^{H}, except for MIS 11 and 13 where the estimates inferred from both proxies converge. While there is no

clear G-IG trends in the differences between the alkenone SST and the TEX_{86}^{H} SST (termed ΔSST), the ΔSST during MIS 11 and 13 are evidently reduced compared to other time intervals. This begs the questions – what causes the differences between the alkenone- and the TEX_{86}^{H}-derived SSTs? Why do they converge during MIS 11 and 13?

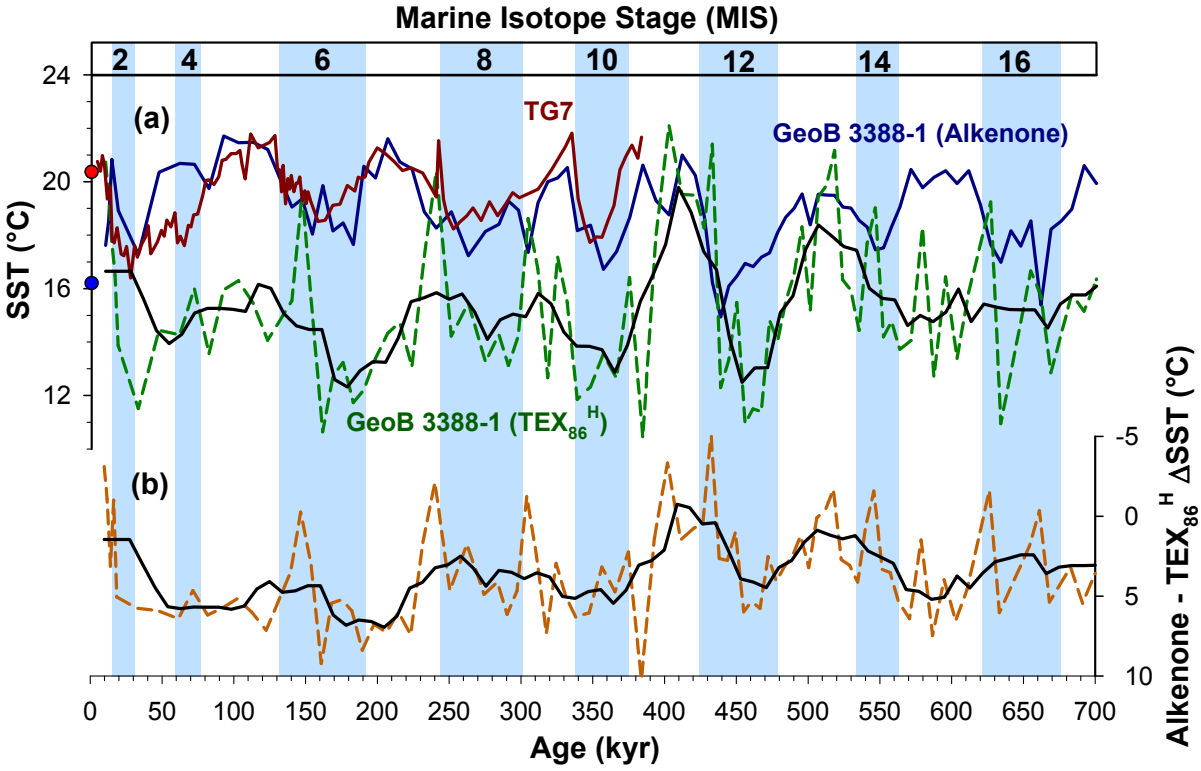

Figure 4.5: Temperature records at site GeoB 3388-1. Black lines denote records smoothed by a running average method. Blue shaded bars represent glacial intervals while the black numbers on top denote the marine isotope stages. (a) Alkenone-derived sea surface temperature records at site GeoB 3388-1 (blue) and TG7 (red) [*Calvo et al.*, 2001], and TEX_{86}^{H}-derived water temperature record (green) at site GeoB 3388-1. The blue and red circles denote the present day WOA09 coldest and warmest months, respectively, at site GeoB 3388-1. (b) The difference between alkenone-derived and TEX_{86}^{H}-derived temperature estimates at site GeoB 3388-1.

Firstly, we explore the plausible reasons for the differences between the two proxies. Taking the SST estimates at face value and assuming that the condition of previous interglacials are comparable to that of present day, one might speculate that the alkenones and the GDGTs are produced during summer and winter, respectively, judging by their agreement with the respective WOA09 seasonal SSTs (see **Figure 4.5**). Nonetheless, this idea cannot be better constrained in the absence of recent sediment sample at the study site (the top of core GeoB 3388-1 is estimated to be 9000 year-old) and sediment trap time series data in this region. A regional core-top alkenone study in the Southeast Pacific indeed suggests that the

sedimentary alkenones in this region register annual mean SST [*Prahl et al.*, 2006], as opposed to our summer-biased alkenone-inferred interglacial SSTs

To the best of our knowledge, there is no reported work on the abundance and seasonal variability of GDGTs in the water column or surface sediment in the vicinity of our study site. Meanwhile, time series data on the prokaryote in the PCC system reveal no seasonal patterns in the abundance of marine archaea (precursors of GDGTs) [*Quiñones et al.*, 2009]. We note that studies from other regions suggested that the Thaumarchaeota thrive during winter in the coastal North Sea [*Wuchter et al.*, 2005]) and the Antarctic coastal waters [*Church et al.*, 2003; *Murray et al.*, 1998]. However, we refrain from extrapolating these findings obtained from studies on shallow coastal waters to our open ocean site, which is situated in a completely different hydrographic and sedimentation setting. This is in light of a recent finding by *Leider et al.* [2010] in a core-top study in the Mediterranean Sea. They attributed the dissimilar TEX_{86}^{H}-SST relationships observed at coastal sites and oceanic sites to differences in the seasonality and/or sedimentation setting. Furthermore, *Giovannoni and Vergin* [2012] also proposed that the microbial communities differ between coastal and open ocean regions, and with latitude.

Alternatively, dissimilar SST values can also arise if the alkenones and the GDGTs record water temperatures at different depths. Unlike the photosynthetic precursor of the alkenones (i.e., haptophyte algae) which are found in the upper photic zone, the chemoautotrophic archaea thrive throughout the water column [e.g., *Karner et al.*, 2001] since their habitat depth is not restricted by light. Off northern Chile, maximum absolute abundance of Thaumarchaeotal cell numbers were found at the oxycline (water depths of ~50 – 200m) above the core of the OMZ [*Belmar et al.*, 2011]. If indeed the GDGTs in the sediment originate from this water depth which coincides with the base of thermocline, they should record water temperatures about 6°C lower than the SST (**Figure 4.6**), in agreement with the ΔSST observed in the alkenone- and TEX_{86}^{H} records. GDGT-based proxies reflecting subsurface temperatures have been reported previously, such as for the Gulf of California [*McClymont et al.*, 2012], the eastern tropical Atlantic [*Lopes dos Santos et al.*, 2010] and the Benguela upwelling system [*Lee et al.*, 2008]. We find this notion more plausible that the seasonality bias, thus adopt it as our working hypothesis for further discussion.

4.4.3. Paleoceanographic implications

Assuming that the alkenones and the GDGTs record water temperatures at the sea surface and the oxycline, respectively, these proxy data suggest that the water column condition is anomalous during MIS 11 and 13, where the oxycline temperatures warm up twice as much as the other time intervals and are almost as warm as the SST. The warming is likely to be restricted to the subsurface since the alkenone-derived MIS 11 and 13 SSTs are not anomalously warm compared to other interglacials. If the archaeal preferred habitat depth remains the same during these intervals, i.e., at the oxycline, significant subsurface warming during MIS 11 and 13 suggests an enhanced influence of warm waters at the oxycline. At present, the oxycline at site GeoB 3388-1 corresponds to the base of the thermocline. As the temperatures at the base of thermocline do not vary much with depth variation (Note: the thermocline is theoretically the boundary between two water masses with specific physical properties), same magnitude of depth shifts in both the oxycline and the thermocline will not lead to large changes in the TEX_{86}^{H}-derived oxycline temperature and in turn the ΔSST. Conversely, substantial oxycline temperature change requires a mismatch in the magnitude of shoaling / deepening of both these hydrographic boundaries.

The variability of the oxycline depth, i.e., the upper boundary of the OMZ, in the subtropical Southeast Pacific is closely linked to the changes in thermocline depth and upwelling intensity [*Fuenzalida et al.*, 2009], which are in turn closely associated with the ENSO variability. During warm El Niño events, large parcel of warm waters accumulates in the eastern Pacific and the upwelling of cold, nutrient rich water at the coastal area is reduced. The depths of both thermocline and oxycline deepen; and the opposite are true for La Niña condition. *Morales et al.* [1999] reported that during an El Niño event offhore Antofagasta (23°S), the thermocline deepened more than did the oxycline. Consequently, the oxycline corresponds to the upper part of the thermocline, unlike during "normal" conditions when the oxycline corresponds to the base of the thermocline. Considering that it is warmer at the upper part of the thermocline than at the base of it, such an El Niño-like reorganization of water column structure would result in smaller temperature difference between the sea surface and the oxycline (**Figure 4.6**). Due to the thicker upper warm water mass, the upwelled water will be warmer than usual, further contribute to decrease the surface-subsurface temperature difference. Putting our temperature reconstruction in this context and assuming that the signal

depths of alkenone and GDGTs are constant through time, smaller ΔSSTs suggest a change in the water column structure analogous to that occurring during the El Niño events.

El Niño-like MIS 11 and 13 in the Southeast Pacific has been previously proposed by *Mohtadi et al.* [2006] based on an independent proxy on core GeoB 3388-1, i.e., foraminiferal $\delta^{13}C$ values. The authors invoked a reorganization of the PCC circulation pattern in the Southeast Pacific to explain the diverging planktonic $\delta^{13}C$ values in the tropical and the subtropical Southeast Pacific during MIS 11 and 13, i.e., the weakened PCC turned westward at a much southerly position than usual leading to this divergence. As argued by the authors, such a shift in the circulation system resembles the El Niño conditions, where weakened Hadley Cell and Walker Circulation lead to a weak gyre circulation and a decreased influence of the ACC (via the PCC) in the equatorial East Pacific. Our water column temperature reconstruction further suggests that during these time intervals, the thermocline deepened more than the oxycline compared to other time intervals over the past 700 kyr.

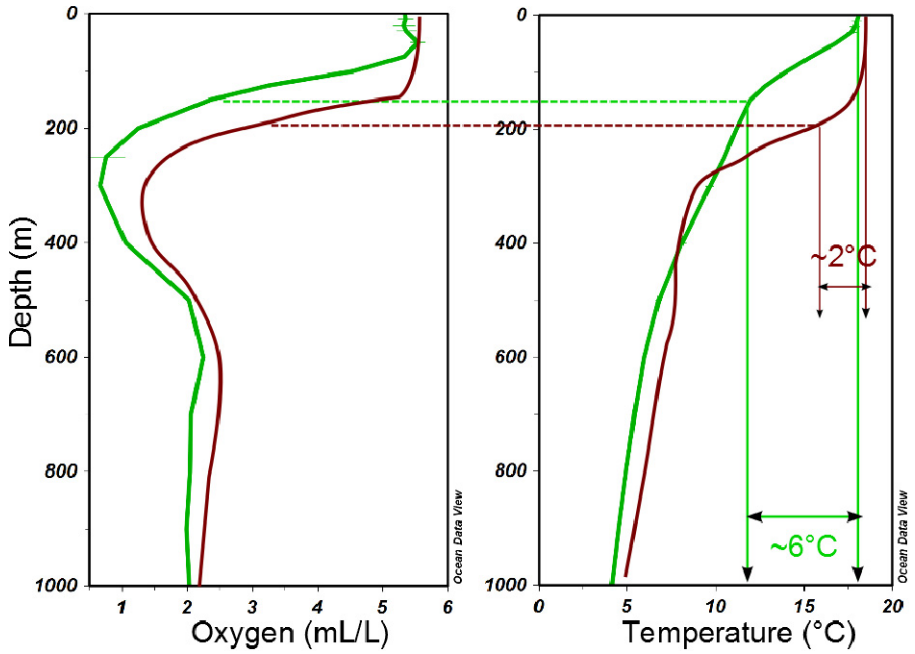

Figure 4.6: Upper water column structure at site GeoB 3388-1 in terms of oxygen concentration and temperature based on the annual mean climatological data of WOA09 (green curves). The red curves are the schematic of the water column structure during El Niño events. The horizontal dashed lines illustrate the position of oxycline and its corresponding temperatures. The arrows depict the difference between the temperatures at the sea surface and the oxycline where the Thaumarchaeota thrive.

4.5. Conclusions

In spite of high BIT index values, it is unlikely that our TEX_{86}^{H} record in the open ocean subtropical Southeast Pacific has been compromised by terrestrial GDGTs because the SST estimates are not anomalously warm and they show no correlation with the BIT index values. The branched GDGTs are probably produced in-situ in the water column or the sediment as proposed for other oceanic regions by previous workers [*Peterse et al.*, 2009; *Zhu et al.*, 2011]. The TEX_{86}^{H}-derived SST estimates are generally 5°C colder than those inferred from the alkenones, probably because the GDGTs record water temperature at the oxycline while the alkenones the surface. This notion is supported by microbial phylogenetic study in the region which found the highest absolute abundance of marine Thaumarchaeota at the oxycline above the oxygen minimum zone [*Belmar et al.*, 2011]. This pattern breaks down during MIS 11 and 13, during which SST estimates derived from both proxies converge. We invoke a drastically deepened thermocline (relative to the oxycline) to explain the substantial warming recorded by the TEX_{86}^{H} during these time intervals. Such a shift resembles the changes in the water column during the El Niño events in modern day. El Niño-like MIS 11 and MIS 13 was previously suggested by *Mohtadi et al.* [2006] based on the foraminiferal $\delta^{13}C$ data measured on the same core.

4.6. Acknowledgments

We thank Carme Huguet and Susanne Fietz for their encouragement and discussion on earlier results. Technical assistance of Ralph Kreutz (handling the HPLC-APCI-MS) is greatly appreciated. We also thank Dierk Hebbeln and Claudio Latorre for providing sediment samples of core GeoB 3388-1 and soil samples from the Atacama Desert, respectively. The POLMAR Graduate School is acknowledged for funding S.L.H.'s PhD study at the Alfred Wegener Institute.

4.7. Supplementary Information

Branched and Isoprenoid Tetraether (BIT) index values following the equation of *Hopmans et al.* [2004], temperature estimates calculated with the TEX_{86}^{H} calibration of *Kim et al.* [2010], and coordinates of the soil samples from the Atacama Desert.

Site	Longitude (°W)	Latitude (°S)	Altitude (m)	BIT	TEX_{86}^{H} T (°C)
L01	67.72	23.50	4480	0.85	28.3
L11	67.85	23.32	3570	0.61	27.3
L16	67.92	23.31	3070	0.72	30.7

Chapter 5: Conclusions and Outlook

5.1. Summary and conclusions

This thesis contributes to a better understanding of organic sea surface temperature (SST) proxies derived from alkenones and archaeal glycerol dialkyl glycerol tetraethers (GDGTs) in three aspects, i.e., the spatial distribution of these lipids, the calibrations and the indices of the proxies, and the resulting paleoclimatic implications.

5.1.1. Lipids occurrence: Where the proxies may be applied

Alkenones are found between the Subtropical Front and the Antarctic Polar Front (APF) in the South Pacific (**Figure 3.1**), with highest abundances found in the shallow waters off New Zealand. Application of alkenone paleothermometry in the cold waters south of the APF and further south in the Antarctic zone would therefore require large amounts of sediment samples to have alkenones in quantifiable abundance. The GDGTs are found in subpolar and polar regions, including all sectors of the Southern Ocean, the North Pacific, the Bering Sea, the Arctic Ocean and the Fram Strait (**Figure 2.1**). The presence of GDGTs at high latitudes renders them promising for SST reconstruction at sites where the absence of the alkenones precludes the application of the better established SST indices e.g., the alkenone-based $U^{K'}_{37}$.

5.1.2. Proxy indices and calibrations: Diverging views from core-top calibration and downcore application

The correlations between the two alkenone unsaturation indices (U^{K}_{37} and $U^{K'}_{37}$) in the South Pacific surface sediments and the annual mean World Ocean Atlas 2009 (WOA09) climatological SSTs (1°C - 12°C) are identical to the commonly used laboratory *E. huxleyi* culture-based calibrations of *Prahl et al.* [1988] (8°C – 25°C) (**Figure 3.3**). The South Pacific alkenone indices – SST correlations are linear, with equally high r^2 values of ~0.9 for both indices. These findings contradict previous studies that suggest a loss of linearity in the alkenone indices – SST relationships at low temperatures [*Conte et al.*, 2006; *Sikes and*

Volkman, 1993; *Sikes et al.*, 1997], and that the $U^{K'}_{37}$-SST correlation (r^2 = 0.9) is better than that of U^{K}_{37}-SST (r^2 = 0.7) [*Sikes et al.*, 1997]. Although the South Pacific core-top data support the use of both alkenone indices for SST reconstruction in the subantarctic region, downcore results suggest otherwise. The two alkenone indices yield diverging Pleistocene SST patterns for the study sites in the subantarctic Southern Ocean (**Figure 3.4**). Judging from the better structural fit with planktonic foraminiferal $\delta^{18}O$ records at these sites and other subantarctic SST records derived from various proxies (**Figure 3.5**), it appears that the original U^{K}_{37} index (instead of the commonly used simplified $U^{K'}_{37}$ index) results in more plausible Pleistocene SST records, hence is a more suitable alkenone SST index in the subantarctic Southern Ocean.

The 160 GDGT indices (TEX_{86} and TEX_{86}^{L}) data presented in this work are discussed in combination with ~470 previously published data to obtain the largest spatial coverage to date (**Figure 2.1**). The correlations of the index values in subpolar and polar core-tops with WOA09 annual mean SST are poor (r^2 values < 0.3) (**Figure 2.4**). Cross-plotting these indices data with seasonal WOA09 SST data sets, and water temperature at various hydrographic boundaries (seasonal thermocline, oxycline, deepest water temperature for each site) does not result in improved correlations (**Figure 2.5** and **Figure 2.6**), suggesting that the scatter in the data is caused by other factors, such as differences in sedimentation setting. Running linear regressions through the new global compilation of core-top GDGT indices data (n = 630) does not yield significantly different equations compared to the previous global calibrations proposed by *Kim et al.* [2010] (**Figure 2.9**). The results from the new global compilation show that the correlation for TEX_{86}-SST is better than that for the TEX_{86}^{L}-SST, and the TEX_{86} index results in better SST estimates for subpolar and polar regions (**Figure 2.7**), in contrast to the conclusions of a previous global core-top calibration study [*Kim et al.*, 2010]. Meanwhile, the new Arctic core-top data presented here show that both GDGT indices overestimate the SST here by up to 30°C (relative to the annual mean SST), especially in the vicinity of the sea ice margin. These Arctic data aside, the scatter at the low temperature end is not more pronounced than that in the mid temperature range, suggesting that the previously suggested loss of temperature dependence at low temperatures might not be true. Therefore, the newly compiled global data set does not suggest the need for different GDGT indices for application at opposite ends of the SST range.

Although the core-top data indicate that GDGT indices correlate better with annual mean SST instead of seasonal SST or subsurface temperatures, a downcore TEX_{86}^{H} (logarithmic version of the TEX_{86} proposed by *Kim et al.* [2010]) record suggests that this might not be the case in the subtropical South Pacific. In this 700 kyr sediment record, the GDGT-derived SSTs are colder than those inferred from the alkenones. The interglacial estimates are colder than annual mean WOA09, and more comparable with modern-day winter SST at the site (**Figure 4.5**). Considering the lack of seasonality in the archaeal abundance in the subtropical South Pacific [*Quiñones et al.*, 2009], it seems that the "cold-biased" GDGT-inferred SSTs here reflect subsurface temperature, plausibly at the oxycline because the source organism, i.e., the Thaumarchaeota, thrive at this hydrographic boundary [*Belmar et al.*, 2011].

5.1.3. Paleo SST estimates: Pleistocene climatic implications

Two subantarctic and one subtropical SST records presented in this thesis shed light on the SST variability in the Southeast Pacific over the past 700 kyr. The subantarctic records are especially important in terms of the long timescale they cover, which is roughly ten times older than the longest SST record in the region. They afford a high-to-low latitudes SST patterns comparison based on records derived from the same proxy (i.e., U^{K}_{37}), which is essential for constraining latitudinal SST gradient calculation. The U^{K}_{37} SST records show that in the Southeast Pacific over the past 700 kyr, the glacial cooling in the subantarctic zone (~8°C) is twice larger than that in the subtropics (~4°C) (**Figure 3.4**), resulting in larger latitudinal SST gradients during glacials (**Figure 3.6**). The extent of glacial cooling here is comparable, if not larger, than what observed in other sectors of the subantarctic Southern Ocean (**Figure 3.5**), in contrast to the findings of *Gersonde et al.* [2005] based on siliceous microfossil transfer functions, which suggest less intense glacial cooling in the Pacific sector. Although sharing a first-order pattern with the Antarctic temperature evolution registered in ice cores [*Jouzel et al.*, 2007; *Petit et al.*, 1999], the subantarctic Pacific SST records do not display a well-expressed Mid-Brunhes Event as in the ice core record. These U^{K}_{37}-derived SSTs imply massive equatorward migrations (by 7 to 9 degrees latitude) of the Antarctic Circumpolar Current frontal systems and enhanced cold water transport to the low latitudes via the Peru-Chile Current (PCC) during glacials.

Whilst the alkenone-inferred interglacial warmth in the subtropics appears to be quite constant over the past 700 kyr, the GDGT-derived temperatures suggest a two-fold subsurface warming at the oxycline during MIS 11 and 13 (**Figure 4.5**). Assuming that the present-day lack of seasonality in the archaeal abundance holds in the past (hence ruling out a shift in archaeal production season), the substantial subsurface warming might be related to an enhanced deepening of the thermocline relative to the oxycline, causing the latter (also the habitat depth of the archaea) to correspond to the upper, warmer part of the thermocline (**Figure 4.6**). Such shifts in the depths of these hydrographic boundaries are analogous to the water column reorganization during modern-day El Niño conditions [*Morales et al.*, 1999].

5.2. Perspectives for future work

"Science is always wrong: It never solves a problem without creating ten more."

George Bernard Shaw (1856-1950)

As solemnly stated in a community White Paper [*Henderson et al.*, 2009] prepared for the National Environment Research Council of the United Kingdom following a symposium on the earth's climate convened by Henry Elderfield and colleagues at the University of Cambridge, "*Despite its importance, careful calibration of a paleoproxy and assessment of its uncertainty can appear less exciting to a researcher or a funding panel than the application of this proxy to a paleoclimate question*". There is clearly room for improvement in proxy calibration and its application.

As discussed thoroughly in previous chapters, choosing the "right" index and calibration is pivotal for reconstructing past SST changes. Indeed, it has been shown that different approaches in terrestrial temperature calibrations alone can result in differences of the same magnitude as the temperature changes in the past millennium reported in the IPCC report [*Esper et al.*, 2005]. In alkenone- and GDGT-inferred SST records, the temporal trends are governed by the definition of the index while the values of the SST estimates depend on the calibration employed. It goes without saying that both the index and the calibration of SST proxies are of paramount importance for accurately reconstructing past SST changes. In light

of the findings presented in this thesis, many more scientific questions arise, which are useful for steering future work to further improve the quality of SST reconstruction.

5.2.1. Refining U^{K}_{37} calibration

Chapter 3 presents South Pacific alkenone core-top calibrations that are comparable with the commonly used *Emiliania huxleyi* culture calibrations [*Prahl et al.*, 1988], but differ systematically from the Southern Ocean core-top calibrations of *Sikes et al.* [1997], especially evident for the U^{K}_{37} index (**Figure 5.1**). Inconsistency in instrumentation and methodology, including chromatogram integration and sample work-up, could be possible causative factors for this offset [personal communication with E. Sikes]. Notwithstanding, given the rarity of the Southern Ocean core-top samples, it is worthy to further examine other potential factors causing the offset, such as non-thermal physiological factors, differences in assemblages or morphotypes in alkenone-producing coccolithophores, before ruling out one of the data sets. This is especially true considering the difficulty in culturing coccolithophores for calibration at temperatures below 5°C. In addition to low growth rates (resulting in a time-consuming experiment), the cold water coccolithophores cultures isolated from the Southern Ocean waters have a small range of preferred growth temperature (~2°C) [*G. Langer*, personal communication] that is not ideal for calibrating the SST proxy.

Furthermore, in light of the new finding presented in this thesis, i.e., the U^{K}_{37} index is a better SST proxy in the subantarctic region at low temperatures (**Section 3.5.1** and **Section 3.5.2**), there is an urgent need to appraise the index at higher temperatures to expand its calibration range. One possible short-term approach would be to combine the South Pacific core-top data with the *E. huxleyi* culture data of *Prahl et al.* [1988], yielding a calibration range from 1 °C to 25°C (compared to 0 °C to 28°C for the global core-top $U^{K'}_{37}$ calibration). Such approach was adopted by *Mashiotta et al.* [1999] for their "hybrid" foraminiferal Mg/Ca calibration, which closely resembles the core-top calibration of *Elderfield and Ganssen* [2000]. Notwithstanding, it is not ideal in theory to combine temporally integrated signals in surface sediments with "snapshot" signals in laboratory cultures. Therefore, the long-term goal should be to generate more U^{K}_{37} data spanning the entire global temperature range, which will not only help to reconcile the differences in various data sets (**Figure 5.1**), but will ultimately contribute to generating a U^{K}_{37} global calibration with a comparable temperature

range to its counterpart $U^{K'}_{37}$. A universal calibration for the entire temperature range would enable a more quantitative comparison of SST records spanning a large latitudinal range.

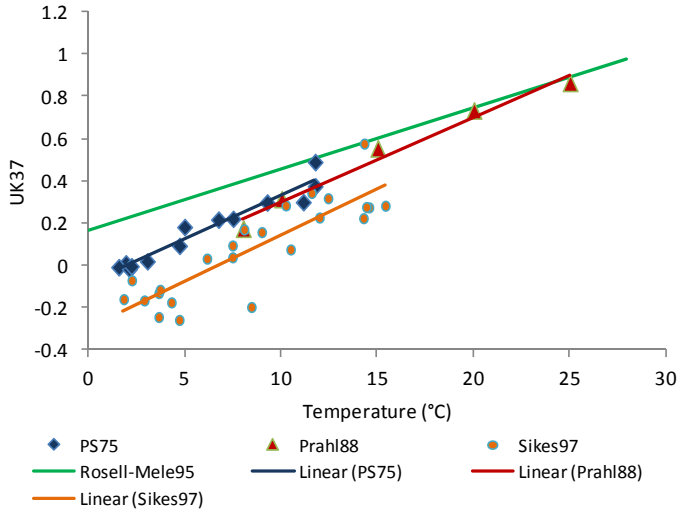

Figure 5.1: U^{K}_{37} calibrations available in the literature. *Prahl et al.* [1988]'s calibration is based on the *Emiliania huxleyi* cultures. Calibrations of *Rosell-Mele et al*. [1995] and *Sikes et al.* [1997] are based on core-top data from the North Atlantic and the Southern Ocean, respectively.

Wide acceptance of the U^{K}_{37} index as SST proxy can be promoted by further evidence that within the same type of alkenone producers (coccolithophore), variations in the relative abundance of $C_{37:4}$ alkenones (termed $\%C_{37:4}$ herein) in the open ocean are not caused by changes in salinity. $\%C_{37:4}$ as a salinity proxy was proposed by *Rosell-Melé* [1998] and *Rosell-Melé et al.* [2002] based on core-top data from the North Atlantic and the Nordic Seas. However, as argued by *Sikes and Sicre* [2002], the proposed relationship could be an artifact due to the strong correlation between temperature and salinity, which incidentally also holds in the South Pacific (**Figure 5.2**). Furthermore, in coastal area, fjords, brackish waters and sea-ice margins, the variations in $\%C_{37:4}$ are likely due to changes in the alkenone producer assemblages [*Bendle et al.*, 2005; *Marlowe et al.*, 1984; *Schulz et al.*, 2000], not because of cellular physiological response to salinity variations. Considering the difficulty to disentangle the effects of these co-varying factors in the natural environments (i.e., shift in assemblages and strong correlation between temperature and salinity), laboratory culture experiments (e.g., growing coccolithophores at constant temperature while changing salinity) will provide more definitive insights into the effect of salinity on $\%C_{37:4}$ in coccolithophores. This might have important implications for future application of alkenones as a SST proxy and/or an indicator for low salinity water masses. Some studies have used the $U^{K'}_{37}$ index in parallel with the

$\%C_{37:4}$ to infer SSTs and the presence of low salinity water, respectively. Although this approach is convenient and has its merits given that a salinity proxy is still elusive, it is lacking a biogeochemical rationale. That is, if salinity does control the alkenone unsaturation pattern (thereby also the $\%C_{37:4}$), it would violate the principle of the $U^{K'}_{37}$ index (which is practically an index that quantifies the degree of unsaturation) as a SST proxy. Alternatively, if the correlation between $\%C_{37:4}$ and salinity stems from the contribution of coastal/brackish water/fresh water alkenone producers which have different alkenone distributions than their open ocean counterparts (i.e., with higher abundance of $C_{37:4}$ alkenones), these alkenones will "contaminate" the signals of marine alkenones, rendering the SST estimates derived from these "mixed alkenones" using the marine core-top calibrations inaccurate. In any case, parallel application of alkenones as both SST and salinity proxy cannot be justified.

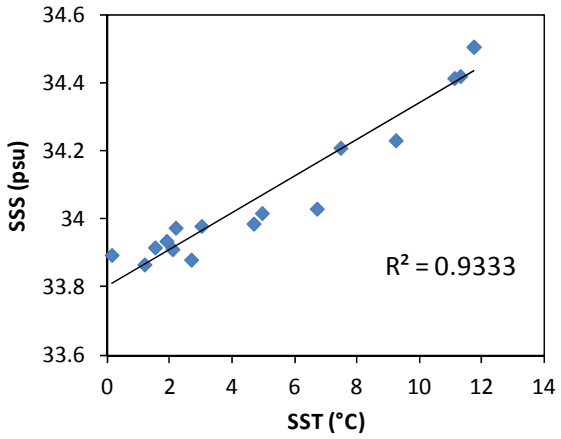

Figure 5.2: Correlation between the sea surface salinity (SSS) and the sea surface temperature (SST) at the core-top sites of PS75 reported in **Chapter 3**. Environmental data are retrieved from the WOA09.

5.2.2. Refining GDGT-based SST calibrations

Compared to the extensively studied alkenone paleothermometry, there is still plenty of room for improvement in GDGT-based proxies due to their more recent discovery (16 years later than the alkenone paleothermometry) and their relatively under-studied archaeal precursors. It is seen in **Chapter 2** that the addition of 230 data points to the global core-top calibration data sets [*Kim et al.*, 2010] does not lead to very different regressions. Instead, the additional data result in larger scatter and hence, larger errors of estimation. This finding suggests that the more urgent issue for GDGT indices is to reduce these errors by investigating the causative factors for the scatter as speculated based on core-top data in

Chapter 2. Such factors include the seasonality in the archaeal abundance and their export to the sediments, potential GDGT contribution from an archaeal group other than the mesophilic Thaumarchaeota, and the archaeal GDGTs originated from subsurface water depths instead of the sea surface.

To test the various hypotheses listed above, sediment trap time series from different hydrographic settings have the potential to unravel regional differences, if any, in the seasonality and the sinking of the GDGT fluxes. To-date, most sediment trap data in the literature are from the tropics and/or shallow continental shelves [*Fallet et al.*, 2011; *Wakeham et al.*, 2003; *Wuchter et al.*, 2006]. Therefore, sediment trap data from open ocean settings and higher latitudes may provide new insights into these issues.

Nonetheless, sediment trap sites worldwide are currently, and will likely be in the future, insufficient to match the broad spatial coverage of the global core-top data set. As an alternative to the sediment trap data, one can probably make use of satellite observations on primary productivity that have global coverage (1° x 1° grid). In addition, the export of primary production from the sea surface can be predicted using biogeochemical models, albeit with some extent of uncertainties inherent to the models. Furthermore, the temperature residuals of TEX_{86}^{L} (**Figure 5.3**) display latitudinal patterns, where overestimates (underestimates) are observed at high (low) latitudes. These patterns resemble the seasonality index calculated by *Schneider et al.* [2010], which shows that primary productivity is positively (negatively) correlated to SST at high (low) latitudes. Therefore, incorporating biogeochemical parameters in TEX_{86} calibrations has the potential to improve the calibration, such as changing the slope of the regression (**Figure 5.4**). Conventionally, seasonality in global calibrations is examined by comparing the r^2 values in the crossplots of the SST index values and seasonal SSTs. However, the seasonal patterns in production and export of organic matter are not comparable at low and high latitudes, with maxima occurring in different seasons. Therefore, a strong justification for correlating index values with seasonal SSTs in global calibrations is lacking.

More confidence in the TEX_{86} paleothermometry will ensue if a better constraint on the original export depth of the GDGTs and more knowledge on the GDGT-producing archaea can be obtained. The fact that the alleged GDGT source organisms (the Thaumarchaeota) thrive throughout the water column casts some doubts on the validity of GDGTs as a SST proxy. The present assumption is that GDGTs are transported to the

sediment via scavenging and fecal pellet formation, thus they reflect the temperatures at upper water depths where an active foodweb exists. Future study is needed to further corroborate this assumption. In this regard, microbial phylogenetic analysis performed in tandem with lipid analysis on suspended matter in the water column at various depths might be useful to improve our understanding of the source organisms and their preferred habitat depth. Such combined analyses on suspended matters in the water column off Chile are currently underway in the laboratory of O. Ulloa, the University of Concepcion in collaboration with R. Summons (Massachusetts Institute of Technology) [*O. Ulloa*, personal communication]. In

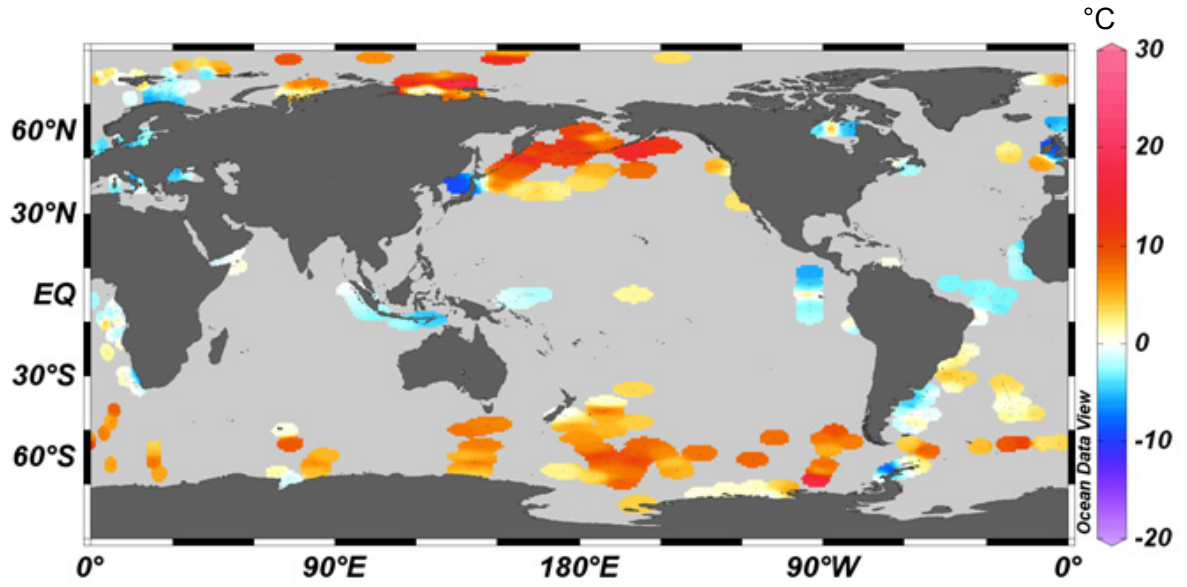

Figure 5.3: TEX_{86}^{L}-derived temperature residuals (difference between estimated SST and climatological SST) by applying the current global calibration of *Kim et al.* [2010] on published data sets [*Ho et al.*, 2011; *Kim et al.*, 2010; *Leider et al.*, 2010; *Shevenell et al.*, 2011] and data presented in **Chapter 2**.

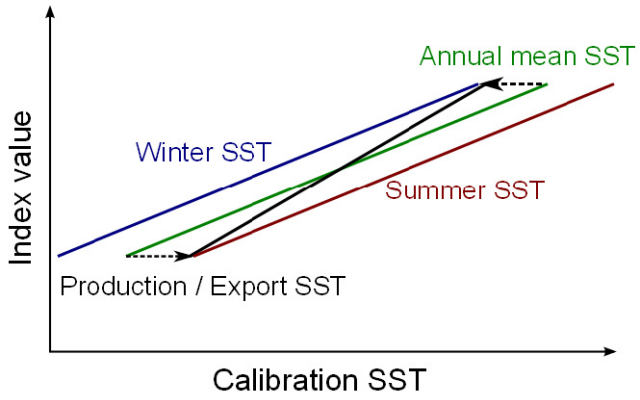

Figure 5.4: Schematic of a possible shift in the global core-top calibrations of TEX_{86} (currently calibrated against annual mean SST) after integrating production and export information, which skew towards warm (cold) seasons at high (low) latitudes.

addition, knowledge on the correlation between the abundances of the archaea and the GDGTs will provide some perspectives on how to translate the currently available archaeal abundance data into the distribution of GDGTs in the water column. Laboratory culture experiment would be ideal for studying GDGT-producing archaea, but culturing mesophilic archaea has proven to be very challenging so far, and there is yet no reported success in culturing the Thaumarchaeota.

5.2.3. Constraining paleo SST reconstruction: Multi-proxy approach

As summarized in **Section 5.1.2**, diverging views on the proxy applicability could be inferred from core-top data and downcore records, suggesting that the modern proxy-SST relationship in the core-top calibration might falter in the past. In this regard, a multi-proxy approach can help to better constrain SST reconstruction. When the proxies are in agreement, they provide additional confidence in the SST estimates. Conversely, disagreements in the proxies might reveal potential bias and prompt us to find the underlying processes to reconcile the differences.

For instance, glacial SSTs at site PS75/034-2 are ~1°C (**Figure 3.4**). At present, such low temperatures are found south of the APF near the winter sea ice edge, where coccolithophores are sparse or absent [*Cubillos et al.*, 2007; *Gravalosa et al.*, 2008; *Hasle*, 1960] and alkenones are at detection limit (note however that alkenones have been found in sediments where the overlying SST is ~0°C in the South Atlantic [*Müller et al.*, 1998]). Notwithstanding, the alkenone abundances in core PS75/034-2 are higher during glacials than interglacials. This suggests that either the alkenones production / preservation is substantially higher during glacials, or the modern alkenone calibration underestimates the glacial SSTs in the past. Additional oceanographic information provided by other SST proxy and sea ice proxy (e.g., diatom assemblages) will be useful to determine which hypothesis is more likely.

Multi-proxy comparison is especially crucial for advancing our understanding of the predictive power of the TEX_{86} index in estimating past temperature changes, considering the uncertainties associated with the depth of origin for GDGTs. In light of sediment trap studies that suggest a subsurface origin for GDGTs [*Huguet et al.*, 2007; *Lee et al.*, 2008], one can examine whether this is true for the past by comparing the TEX_{86} records with other SST proxies and subsurface temperature proxies (e.g., Mg/Ca on deep-dwelling foraminifera such

as *G. inflata* and *G. truncatulinoides*) records measured on the same sediment cores. More importantly, such comparison will also yield insights into whether the source depth for GDGTs has shifted in the past. This has implications for the assumption made (that the GDGT signal depth remains invariant in the past) in the hypothesis put forward in **Chapter 4** to explain the substantial warming registered in the GDGT-derived temperature record during MIS 11 and 13.

5.2.4. Towards the "big picture"

As stated in **Chapter 1**, the ultimate goal of all branches of climate research is to have an accurate projection of future climate change, in order to better prepare for its consequences on human's society. Since proxy data are widely used to validate numerical models, improvements of both proxies and models are pivotal towards achieving that ultimate goal. Recent development has seen heightened awareness in the scientific community regarding the importance of bringing together paleoclimatology and modeling. Further examination on proxy calibrations and the quantification of their uncertainties have the potential to contribute to this cause. Some studies have shown that the temperature variations simulated by climate models are smaller than those observed in proxy data [*Braconnot et al.*, 2012; *Lohmann et al.*, 2012; *Lorenz et al.*, 2006; *Schneider et al.*, 2010]. As proposed in **Section 5.2.2**, integrating biogeochemical parameters such as production or export might lead to a shift in the slope of the global calibration, resulting in smaller amplitudes of the SST variation for the same range of index values. Therefore, future work shall go beyond the conventional scope of paleo proxy work and attempt to place proxy studies in the context of model-data comparison. The advantages of model-proxy comparison are analogous to those of the multi-proxy comparison, i.e., agreement shall bring confidence in both models and proxy data; while disagreements encourage the community to strive harder to understand underlying causes of the mismatch. Furthermore, changes in global calibrations shall have far-reaching implications for the calculations of climate sensitivity over glacial-interglacial cycles, which in turn affect the projection of future climate with a doubling of atmospheric CO_2.

References

Alonso-Sáez, L., Sánchez, O., Gasol, J.M., Balagué, V., Pedrós-Alio, C., 2008. Winter-to-summer changes in the composition and single-cell activity of near-surface Arctic prokaryotes. Environmental Microbiology 10, 2444-2454.

Bano, N., Ruffin, S., Ransom, B., Hollibaugh, J.T., 2004. Phylogenetic composition of Arctic Ocean archaeal assemblages and comparison with Antarctic assemblages. Applied and Environmental Microbiology 70, 781-789.

Bard, E., 2001. Comparison of alkenone estimates with other paleotemperature proxies. Geochemistry Geophysics Geosystems 2, 1002.

Bard, E., Rickaby, R.E.M., 2009. Migration of the subtropical front as a modulator of glacial climate. Nature 460, 380-383.

Barker, S., Cacho, I., Benway, H., Tachikawa, K., 2005. Planktonic foraminiferal Mg/Ca as a proxy for past oceanic temperatures: a methodological overview and data compilation for the Last Glacial Maximum. Quaternary Science Reviews 24, 821-834.

Barrows, T.T., Juggins, S., 2005. Sea-surface temperatures around the Australian margin and Indian Ocean during the Last Glacial Maximum. Quaternary Science Reviews 24, 1017-1047.

Beck, J.W., Edwards, R.L., Ito, E., Taylor, F.W., Recy, J., Rougerie, F., Joannot, P., Henin, C., 1992. Sea-Surface Temperature from Coral Skeletal Strontium/Calcium Ratios. Science 257, 644-647.

Becquey, S., Gersonde, R., 2002. Past hydrographic and climatic changes in the Subantarctic Zone of the South Atlantic - The Pleistocene record from ODP Site 1090. Palaeogeography, Palaeoclimatology, Palaeoecology 182, 221-239.

Becquey, S., Gersonde, R., 2003. A 0.55-Ma paleotemperature record from the Subantarctic zone: Implications for Antarctic Circumpolar Current development. Paleoceanography 18, 1014.

Bell, M.V., Pond, D., 1996. Lipid composition during growth of motile and coccolith forms of Emiliania huxleyi. Phytochemistry 41, 465-471.

Belmar, L., Molina, V., Ulloa, O., 2011. Abundance and phylogenetic identity of archaeoplankton in the permanent oxygen minimum zone of the eastern tropical South Pacific. FEMS Microbiology Ecology 78, 314-326.

Bendle, J., Rosell-Melé, A., 2004. Distributions of U^{K}_{37} and $U^{K'}_{37}$ in the surface waters and sediments of the Nordic Seas: Implications for paleoceanography. Geochemistry Geophysics Geosystems 5, Q11013.

Bendle, J., Rosell-Melé, A., Ziveri, P., 2005. Variability of unusual distributions of alkenones in the surface waters of the Nordic seas. Paleoceanography 20, PA2001.

Benthien, A., Müller, P.J., 2000. Anomalously low alkenone temperatures caused by lateral particle and sediment transport in the Malvinas Current region, western Argentine Basin. Deep-Sea Research Part I-Oceanographic Research Papers 47, 2369-2393.

Blaga, C.I., Reichart, G.J., Heiri, O., Damste, J.S.S., 2009. Tetraether membrane lipid distributions in water-column particulate matter and sediments: a study of 47 European lakes along a north-south transect. Journal of Paleolimnology 41, 523-540.

Braconnot, P., Harrison, S.P., Kageyama, M., Bartlein, P.J., Masson-Delmotte, V., Abe-Ouchi, A., Otto-Bliesner, B., Zhao, Y., 2012. Evaluation of climate models using palaeoclimatic data. Nature Climate Change 2, 417-424.

Brassell, S.C., Eglinton, G., Marlowe, I.T., Pflaumann, U., Sarnthein, M., 1986. Molecular stratigraphy - a new tool for climatic assessment. Nature 320, 129-133.

Brochier-Armanet, C., Boussau, B., Gribaldo, S., Forterre, P., 2008. Mesophilic crenarchaeota: proposal for a third archaeal phylum, the Thaumarchaeota. Nature Reviews Microbiology 6, 245-252.

Caley, T., Kim, J.-H., Malaize, B., Giraudeau, J., Laepple, T., Caillon, N., Charlier, K., Rebaubier, H., Rossignol, L., Castaneda, I.S., Schouten, S., Sinninghe Damste, J.S., 2011. High-latitude obliquity as a dominant forcing in the Agulhas current system. Climate of the Past 7, 1285 -1296.

Calvo, E., Grimalt, J.O., Jansen, E., 2002. High resolution U^{K}_{37} sea surface temperature reconstruction in the Norwegian Sea during the Holocene. Quaternary Science Reviews 21, 1385-1394.

Calvo, E., Pelejero, C., Herguera, J.C., Palanques, A., Grimalt, J.O., 2001. Insolation dependence of the southeastern Subtropical Pacific sea surface temperature over the last 400 kyrs. Geophysical Research Letters 28, 2481-2484.

Caniupán, M., Lamy, F., Lange, C.B., Kaiser, J., Arz, H., Kilian, R., Baeza Urrea, O., Aracena, C., Hebbeln, D., Kissel, C., Laj, C., Mollenhauer, G., Tiedemann, R., 2011. Millennial-scale sea surface temperature and Patagonian Ice Sheet changes off southernmost Chile (53°S) over the past 60 kyr. Paleoceanography 26, PA3221.

Casey, K.S., Cornillon, P., 1999. A comparison of satellite and in situ based sea surface temperature climatologies. Journal of Climate 12, 3801-3818.

Castañeda, I.S., Schefuß, E., Pätzold, J., Sinninghe Damsté, J.S., Weldeab, S., Schouten, S., 2010. Millennial-scale sea surface temperature changes in the eastern Mediterranean (Nile River Delta region) over the last 27,000 years. Paleoceanography 25, PA1208.

Chaigneau, A., Pizarro, O., 2005. Surface circulation and fronts of the South Pacific Ocean, east of 120°W. Geophysical Research Letters 32, L08605.

Chave, K.E., 1954. Aspects of the biogeochemistry of magnesium: 1. Calcareous marine organisms. Journal of Geology, 266-283.

Chavez, F.P., Messié, M., 2009. A comparison of Eastern Boundary Upwelling Ecosystems. Progress In Oceanography 83, 80-96.

Church, M.J., DeLong, E.F., Ducklow, H.W., Karner, M.B., Preston, C.M., Karl, D.M., 2003. Abundance and distribution of planktonic Archaea and Bacteria in the waters west of the Antarctic Peninsula. Limnolog and Oceanography 48, 1893-1902.

Conte, M.H., Eglinton, G., 1993. Alkenone and Alkenoate Distributions within the Euphotic Zone of the Eastern North-Atlantic - Correlation with Production Temperature. Deep-Sea Research Part I- Oceanographic Research Pappers 40, 1935-1961.

Conte, M.H., Sicre, M.A., Ruhlemann, C., Weber, J.C., Schulte, S., Schulz-Bull, D., Blanz, T., 2006. Global temperature calibration of the alkenone unsaturation index ($U^{K'}_{37}$) in surface waters and comparison with surface sediments. Geochemistry Geophysics Geosystems 7, Q02005.

Cortese, G., Abelmann, A., 2002. Radiolarian-based paleotemperatures during the last 160 kyr at ODP Site 1089 (Southern Ocean, Atlantic Sector). Palaeogeography, Palaeoclimatology, Palaeoecology 182, 259-286.

Crosta, X., Sturm, A., Armand, L., Pichon, J.-J., 2004. Late Quaternary sea ice history in the Indian sector of the Southern Ocean as recorded by diatom assemblages. Marine Micropaleontology 50, 209-223.

Cubillos, J.C., Wright, S.W., Nash, G., de Salas, M.F., Griffiths, B., Tilbrook, B., Poisson, A., Hallegraeff, G.M., 2007. Calcification morphotypes of the coccolithophorid Emiliania huxleyi in the Southern Ocean: changes in 2001 to 2006 compared to historical data. Marine Ecology Progress Series 348, 47-54.

Cunningham, S.A., Alderson, S.G., King, B.A., Brandon, M.A., 2003. Transport and variability of the Antarctic Circumpolar Current in Drake Passage. Journal of Geophysical Research 108, 8084.

de Leeuw, J.W., v.d. Meer, F.W., Rijpstra, W.I.C., Schenck, P.A., 1980. On the occurrence and structural identification of long chain unsaturated ketones and hydrocarbons in sediments. Physics and Chemistry of The Earth 12, 211-217.

De Rosa, M., Gambacorta, A., 1988. The lipids of archaebacteria. Progress in Lipid Research 27, 153-175.

de Vernal, A., Rosell-Melé, A., Kucera, M., Hillaire-Marcel, C., Eynaud, F., Weinelt, M., Dokken, T., Kageyama, M., 2006. Comparing proxies for the reconstruction of LGM sea-surface conditions in the northern North Atlantic. Quaternary Science Reviews 25, 2820-2834.

Deser, C., Alexander, M.A., Xie, S.-P., Phillips, A.S., 2010. Sea Surface Temperature Variability: Patterns and Mechanisms. Annual Review of Marine Science 2, 115-143.

Elderfield, H., Ganssen, G., 2000. Past temperature and $\delta^{18}O$ of surface ocean waters inferred from foraminiferal Mg/Ca ratios. Nature 405, 442-445.

Emiliani, C., 1955. Pleistocene temperatures. Journal of Geology 63, 538-578.

Epstein, B.L., D'Hondt, S., Hargraves, P.E., 2001. The possible metabolic role of C-37 alkenones in Emiliania huxleyi. Organic Geochemistry 32, 867-875.

Epstein, S., Buchsbaum, R., Lowenstam, H.A., Urey, H.C., 1953. Revised carbonate-water isotopic temperature scale. Geological Society of America Bulletin 64, 1315-1326.

Escala, M., Rosell-Melé, A., Masque, P., 2007. Rapid screening of glycerol dialkyl glycerol tetraethers in continental Eurasia samples using HPLC/APCI-ion trap mass spectrometry. Organic Geochemistry 38, 161-164.

Esper, J., Frank, D.C., Wilson, R.J.S., Briffa, K.R., 2005. Effect of scaling and regression on reconstructed temperature amplitude for the past millennium. Geophysical Research Letters 32, L07711.

Fallet, U., Ullgren, J.E., Castañeda, I.S., van Aken, H.M., Schouten, S., Ridderinkhof, H., Brummer, G.-J.A., 2011. Contrasting variability in foraminiferal and organic paleotemperature proxies in sedimenting particles of the Mozambique Channel (SW Indian Ocean). Geochimica et Cosmochimica Acta 75, 5834-5848.

Feldberg, M.J., Mix, A.C., 2002. Sea-surface temperature estimates in the Southeast Pacific based on planktonic foraminiferal species; modern calibration and Last Glacial Maximum. Marine Micropaleontology 44, 1-29.

Feldberg, M.J., Mix, A.C., 2003. Planktonic foraminifera, sea surface temperatures, and mechanisms of oceanic change in the Peru and south equatorial currents, 0-150 ka BP. Paleoceanography 18, 1016.

Fietz, S., Huguet, C., Bendle, J., Escala, M., Gallacher, C., Herfort, L., Jamieson, R., Martínez-Garcia, A., McClymont, E.L., Peck, V.L., Prahl, F.G., Rossi, S., Rueda, G., Sanson-Barrera, A., Rosell-Melé, A., 2012. Co-variation of crenarchaeol and branched GDGTs in globally-distributed marine and freshwater sedimentary archives. Global and Planetary Change 92–93, 275-285.

Fietz, S., Martínez-Garcia, A., Huguet, C., Rueda, G., Rosell-Melé, A., 2011. Constraints in the application of the Branched and Isoprenoid Tetraether index as a terrestrial input proxy. Journal of Geophysical Research-Oceans 116, C10032.

Fischer, H., Schmitt, J., Lüthi, D., Stocker, T.F., Tschumi, T., Parekh, P., Joos, F., Köhler, P., Völker, C., Gersonde, R., Barbante, C., Le Floch, M., Raynaud, D., Wolff, E., 2010. The role of Southern Ocean processes in orbital and millennial CO_2 variations – A synthesis. Quaternary Science Reviews 29, 193-205.

Fuenzalida, R., Schneider, W., Garcés-Vargas, J., Bravo, L., Lange, C., 2009. Vertical and horizontal extension of the oxygen minimum zone in the eastern South Pacific Ocean. Deep Sea Research Part II: Topical Studies in Oceanography 56, 992-1003.

Gagan, M.K., Ayliffe, L.K., Beck, J.W., Cole, J.E., Druffel, E.R.M., Dunbar, R.B., Schrag, D.P., 2000. New views of tropical paleoclimates from corals. Quaternary Science Reviews 19, 45-64.

Gaines, S.M., Eglinton, G., Rullkotter, J., 2008. Echoes of Life: What Fossil Molecules Reveal about Earth History. Oxford University Press.

Gersonde, R., 2011. The expedition of the research vessel "Polarstern" to the polar South Pacific in 2009/2010 (ANT-XXVI/2 - BIPOMAC), In: Gersonde, R. (Ed.), Berichte zur Polar- und Meeresforschung (Reports on Polar and Marine Research). Alfred Wegener Institute for Polar and Marine Research, Bremerhaven, p. 330.

Gersonde, R., Abelmann, A., Brathauer, U., Becquey, S., Bianchi, C., Cortese, G., Grobe, H., Kuhn, G., Niebler, H.S., Segl, M., Sieger, R., Zielinski, U., Futterer, D.K., 2003. Last glacial sea surface temperatures and sea-ice extent in the Southern Ocean (Atlantic-Indian sector): A multiproxy approach. Paleoceanography 18.

Gersonde, R., Crosta, X., Abelmann, A., Armand, L., 2005. Sea-surface temperature and sea ice distribution of the Southern Ocean at the EPILOG Last Glacial Maximum - A circum-Antarctic view based on siliceous microfossil records. Quaternary Science Reviews 24, 869-896.

Giovannoni, S.J., Vergin, K.L., 2012. Seasonality in Ocean Microbial Communities. Science 335, 671-676.

Gliozzi, A., Paoli, G., De Rosa, M., Gambacorta, A., 1983. Effect of isoprenoid cyclization on the transition temperature of lipids in thermophilic archaebacteria. Biochimica et Biophysica Acta - Biomembranes 735, 234-242.

Gliozzi, A., Relini, A., Chong, P.L.G., 2002. Structure and permeability properties of biomimetic membranes of bolaform archaeal tetraether lipids. Journal of Membrane Science 206, 131-147.

Gravalosa, J.M., Flores, J.A., Sierro, F.J., Gersonde, R., 2008. Sea surface distribution of coccolithophores in the eastern Pacific sector of the Southern Ocean (Bellingshausen and Amundsen Seas) during the late austral summer of 2001. Marine Micropaleontology 69, 16-25.

Harada, N., Ahagon, N., Sakamoto, T., Uchida, M., Ikehara, M., Shibata, Y., 2006. Rapid fluctuation of alkenone temperature in the southwestern Okhotsk Sea during the past 120 ky. Global and Planetary Change 53, 29-46.

Hasle, G.R., 1960. Plankton coccolithophorids from the Subantarctic and Equatorial Pacific. Nytt Magasin for Botanikk 8, 77-88.

Hastie, T., Tibshirani, R., 1990. Generalized Additive Models. Chapman & Hall, London.

Hays, J.D., Imbrie, J., Shackleton, N.J., 1976. Variations in the earth's orbit: Pacemaker of the ice ages. Science 194, 1121-1132.

Hazel, J.R., 1988. Homeoviscous adaptation in animal cell membranes, Physiological Regulation of Membrane Fluidity, pp. 149-188.

Hebbeln, D., Wefer, G., Participants, C., 1995. Cruise report of R/V *Sonne* cruise 102, Valparaiso-Valparaiso,, Rep. 68. Univ. Bremen, Bremen, p. 166.

Helly, J.J., Levin, L.A., 2004. Global distribution of naturally occurring marine hypoxia on continental margins. Deep-Sea Res. Pt. I 51, 1159-1168.

Henderson, G., Collins, M., Hall, I., Lockwood, M., Palike, H., Rickaby, R., Schmidt, G., Turney, C., Wolff, E., 2009. Improving future climate prediction using palaeoclimate data, pp. 1-28.

Hendy, E.J., Gagan, M.K., Alibert, C.A., McCulloch, M.T., Lough, J.M., Isdale, P.J., 2002. Abrupt Decrease in Tropical Pacific Sea Surface Salinity at End of Little Ice Age. Science 295, 1511-1514.

Herbert, T.D., 2003. Alkenone Paleotemperature Determinations, In: Holland, H.D., Turekian, K.K. (Eds.), Treatise on Geochemistry. Pergamon, Oxford, pp. 391-432.

Ho, S.L., Mollenhauer, G., Lamy, F., Martínez-Garcia, A., Mohtadi, M., Gersonde, R., Hebbeln, D., Nunez Ricardo, S., Rosell-Melé, A., Tiedemann, R., in press. Sea surface temperature variability in the Pacific sector of the Southern Ocean over the past 700 kyr. Paleoceanography.

Ho, S.L., Yamamoto, M., Mollenhauer, G., Minagawa, M., 2011. Core top TEX_{86} values in the south and equatorial Pacific. Organic Geochemistry 42, 94-99.

Honda, M.C., Imai, K., Nojiri, Y., Hoshi, F., Sugawara, T., Kusakabe, M., 2002. The biological pump in the northwestern North Pacific based on fluxes and major components of particulate matter obtained by sediment-trap experiments (1997-2000). Deep-Sea Research Part II-Topical Studies in Oceanography 49, 5595-5625.

Honjo, S., Francois, R., Manganini, S., Dymond, J., Collier, R., 2000. Particle fluxes to the interior of the Southern Ocean in the Western Pacific sector along 170 degrees W. Deep-Sea Research Part II-Topical Studies in Oceanography 47, 3521-3548.

Hopmans, E.C., Schouten, S., Pancost, R.D., van der Meer, M.T.J., Sinninghe Damsté, J.S., 2000. Analysis of intact tetraether lipids in archaeal cell material and sediments by high performance liquid chromatography/atmospheric pressure chemical ionization mass spectrometry. Rapid Communication in Mass Spectrometry 14, 585-589.

Hopmans, E.C., Weijers, J.W.H., Schefuss, E., Herfort, L., Sinninghe Damsté, J.S., Schouten, S., 2004. A novel proxy for terrestrial organic matter in sediments based on branched and isoprenoid tetraether lipids. Earth and Planetary Science Letters 224, 107-116.

Horikawa, K., Murayama, M., Minagawa, M., Kato, Y., Sagawa, T., 2010. Latitudinal and downcore (0–750 ka) changes in n-alkane chain lengths in the eastern equatorial Pacific. Quaternary Research 73, 573-582.

Howard, W.R., Prell, W.L., 1992. Late Quaternary Surface Circulation of the Southern Indian Ocean and its Relationship to Orbital Variations. Paleoceanography 7, 79-117.

Huguet, C., Cartes, J.E., Sinninghe Damsté, J.S., Schouten, S., 2006a. Marine crenarchaeotal membrane lipids in decapods: Implications for the TEX_{86} paleothermometer. Geochemistry Geophysics Geosystems 7, Q11010.

Huguet, C., Kim, J.H., Sinninghe Damsté, J.S., Schouten, S., 2006b. Reconstruction of sea surface temperature variations in the Arabian Sea over the last 23 kyr using organic proxies (TEX_{86} and $U^{K'}_{37}$). Paleoceanography 21, PA3003.

Huguet, C., Martrat, B., Grimalt, J.O., Sinninghe Damsté, J.S., Schouten, S., 2011. Coherent millennial-scale patterns in $U^{K'}_{37}$ and TEX^{H}_{86} temperature records during the penultimate interglacial-to-glacial cycle in the western Mediterranean. Paleoceanography 26, PA2218.

Huguet, C., Schimmelmann, A., Thunell, R., Lourens, L.J., Sinninghe Damsté, J.S., Schouten, S., 2007. A study of the TEX_{86} paleothermometer in the water column and sediments of the Santa Barbara Basin, California. Paleoceanography 22, PA3203.

Huybers, P., Wunsch, C., 2010. Paleophysical Oceanography with an Emphasis on Transport Rates. Annual Review of Marine Science 2, 1-34.

Imbrie, J., Kipp, N.G., 1977. A new micropaleontological method for Quantitative Paleoclimatology: Application to a late PleistoceneCaribbean Core., In: Turekian, K.K. (Ed.), The Late Cenozoic Glacial Ages. Yale University Press, New Haven, pp. 71-181.

Jouzel, J., Masson-Delmotte, V., Cattani, O., Dreyfus, G., Falourd, S., Hoffmann, G., Minster, B., Nouet, J., Barnola, J.M., Chappellaz, J., Fischer, H., Gallet, J.C., Johnsen, S., Leuenberger, M., Loulergue, L., Luethi, D., Oerter, H., Parrenin, F., Raisbeck, G., Raynaud, D., Schilt, A., Schwander, J., Selmo, E., Souchez, R., Spahni, R., Stauffer, B., Steffensen, J.P., Stenni, B., Stocker, T.F., Tison, J.L., Werner, M., Wolff, E.W., 2007. Orbital and millennial Antarctic climate variability over the past 800,000 years. Science 317, 793-796.

Junge, K., Eicken, H., Deming, J.W., 2004. Bacterial Activity at −2 to −20°C in Arctic Wintertime Sea Ice. Applied and Environmental Microbiology 70, 550-557.

Kaiser, J., Lamy, F., Hebbeln, D., 2005. A 70-kyr sea surface temperature record off southern Chile (Ocean Drilling Program Site 1233). Paleoceanography 20, PA4009.

Kalanetra, K.M., Bano, N., Hollibaugh, J.T., 2009. Ammonia-oxidizing Archaea in the Arctic Ocean and Antarctic coastal waters. Environ Microbiol 11, 2434-2445.

Karner, M.B., DeLong, E.F., Karl, D.M., 2001. Archaeal dominance in the mesopelagic zone of the Pacific Ocean. Nature 409, 507-510.

Kidston, J., Taschetto, A.S., Thompson, D.W.J., England, M.H., 2011. The influence of Southern Hemisphere sea-ice extent on the latitude of the mid-latitude jet stream. Geophysical Research Letters 38, L15804.

Kienast, M., MacIntyre, G., Dubois, N., Higginson, S., Normandeau, C., Chazen, C., Herbert, T.D., 2012. Alkenone unsaturation in surface sediments from the eastern equatorial Pacific: Implications for SST reconstructions. Paleoceanography 27, PA1210.

Kim, J.H., Schneider, R.R., Hebbeln, D., Müller, P.J., Wefer, G., 2002. Last deglacial sea-surface temperature evolution in the Southeast Pacific compared to climate changes on the South American continent. Quaternary Science Reviews 21, 2085-2097.

Kim, J.H., Schouten, S., Hopmans, E.C., Donner, B., Sinninghe Damsté, J.S., 2008. Global sediment core-top calibration of the TEX_{86} paleothermometer in the ocean. Geochimica et Cosmochimica Acta 72, 1154-1173.

Kim, J.H., van der Meer, J., Schouten, S., Helmke, P., Willmott, V., Sangiorgi, F., Koc, N., Hopmans, E.C., Sinninghe Damsté, J.S., 2010. New indices and calibrations derived from the distribution of crenarchaeal isoprenoid tetraether lipids: Implications for past sea surface temperature reconstructions. Geochimica et Cosmochimica Acta 74, 4639-4654.

Könneke, M., Bernhard, A.E., de la Torre, J.R., Walker, C.B., Waterbury, J.B., Stahl, D.A., 2005. Isolation of an autotrophic ammonia-oxidizing marine archaeon. Nature 437, 543-546.

Kucera, M., Rosell-Melé, A., Schneider, R., Waelbroeck, C., Weinelt, M., 2005. Multiproxy approach for the reconstruction of the glacial ocean surface (MARGO). Quaternary Science Reviews 24, 813-819.

Lamy, F., Hebbeln, D., Wefer, G., 1998. Terrigenous sediment supply along the Chilean continental margin: modern regional patterns of texture and composition. Geologische Rundschau 87, 477-494.

Lamy, F., Kaiser, J., Ninnemann, U., Hebbeln, D., Arz, H.W., Stoner, J., 2004. Antarctic Timing of Surface Water Changes off Chile and Patagonian Ice Sheet Response. Science 304, 1959-1962.

Lang, N., Wolff, E.W., 2011. Interglacial and glacial variability from the last 800 ka in marine, ice and terrestrial archives. Climate of the Past 7, 361-380.

Lee, K.E., Kim, J.H., Wilke, I., Helmke, P., Schouten, S., 2008. A study of the alkenone, TEX_{86}, and planktonic foraminifera in the Benguela Upwelling System: Implications for past sea surface temperature estimates. Geochemistry Geophysics Geosystems 9, Q10019.

Leider, A., Hinrichs, K.-U., Mollenhauer, G., Versteegh, G.J.M., 2010. Core-top calibration of the lipid-based and TEX_{86} temperature proxies on the southern Italian shelf (SW Adriatic Sea, Gulf of Taranto). Earth and Planetary Science Letters 300, 112-124.

Lipp, J.S., Hinrichs, K.U., 2009. Structural diversity and fate of intact polar lipids in marine sediments. Geochimica et Cosmochimica Acta 73, 6816-6833.

Lisiecki, L.E., Raymo, M.E., 2005. A Pliocene-Pleistocene stack of 57 globally distributed benthic $\delta^{18}O$ records. Paleoceanography 20, PA1003.

Liu, Z.H., Pagani, M., Zinniker, D., DeConto, R., Huber, M., Brinkhuis, H., Shah, S.R., Leckie, R.M., Pearson, A., 2009. Global Cooling During the Eocene-Oligocene Climate Transition. Science 323, 1187-1190.

Locarnini, R.A., Mishonov, A.V., Antonov, J.I., Boyer, T.P., Garcia, H.E., Baranova, O.K., Zweng, M.M., Johnson, D.R., 2010. World Ocean Atlas 2009: Volume 1: Temperature, In: Levitus, S. (Ed.), NOAA Atlas NESDIS 68. U.S. Government Printing Office, Washington, D.C., p. 184.

Lohmann, G., Pfeiffer, M., Laepple, T., Leduc, G., Kim, J.H., 2012. A model-data comparison of the Holocene global sea surface temperature evolution. Climate of the Past Discussion 8, 1005-1056.

Lopes dos Santos, R.A., Prange, M., Castañeda, I.S., Schefuß, E., Mulitza, S., Schulz, M., Niedermeyer, E.M., Sinninghe Damsté, J.S., Schouten, S., 2010. Glacial–interglacial variability in Atlantic meridional overturning circulation and thermocline adjustments in the tropical North Atlantic. Earth and Planetary Science Letters 300, 407-414.

Lorenz, S.J., Kim, J.-H., Rimbu, N., Schneider, R.R., Lohmann, G., 2006. Orbitally driven insolation forcing on Holocene climate trends: Evidence from alkenone data and climate modeling. Paleoceanography 21, PA1002.

Luz, B., 1977. Late Pleistocene paleoclimates of the South Pacific based on statistical analysis of planktonic foraminifers. Palaeogeography, Palaeoclimatology, Palaeoecology 22, 61-78.

Malmgren, B.A., Kucera, M., Nyberg, J., Waelbroeck, C., 2001. Comparison of Statistical and Artificial Neural Network Techniques for Estimating Past Sea Surface Temperatures from Planktonic Foraminifer Census Data. Paleoceanography 16, 520-530.

Margot, H., Acebal, C., Toril, E., Amils, R., Fernandez Puentes, J., 2002. Consistent association of crenarchaeal Archaea with sponges of the genus *Axinella*. Marine Biology 140, 739-745.

Marlowe, I.T., Brassell, S.C., Eglinton, G., Green, J.C., 1990. Long-Chain Alkenones and Alkyl Alkenoates and the Fossil Coccolith Record of Marine-Sediments. Chemical Geology 88, 349-375.

Marlowe, I.T., Green, J.C., Neal, A.C., Brassell, S.C., Eglinton, G., Course, P.A., 1984. Long chain (n-C_{37}–C_{39}) alkenones in the Prymnesiophyceae. Distribution of alkenones and other lipids and their taxonomic significance. British Phycological Journal 19, 203-216.

Marshall, J., Speer, K., 2012. Closure of the meridional overturning circulation through Southern Ocean upwelling. Nature Geoscience 5, 171-180.

Martínez-Garcia, A., Rosell-Melé, A., Geibert, W., Gersonde, R., Masque, P., Gaspari, V., Barbante, C., 2009. Links between iron supply, marine productivity, sea surface temperature, and CO_2 over the last 1.1 Ma. Paleoceanography 24, PA1207.

Martínez-Garcia, A., Rosell-Melé, A., McClymont, E.L., Gersonde, R., Haug, G.H., 2010. Subpolar link to the emergence of the modern equatorial Pacific cold tongue. Science 328, 1550-1553.

Mashiotta, T.A., Lea, D.W., Spero, H.J., 1999. Glacial-interglacial changes in Subantarctic sea surface temperature and delta O-18-water using foraminiferal Mg. Earth and Planetary Science Letters 170, 417-432.

McClymont, E.L., Ganeshram, R.S., Pichevin, L.E., Talbot, H.M., van Dongen, B.E., Thunell, R.C., Haywood, A.M., Singarayer, J.S., Valdes, P.J., 2012. Sea-surface temperature records of Termination 1 in the Gulf of California: Challenges for seasonal and interannual analogues of tropical Pacific climate change. Paleoceanography 27, PA2202.

McClymont, E.L., Martinez-Garcia, A., Rosell-Mele, A., 2007. Benefits of freeze-drying sediments for the analysis of total chlorins and alkenone concentrations in marine sediments. Organic Geochemistry 38, 1002-1007.

Mohtadi, M., Hebbeln, D., 2004. Mechanisms and variations of the paleoproductivity off northern Chile (24°S & 33°S) during the last 40,000 years. Paleoceanography 19, PA2023.

Mohtadi, M., Hebbeln, D., Nuñez Ricardo, S., Lange, C.B., 2006. El Niño-like pattern in the Pacific during marine isotope stages (MIS) 13 and 11? Paleoceanography 21, PA1015.

Mollenhauer, G., Eglinton, T.I., Hopman, E.C., Sinninghe Damsté, J.S., 2008. A radiocarbon-based assessment of the preservation characteristics of crenarchaeol and alkenones from continental margin sediments. Organic Geochemistry 39, 1039-1045.

Mollenhauer, G., Inthorn, M., Vogt, T., Zabel, M., Sinninghe Damsté, J.S., Eglinton, T.I., 2007. Aging of marine organic matter during cross-shelf lateral transport in the Benguela upwelling system revealed by compound-specific radiocarbon dating. Geochemistry Geophysics Geosystems 8, Q09004.

Mollenhauer, G., McManus, J.F., Benthien, A., Müller, P.J., Eglinton, T.I., 2006. Rapid lateral particle transport in the Argentine Basin: Molecular ^{14}C and $^{230}Th_{xs}$ evidence. Deep-Sea Research Part I: Oceanographic Research Papers 53, 1224-1243.

Morales, C.E., Hormazabal, S.E., Blanco, J., 1999. Interannual variability in the mesoscale distribution of the depth of the upper boundary of the oxygen minimum layer off northern Chile (18–24°S): Implications for the pelagic system and biogeochemical cycling. Journal of Marine Research 57, 909-932.

Müller, P.J., Cepek, M., Ruhland, G., Schneider, R.R., 1997. Alkenone and coccolithophorid species changes in late Quaternary sediments from the Walvis Ridge: Implications for the alkenone paleotemperature method. Palaeogeography, Palaeoclimatology, Palaeoecology 135, 71-96.

Müller, P.J., Kirst, G., Ruhland, G., von Storch, I., Rosell-Melé, A., 1998. Calibration of the alkenone paleotemperature index $U_{37}^{K'}$ based on core-tops from the eastern South Atlantic and the global ocean (60 °N-60 °S). Geochimica et Cosmochimica Acta 62, 1757-1772.

Murray, A.E., Preston, C.M., Massana, R., Taylor, L.T., Blakis, A., Wu, K., DeLong, E.F., 1998. Seasonal and spatial variability of bacterial and archaeal assemblages in the coastal waters near Anvers Island, Antarctica. Applied and Environmental Microbiology 64, 2585-2595.

Naafs, B.D.A., Hefter, J., Stein, R., 2012. Application of the long chain diol index (LDI) paleothermometer to the early Pleistocene (MIS 96). Organic Geochemistry 49, 83-85.

Nuernberg, D., 1995. Magnesium in tests of Neogloboquadrina pachyderma sinistral from high northern and southern latitudes. The Journal of Foraminiferal Research 25, 350-368.

Orsi, A.H., Whitworth, T., Nowlin, W.D., 1995. On the meridional extent and fronts of the Antarctic Circumpolar Current. Deep-Sea Research Part I: Oceanographic Research Papers 42, 641-673.

Pahnke, K., Zahn, R., Elderfield, H., Schulz, M., 2003. 340,000-Year Centennial-Scale Marine Record of Southern Hemisphere Climatic Oscillation. Science 301, 948-952.

Paillard, D., Labeyrie, L., Yiou, P., 1996. Macintosh Program performs time-series analysis. Eos Transactions AGU 77, 379-379.

Parrenin, F., Barnola, J.M., Beer, J., Blunier, T., Castellano, E., Chappellaz, J., Dreyfus, G., Fischer, H., Fujita, S., Jouzel, J., Kawamura, K., Lemieux-Dudon, B., Loulergue, L., Masson-Delmotte, V., Narcisi, B., Petit, J.R., Raisbeck, G., Raynaud, D., Ruth, U., Schwander, J., Severi, M., Spahni, R., Steffensen, J.P., Svensson, A., Udisti, R., Waelbroeck, C., Wolff, E., 2007. The EDC3 chronology for the EPICA dome C ice core. Climate of the Past 3, 485-497.

Peterse, F., Kim, J.H., Schouten, S., Kristensen, D.K., Koc, N., Sinninghe Damsté, J.S., 2009. Constraints on the application of the MBT/CBT palaeothermometer at high latitude environments (Svalbard, Norway). Organic Geochemistry 40, 692-699.

Petit, J.R., Jouzel, J., Raynaud, D., Barkov, N.I., Barnola, J.M., Basile, I., Bender, M., Chappellaz, J., Davis, M., Delaygue, G., Delmotte, M., Kotlyakov, V.M., Legrand, M., Lipenkov, V.Y., Lorius, C., Pepin, L., Ritz, C., Saltzman, E., Stievenard, M., 1999. Climate and atmospheric history of the past 420,000 years from the Vostok ice core, Antarctica. Nature 399, 429-436.

Pflaumann, U., Duprat, J., Pujol, C., Labeyrie, L.D., 1996. SIMMAX: A Modern Analog Technique to Deduce Atlantic Sea Surface Temperatures from Planktonic Foraminifera in Deep-Sea Sediments. Paleoceanography 11, 15-35.

Prahl, F.G., Mix, A.C., Sparrow, M.A., 2006. Alkenone paleothermometry: Biological lessons from marine sediment records off western South America. Geochimica et Cosmochimica Acta 70, 101-117.

Prahl, F.G., Muehlhausen, L.A., Zahnle, D.L., 1988. Further evaluation of long-chain alkenones as indicators of paleoceanographic conditions. Geochimica et Cosmochimica Acta 52, 2303-2310.

Prahl, F.G., Wakeham, S.G., 1987. Calibration of unsaturation patterns in long-chain ketone compositions for paleotemperature assessment. Nature 330, 367-369.

Prell, W.L., 1985. The stability of low-latitude sea-surface temperatures: An evaluation of the CLIMAP reconstruction with emphasis on the positive SST anomalies,, US Department of Energy, Washington, DC., pp. 1-60.

Quiñones, R.A., Levipan, H.A., Urrutia, H., 2009. Spatial and temporal variability of planktonic archaeal abundance in the Humboldt Current System off Chile. Deep Sea Research Part II: Topical Studies in Oceanography 56, 1073-1082.

Rampen, S.W., Willmott, V., Kim, J.-H., Uliana, E., Mollenhauer, G., Schefuß, E., Sinninghe Damsté, J.S., Schouten, S., 2012. Long chain 1,13- and 1,15-diols as a potential proxy for palaeotemperature reconstruction. Geochimica et Cosmochimica Acta 84, 204-216.

Rechka, J.A., Maxwell, J.R., 1988. Unusual long chain ketones of algal origin. Tetrahedron Letters 29, 2599-2600.

Rincón-Martínez, D., Lamy, F., Contreras, S., Leduc, G., Bard, E., Saukel, C., Blanz, T., Mackensen, A., Tiedemann, R., 2010. More humid interglacials in Ecuador during the past 500 kyr linked to latitudinal shifts of the equatorial front and the Intertropical Convergence Zone in the eastern tropical Pacific. Paleoceanography 25, PA2210.

Roemmich, D., John Gould, W., Gilson, J., 2012. 135 years of global ocean warming between the Challenger expedition and the Argo Programme. Nature Climate Change 2, 425-428.

Romero, O.E., Kim, J.-H., Hebbeln, D., 2006. Paleoproductivity evolution off central Chile from the Last Glacial Maximum to the Early Holocene. Quaternary Research 65, 519-525.

Rosell-Melé, A., 1998. Interhemispheric appraisal of the value of alkenone indices as temperature and salinity proxies in high-latitude locations. Paleoceanography 13, 694-703.

Rosell-Melé, A., Carter, J., Eglinton, G., 1994. Distributions of long-chain alkenones and alkyl alkenoates in marine surface sediments from the North East Atlantic. Organic Geochemistry 22, 501-509.

Rosell-Melé, A., Comes, P., 1999. Evidence for a warm Last Glacial Maximum in the Nordic seas or an example of shortcomings in $U^{K'}_{37}$ and U^{K}_{37} to estimate low sea surface temperature? Paleoceanography 14, 770-776.

Rosell-Melé, A., Eglinton, G., Pflaumann, U., Sarnthein, M., 1995. Atlantic core-top calibration of the U_{37}^{K} index as a sea-surface palaeotemperature indicator. Geochimica et Cosmochimica Acta 59, 3099-3107.

Rosell-Melé, A., Jansen, E., Weinelt, M., 2002. Appraisal of a molecular approach to infer variations in surface ocean freshwater inputs into the North Atlantic during the last glacial. Global and Planetary Change 34, 143-152.

Rühlemann, C., Butzin, M., 2006. Alkenone temperature anomalies in the Brazil-Malvinas Confluence area caused by lateral advection of suspended particulate material. Geochemistry Geophysics Geosyststems 7, Q10015.

Saavedra-Pellitero, M., Flores, J.A., Lamy, F., Sierro, F.J., Cortina, A., 2011. Coccolithophore estimates of paleotemperature and paleoproductivity changes in the southeast Pacific over the past 27 kyr. Paleoceanography 26, PA1201.

Saukel, C., Lamy, F., Stuut, J.-B.W., Tiedemann, R., Vogt, C., 2011. Distribution and provenance of wind-blown SE Pacific surface sediments. Marine Geology 280, 130-142.

Sawada, K., Shiraiwa, Y., 2004. Alkenone and alkenoic acid compositions of the membrane fractions of Emiliania huxleyi. Phytochemistry 65, 1299-1307.

Schaefer, G., Rodger, J.S., Hayward, B.W., Kennett, J.P., Sabaa, A.T., Scott, G.H., 2005. Planktic foraminiferal and sea surface temperature record during the last 1 Myr across the Subtropical Front, Southwest Pacific. Marine Micropaleontology 54, 191-212.

Schlitzer, R., 2011. Ocean Data View, http://odv.awi.de.

Schneider-Mor, A., Yam, R., Bianchi, C., Kunz-Pirrung, M., Gersonde, R., Shemesh, A., 2008. Nutrient regime at the siliceous belt of the Atlantic sector of the Southern Ocean during the past 660 ka. Paleoceanography 23, PA3217.

Schneider, B., Leduc, G., Park, W., 2010. Disentangling seasonal signals in Holocene climate trends by satellite-model-proxy integration. Paleoceanography 25, PA4217.

Schneider, R.R., Müller, P.J., Acheson, R., 1999. Atlantic alkenone sea-surface temperature records: Low versus mid latitudes and differences between hemispheres, In: Abrantes, F., Mix, A.C. (Eds.), Reconstructing Ocean History: A Window into the Future. Kluwer Academic / Plenum Publishers, New York, pp. 33-55.

Schouten, S., Hopmans, E.C., Pancost, R.D., Damsté, J.S.S., 2000. Widespread occurrence of structurally diverse tetraether membrane lipids: Evidence for the ubiquitous presence of low-temperature relatives of hyperthermophiles. Proceedings of the National Academy of Sciences 97, 14421-14426.

Schouten, S., Hopmans, E.C., Schefuss, E., Sinninghe Damsté, J.S., 2002. Distributional variations in marine crenarchaeotal membrane lipids: a new tool for reconstructing ancient sea water temperatures? Earth and Planetary Science Letters 204, 265-274.

Schouten, S., Hopmans, E.C., Sinninghe Damsté, J.S., 2004. The effect of maturity and depositional redox conditions on archaeal tetraether lipid palaeothermometry. Organic Geochemistry 35, 567-571.

Schouten, S., Huguet, C., Hopmans, E.C., Kienhuis, M.V., Sinninghe Damsté, J.S., 2007. Analytical methodology for TEX_{86} paleothermometry by high-performance liquid chromatography/atmospheric pressure chemical ionization-mass spectrometry. Analytical Chemistry 79, 2940-2944.

Schulz, H.-M., Schöner, A., Emeis, K.-C., 2000. Long-chain alkenone patterns in the Baltic sea—an ocean-freshwater transition. Geochimica et Cosmochimica Acta 64, 469-477.

Shackleton, N.J., 1987. Oxygen isotopes, ice volume and sea level. Quaternary Science Reviews 6, 183-190.

Shackleton, N.J., Berger, A., Peltier, W.R., 1990. An alternative astronomical calibration of the lower Pleistocene timescale based on ODP Site 677. Earth and Environmental Science Transactions of the Royal Society of Edinburgh 81, 251-261.

Shah, S.R., Mollenhauer, G., Ohkouchi, N., Eglinton, T.I., Pearson, A., 2008. Origins of archaeal tetraether lipids in sediments: Insights from radiocarbon analysis. Geochimica et Cosmochimica Acta 72, 4577-4594.

Shemesh, A., Charles, C.D., Fairbanks, R.G., 1992. Oxygen Isotopes in Biogenic Silica: Global Changes in Ocean Temperature and Isotopic Composition. Science 256, 1434-1436.

Shevenell, A.E., Ingalls, A.E., Domack, E.W., Kelly, C., 2011. Holocene Southern Ocean surface temperature variability west of the Antarctic Peninsula. Nature 470, 250-254.

Sikes, E.L., Sicre, M.A., 2002. Relationship of the tetra-unsaturated C_{37} alkenone to salinity and temperature: Implications for paleoproxy applications. Geochemistry Geophysics Geosystems 3, 1063.

Sikes, E.L., Volkman, J.K., 1993. Calibration of alkenone unsaturation ratios ($U^{k'}_{37}$) for paleotemperature estimation in cold polar waters. Geochimica et Cosmochimica Acta 57, 1883-1889.

Sikes, E.L., Volkman, J.K., Robertson, L.G., Pichon, J.J., 1997. Alkenones and alkenes in surface waters and sediments of the Southern Ocean: Implications for paleotemperature estimation in polar regions. Geochimica et Cosmochimica Acta 61, 1495-1505.

Sinninghe Damsté, J.S., Ossebaar, J., Abbas, B., Schouten, S., Verschuren, D., 2009. Fluxes and distribution of tetraether lipids in an equatorial African lake: Constraints on the application of the TEX_{86} palaeothermometer and BIT index in lacustrine settings. Geochimica et Cosmochimica Acta 73, 4232-4249.

Sinninghe Damsté, J.S., Rijpstra, W.I.C., Hopmans, E.C., Prahl, F.G., Wakeham, S.G., Schouten, S., 2002a. Distribution of membrane lipids of planktonic Crenarchaeota in the Arabian sea. Applied and Environmental Microbiology 68, 2997-3002.

Sinninghe Damsté, J.S., Schouten, S., Hopmans, E.C., van Duin, A.C.T., Geenevasen, J.A.J., 2002b. Crenarchaeol: the characteristic core glycerol dibiphytanyl glycerol tetraether membrane lipid of cosmopolitan pelagic crenarchaeota. Journal of Lipid Research 43, 1641-1651.

Sluijs, A., Schouten, S., Pagani, M., Woltering, M., Brinkhuis, H., Sinninghe Damsté, J.S., Dickens, G.R., Huber, M., Reichart, G.J., Stein, R., Matthiessen, J., Lourens, L.J., Pedentchouk, N., Backman, J., Moran, K., Scientists, E., 2006. Subtropical arctic ocean temperatures during the Palaeocene/Eocene thermal maximum. Nature 441, 610-613.

Smith, R.W., Bianchi, T.S., Li, X., 2012. A re-evaluation of the use of branched GDGTs as terrestrial biomarkers: Implications for the BIT Index. Geochimica et Cosmochimica Acta 80, 14-29.

Sonzogni, C., Bard, E., Rostek, F., Lafont, R., Rosell-Melé, A., Eglinton, G., 1997. Core-top calibration of the alkenone index vs sea surface temperature in the Indian Ocean. Deep-Sea Research Part II- Topical Studies in Oceanography 44, 1445-1460.

Stephens, B.B., Keeling, R.F., 2000. The influence of Antarctic sea ice on glacial-interglacial CO^2 variations. Nature 404, 171-174.

Strub, P.T., Mesias, J.M., Montecino, V., Rutlant, J., Salinas, S., 1998. Coastal ocean circulation off western South America. Wiley, New York.

Stuut, J.-B.W., Lamy, F., 2004. Climate variability at the southern boundaries of the Namib (southwestern Africa) and Atacama (northern Chile) coastal deserts during the last 120,000 yr. Quaternary Research 62, 301-309.

Talley, L.D., Pickard, G.L., Emery, W.J., Swift, J.H., 2011. Descriptive Physical Oceanograpgy: an Introduction, 6 ed. Academic Press.

Toggweiler, J.R., Russell, J., 2008. Ocean circulation in a warming climate. Nature 451, 286-288.

Tomczak, M., Godfrey, J.S., 2003. Regional Oceanography: an Introduction, 2nd ed. Daya Publishing House, Delhi.

Uda, I., Sugai, A., Itoh, Y.H., Itoh, T., 2001. Variation on molecular species of polar lipids from *Thermoplasma acidophilum* depends on growth temperature. Lipids 36, 103-105.

Urey, H.C., 1947. The thermodynamic properties of isotopic substances. Journal of Chemical Society, 562-581.

Venz, K.A., Hodell, D.A., 2002. New evidence for changes in Plio-Pleistocene deep water circulation from Southern Ocean ODP Leg 177 Site 1090. Palaeogeography, Palaeoclimatology, Palaeoecology 182, 197-220.

Verleye, T.J., Louwye, S., 2010. Late Quaternary environmental changes and latitudinal shifts of the Antarctic Circumpolar Current as recorded by dinoflagellate cysts from offshore Chile (41°S). Quaternary Science Reviews 29, 1025-1039.

Versteegh, G.J.M., Bosch, H.J., De Leeuw, J.W., 1997. Potential palaeoenvironmental information of C24 to C36 mid-chain diols, keto-ols and mid-chain hydroxy fatty acids; a critical review. Organic Geochemistry 27, 1-13.

Villanueva, J., Grimalt, J.O., 1996. Pitfalls in the chromatographic determination of the alkenone Uk37 index for paleotemperature estimation. Journal of Chromatography A 723, 285-291.

Waelbroeck, C., Labeyrie, L., Duplessy, J.C., Guiot, J., Labracherie, M., Leclaire, H., Duprat, J., 1998. Improving Past Sea Surface Temperature Estimates Based on Planktonic Fossil Faunas. Paleoceanography 13, 272-283.

Wakeham, S.G., Lewis, C.M., Hopmans, E.C., Schouten, S., Sinninghe Damsté, J.S., 2003. Archaea mediate anaerobic oxidation of methane in deep euxinic waters of the Black Sea. Geochimica et Cosmochimica Acta 67, 1359-1374.

Walsh, J.E., 1978. A data set on Northern Hemisphere sea ice extent, World Data Center-A for Glaciology (Snow and Ice), "Glaciological Data, Report GD-2", pp. 49 - 51.

Weijers, J.W.H., Schouten, S., Spaargaren, O.C., Sinninghe Damsté, J.S., 2006. Occurrence and distribution of tetraether membrane lipids in soils: Implications for the use of the TEX_{86} proxy and the BIT index. Organic Geochemistry 37, 1680-1693.

Wells, P., Okada, H., 1997. Response of nannoplankton to major changes in sea-surface temperature and movements of hydrological fronts over Site DSDP 594 (south Chatham Rise, southeastern New Zealand), during the last 130 kyr. Marine Micropaleontology 32, 341-363.

Wuchter, C., Schouten, S., Coolen, M.J.L., Sinninghe Damsté, J.S., 2004. Temperature-dependent variation in the distribution of tetraether membrane lipids of marine Crenarchaeota: Implications for TEX_{86} paleothermometry. Paleoceanography 19, PA4028.

Wuchter, C., Schouten, S., Wakeham, S.G., Sinninghe Damsté, J.S., 2005. Temporal and spatial variation in tetraether membrane lipids of marine Crenarchaeota in particulate organic matter: Implications for TEX_{86} paleothermometry. Paleoceanography 20, PA3013.

Wuchter, C., Schouten, S., Wakeham, S.G., Sinninghe Damsté, J.S.S., 2006. Archaeal tetraether membrane lipid fluxes in the northeastern Pacific and the Arabian Sea: Implications for TEX_{86} paleothermometry. Paleoceanography 21, PA4208.

Wyrtki, K., 1965. Oceanography of the eastern equatorial Pacific Ocean. Oceanography and Marine Biology 4, 33-68.

Zhu, C., Weijers, J.W.H., Wagner, T., Pan, J.M., Chen, J.F., Pancost, R.D., 2011. Sources and distributions of tetraether lipids in surface sediments across a large river-dominated continental margin. Organic Geochemistry 42, 376-386.

Zielinski, U., Gersonde, R., 2002. Plio–Pleistocene diatom biostratigraphy from ODP Leg 177, Atlantic sector of the Southern Ocean. Marine Micropaleontology 45, 225-268.

Zwally, H.J., Comiso, J.C., Parkinson, C.L., Campbell, W.J., Carsey, F.D., Gloersen, P., 1983. Antarctic sea ice, 1973-1976: satellite passive-microwave observations, NASA Special Publications SP-459. National Aeronatics and Space Administration, Washington, D.C., p. 206.

Data handling

All data presented in this thesis will be publicly available on the Pangaea database (www.pangaea.de) once the manuscripts are published online.

Data from the manuscript in **Chapter 3**: http://doi.pangaea.de/10.1594/PANGAEA.792642

Data from the manuscript in **Appendix 5**: http://doi.pangaea.de/10.1594/PANGAEA.767415

Appendix 1: Abbreviations and acronyms

ACC	Antarctic Circumpolar Current
AMJ	April May June
ANN	Artificial Neural Network
APCI	Atmospheric pressure chemical ionization
APF	Antarctic Polar Front
ARGO	Array for Real-time Geostrophic Oceanography
ASE	Accelerated solvent extractor
AVHRR	Advanced Very High Resolution Radiometer
BIT	Branched and Isoprenoid Tetraether index
CHC	Cape Horn Current
Cren'	Crenarchaeol regioisomer
EPICA	European Project for Ice Coring in Antarctica
EEP	Eastern Equatorial Pacific
ENSO	El Niño – Southern Oscillation
EUC	Equatorial Undercurrent
FID	Flame ionization detector
GAM	Generalized additive model
GC	Gas chromatography
GDGT	Glycerol dialkyl glycerol tetraether
G-IG	Glacial - interglacial
HMS	Her/His Majesty's Ship
HPLC	High performance liquid chromatography
ICOADS	International Comprehensive Atmosphere-Ocean Data Set
IKM	Imbrie and Kipp method
IPCC	Intergovernmental Panel on Climate Change
IRD	Ice-rafted debris
ITCZ	Intertropical Convergence Zone
IUPAC	International Union of Pure and Applied Chemistry
JAS	July August September
JFM	January February March
LDI	Long-chain Diol Index
LGM	Last Glacial Maximum
LSR	Linear sedimentation rate
MARGO	Multiproxy Approach for the Reconstruction of the Glacial Ocean surface
MAT	Modern analog technique
MBE	Mid Brunhes Event
MIS	Marine Isotope Stage
MS	Mass spectrometer
MSD	Mass Selective Detector
NBS	National Bureau of Standards
NIOZ	Netherlands Institute for Sea Research
NSIPP	NASA (National Aeronautics and Space Adminitration) Seasonal-To-Interannual Prediction Project
ODV	Ocean Data View
OMZ	Oxygen minimum zone
OND	October November December
PCA	Principal component analysis
PCC	Peru-Chile Current

PETM	Paleocene-Eocene Thermal Maximum
PUC	Peru-Chile Undercurrent
RAM	Revised analog method
SAF	Subantarctic Front
SCAR	Scientific Committee on Antarctic Science
SEC	South Equatorial Current
SIM	Selected ion monitoring
SIMMAX	Modern analog technique with a similarity index
SSI	Summer sea ice extent
SST	Sea surface temperature
STF	Subtropical Front
TEX_{86}	TetraEther indeX with 86 carbon atoms
TEX_{86}^{H}	Modified TEX_{86}; TetraEther indeX with 86 carbon atoms for reconstructing sea surface temperature Higher 15°C
TEX_{86}^{L}	Modified TEX_{86}; TetraEther indeX with 86 carbon atoms for reconstructing sea surface temperature Lower than 15°C
TF	Transfer function
U^{K}_{37}	Unsaturation of Ketone with 37 carbon atoms (isomers with two, three and four double-bonds)
$U^{K'}_{37}$	Simplified U^{K}_{37}; Unsaturation of Ketone with 37 carbon atoms (isomers with two and three double-bonds)
VPDB	Vienna Pee Dee Belemnite
WOA	World Ocean Atlas
WOCE	World Ocean Circulation Experiment
WOD	World Ocean Data
WSI	Winter sea-ice extent

Appendix 2: Units and chemical nomenclatures

%	percent
‰	per mil
°N/S/W/E	degree North/South/West/East
°C	degree Celsius
Ca	Calcium
cm	centimeter (10^{-2} meter)
DCM	Dichloromethane
KOH	Potassium hydroxide
kV	kilovolt (10^{3} volt)
kyr	kiloyear (10^{3} year)
m	meter
Mg	Magnesium
min	minute
mL	milliliter (10^{-3} liter)
mm	millimeter (10^{-3} meter)
ms	millisecond (10^{-3} second)
mTorr	millitorr
µA	microampere **(**10^{-6} ampere**)**
µL	microliter (10^{-6} liter)
µm	micrometer (10^{-6} meter)
N_2	Nitrogen
ng	nanogram (10^{-9} gram)
PTFE	Polytetrafluoroethylene
r^2	coefficient of determination
SiO	Silica
Sr	Strontium
Sv	Sverdrup
v/v	volume / volume

Appendix 3: List of figures

Figure	**1.1**	Major components of the climate system. (from Roger Pielke Sr.'s www.pielkeclimatesci.wordpress.com).	1
Figure	**1.2**	A schematic of the framework for projecting future climate using climate models (from Goosse et al.'s online textbook at www.climate.be/textbook/).	2
Figure	**1.3**	Molecular structure and standard IUPAC names of C_{37} alkenones with 2, 3, and 4 double bonds (Figure from *Marlowe et al.* [1990], following structure verification by *Rechka and Maxwell* [1988] and double-bond position identification by *de Leeuw* et al. [1980]).	5
Figure	**1.4**	Molecular structure of isoprenoid glycerol dialkyl glycerol tetraether (GDGT) lipids with different ring moieties (from *Ho et al.* [2011])	8
Figure	**1.5**	Literature review of paleo sea surface temperature reconstruction in the subantarctic South Pacific south of 40°S.	11
Figure	**1.6**	Crossplots of GDGT-based indices, i.e., TEX_{86} and TEX_{86}^{L}, with satellite SSTs from *Kim et al.* [2010].	12
Figure	**1.7**	Location of marine sediments used in this study.	16
Figure	**1.8**	Types of biomarkers and their precursors in the three domains of life.	17
Figure	**1.9**	Schematic of silica or alumina column chromatography to separate a mixture of organic compounds into different fractions prior to analysis. (Figure from explow.com/chromatography)	18
Figure	**1.10**	South Pacific core-top alkenone index values with and without saponification	19
Figure	**1.11**	Correlation between the climatology SST data sets from the NSIPP AVHRR Pathfinder and Erosion Global 9km [*Casey and Cornillon*, 1999] and the World Ocean Atlas 2009 [*Locarnini et al.*, 2010].	21
Figure	**2.1**	Location of study sites in the global ocean.	27
Figure	**2.2**	Principal component analysis on the individual GDGTs in the compilation of the data in this study and the published core-top data by *Kim et al.* [2008], *Kim et al.* [2010] and *Ho et al.* [2011]	30
Figure	**2.3**	Relationship between the fractional abundance of individual GDGTs and the WOA09 annual mean SSTs..	32
Figure	**2.4**	Correlation plots of TEX_{86} and TEX_{86}^{L} values with annual mean sea surface temperature derived from World Ocean Atlas 2009 (WOA09).	33
Figure	**2.5**	Correlation plots of TEX_{86} and TEX_{86}^{L} values with water temperatures derived from World Ocean Atlas 2009 (WOA09) at various depths.	35
Figure	**2.6**	Correlation plots of TEX_{86} and TEX_{86}^{L} values with mean seasonal sea surface temperature derived from World Ocean Atlas 2009 (WOA09).	36
Figure	**2.7**	The residuals of temperature estimates derived from the latest global core-top calibrations for TEX_{86} and TEX_{86}^{L} [*Kim et al.*, 2010].	37
Figure	**2.8**	Close-up of the residuals of TEX_{86} and TEX_{86}^{L} derived SST estimates relative to World Ocean Atlas 2009 (WOA09) summer SST in the Arctic.	40
Figure	**2.9**	Compilation of the TEX_{86} and TEX_{86}^{L} data from this study and the published data set of *Kim et al.* [2010], *Kim et al.* [2008], *Leider et al.*	44

		[2010], *Ho et al*. [2011] and *Shevenell et al*. [2011], as a function of World Ocean Atlas 2009 (WOA09) annual mean SST.	
Figure	**3.1**	Location of sites and major oceanic currents discussed in this work.	50
Figure	**3.2**	Age models and linear sedimentation rates at core sites GeoB 3388-1, GeoB 3327-5 and PS75/034-2.	57
Figure	**3.3**	Correlations of alkenone indices, i.e., $U^{K'}_{37}$ and U^{K}_{37} with temperature.	58
Figure	**3.4**	Planktic $\delta^{18}O$ and alkenone-based SST records.	60
Figure	**3.5**	Comparison of temperature records from the Southern Ocean and Antarctica based on different proxies.	66
Figure	**3.6**	Meridional gradients of alkenone-inferred SSTs and mean annual insolation along the Southeast Pacific and SST evolution in the tropical Pacific.	68
Figure	**4.1**	Core locations of GeoB 3388-1 and TG7 [*Calvo et al.*, 2001], and major hydrographic features in the southeast Pacific.	75
Figure	**4.2**	Molecular structures of glycerol dialkyl glycerol tetraethers (GDGTs) used for the calculation of the TEX_{86}^{H} and BIT indices.	76
Figure	**4.3**	Glycerol dialkyl glycerol tetraether (GDGT) parameters and benthic $\delta^{18}O$ record of core GeoB 3388-1.	77
Figure	**4.4**	Correlation between the Branched and Isoprenoid Tetraether (BIT) index values and the TEX_{86}^{H}-derived SST estimates calculated with the global core-top calibration of *Kim et al.* [2010].	79
Figure	**4.5**	Temperature records at site GeoB 3388-1.	80
Figure	**4.6**	Upper water column structure at site GeoB 3388-1 in terms of oxygen concentration and temperature based on the annual mean climatological data of WOA09	83
Figure	**5.1**	U^{K}_{37} calibrations available in the literature.	91
Figure	**5.2**	Correlation between the sea surface salinity (SSS) and the sea surface temperature (SST) at the core-top sites of PS75 reported in **Chapter 3**.	92
Figure	**5.3**	TEX_{86}^{L}-derived temperature residuals (difference between estimated SST and climatological SST) by applying the current global calibration of *Kim et al*. [2010] on published data sets [*Ho et al.*, 2011; *Kim et al.*, 2010; *Leider et al.*, 2010; *Shevenell et al.*, 2011] and data presented in **Chapter 2**.	94
Figure	**5.4**	Schematic of a possible shift in the global core-top calibrations of TEX_{86} (currently calibrated against annual mean SST) after integrating production and export information, which skew towards warm (cold) seasons at high (low) latitudes.	94

Appendix 4: List of tables

Table	**1.1**	Overview of paleo sea surface temperature (SST) proxies.	4
Table	**1.2**	Short description of several modified GDGT-based indices and calibrations that deviate from the commonly applied global core-top calibrations of *Schouten et al.* [2002], *Kim et al.* [2008] and *Kim et al.* [2010].	9
Table	**1.3**	Details of previous paleo sea surface temperature studies in the subantarctic Southeast Pacific (south of 40°S).	11
Table	**3.1**	Site information and alkenone index values of the Southern Ocean core-top samples retrieved via multicoring.	52

Appendix 5: Additional first-authored manuscripts

"**Alkenone paleothermometry based on the haptophyte algae**", in *Encyclopedia of Quaternary Science*, Elsevier (in press)

By Ho, S.L., Naafs, B.D.A., and Lamy, F.

- This review contains a comprehensive description of many aspects of the alkenone paleothermometry, including a brief history of the development of this proxy, chemical structures, genetic evolution of the source organism, the relationship between the alkenone unsaturation and temperature in suspended matter, laboratory cultures and sediments, and some secondary effects (such as non-thermal physiological factors and degradation) that might affect the use of this paleothermometry.

"**Core top TEX_{86} values in the south and equatorial Pacific**", published in *Organic Geochemistry* 42, pages 94-99 (2011)

By Ho, S.L., Yamamoto, M., Mollenhauer, G., and Minagawa, M.

- This paper discusses whether there is a regional bias in the TEX_{86}-SST relationship in the Pacific, given that this ocean is under-represented in the global core-top calibration of *Kim et al.* [2010]. The appraisal is based on the relative distribution of individual GDGTs, the crossplots of the index values with atlas SSTs and the residuals of the temperature estimates. The small data set presented here encompasses diverse oceanic provinces (e.g., eastern equatorial Pacific cold tongue, west Pacific warm pool, the Southern Ocean) from low to high latitudes.